Thesis for the degree of Doctor of Philosophy

Continuous wave and pulsed erbium-doped fiber lasers for microwave photonics applications

Guillermo Eduardo Villanueva Ibáñez

Supervisors:

Dr. Pere Pérez Millán
Prof. Javier Martí Sendra

Valencia, November 2012

Agradecimientos

La realización de una tesis doctoral no es un trabajo de carácter individual, sino el fruto de numerosas colaboraciones con compañeros y colegas que hacen posible obtener resultados de calidad, y esta tesis no es una excepción. Sin la ayuda de estas personas, no sólo en el ámbito profesional sino en el emocional, habría sido imposible completar este trabajo de tesis. En esta parte del documento me gustaría transmitir mi agradecimiento a todos ellos.

En primer lugar quiero mostrar mi más profundo agradecimiento a mis directores de tesis. Gracias a Javier Martí por ofrecerme la oportunidad de formar parte del Centro de Tecnología Nanofotónica, donde he podido desarrollar una excelente carrera investigadora durante los últimos cinco años. Siempre ha mostrado un apoyo y confianza constante en mi labor que nunca olvidaré. Gracias a Pere Pérez por tomar la codirección de mi tesis en una etapa delicada de la misma. Toda la dedicación, consejos y confianza que ha depositado en mí han sido inestimables para sacar adelante esta tesis doctoral. Pero más allá del trabajo de investigación realizado está la amistad que se ha forjado durante estos años. Espero que nuestras colaboraciones se extiendan muchos años más en el futuro.

Durante los años transcurridos en el Centro de Tecnología Nanofotónica he tenido la suerte de entablar amistad con fantásticos compañeros de trabajo. Necesariamente mi lista de agradecimientos la encabeza José Vicente Galán. Gracias a su consejo me incorporé a este instituto, y constantemente me ha echado una mano cuando lo he necesitado. Cómo no agradecer la compañía de Jesús Palací y Jordi Peiró, que han inundado de almuerzacos, desafíos y carcajadas el día a día de trabajo. Agradezco sobremanera los buenos ratos pasados con los "metas" Carlos García, Rubén Ortuño y Pak. En todo momento he contado con el apoyo de mis compañeros de área María Morant, Marta Beltrán, Ruth Vilar, Joaquín Matres y Sara Mas. Gracias también a Josema Escalante, Javier García, Mercé Llopis, Antoine Brimont, Ana Gutierrez, Mariam Aamer, Clara Calvo, Susana Pérez, Carlos García y Caterina Calatayud por su compañerismo y amistad. También agradezco la ayuda recibida por parte de Jaime García, Borja Vidal, Teresa Mengual y Javier Herrera. Y a todos aquellos que ya no forman parte del instituto y que también me han brindado su apoyo y amistad: Claudio Otón, Veronica Toccafondo, Ingrid Niño, Rubén Alemany, Rakesh Sambaraju, José Caraquitena, Ignacio Solanes, Vicente Herrero, Vicent Gavino, Valentín Polo, y

un largo etcétera.

Además, la realización de esta tesis ha servido para formar fructíferas colaboraciones con otros grupos investigadores. En este aspecto quería agradecer a Miguel Andrés y José Luis Cruz de la Universidad de Valencia por toda su ayuda, consejo y predisposición a la hora de realizar redes de difracción en fibra. A Paolo Ghelfi, Claudio Porzi y Giovanni Serafino por acogernos a Jesús y a mí en Scuola Superiore Sant'Anna, en Pisa. A Jaques Albert por darme la oportunidad de incorporarme a su grupo en la Carleton University, Ottawa, durante cuatro meses. Y a Dmitry Turchinovich por recibirme en otra estancia predoctoral de tres meses en la Technical University of Denmark.

Fuera del ambiente de trabajo, pero no por ello de manera menos importante, otras muchas personas han contribuido indirectamente a la realización de esta tesis doctoral. Gracias a mis amigos de carrera Luis, Daniel, Rita, Alejandro, María, Rebeca y Queca. Su inestimable amistad siempre ha sido una gran motivación para mí. Por supuesto, en estos agradecimientos no puede faltar mi pequeño y apreciado grupo de tarados. Gracias a David, Edu, Jon, Benjamín, Jorge, Alex y todos los demás por proveerme siempre de risas y sacarme de vez en cuando del plano racional.

Esta tesis nunca se habría podido llevar a cabo sin el apoyo incondicional de mi familia. Gracias a mis hermanos Isabel, Vicente y Regina, y a mis padres por todo el cariño y comprensión que siempre han volcado en mí.

Gracias a Esteban y Vale. Su apoyo (y sus provisiones de leguminosas) me han dado fuerzas a lo largo de todos estos años.

Finalmente quería transmitir mi agradecimiento a una persona muy especial en mi vida. No sólo su apoyo, cariño y compresión han permitido realizar esta tesis doctoral, sino que han sido capaces de transformarme en una persona mejor. Los nueve años al lado de mi novia Patricia han sido los mejores años de mi vida. Contigo abrazada a mí siento que no hay proyecto al que no pueda enfrentarme. Gracias Patricia por compartir tu corazón conmigo, te quiero.

Abstract

This thesis studies optical fiber lasers for microwave photonics applications. Performance of traditional electronics counterparts turns out to be limited for high frequencies ranging tens of GHz. In this context, optics has found potential application to contribute towards the extension of microwave system features. In particular, fiber lasers have shown to be cost-effective reliable sources which are gaining increasing interest as a compact solution in comparison with solid-state lasers. The aim of this thesis is the design, fabrication and characterization of compact fiber laser optical sources for microwave photonics applications such as microwave-millimeter wave generation and photonic-assisted analog to digital conversion.

A tunable dual-wavelength distributed feedback (DFB) fiber laser for continuous wave microwave generation by photomixing is presented. A fiber Bragg grating written in an erbium–doped fiber with two induced phase shifts constitutes the laser cavity. The dynamic wavelength difference tunability is achieved through two piezoelectric actuators controlled by a DC voltage source. After photodetection of the dual-wavelength laser output, a microwave signal with a continuously 0.12-7 GHz tuning range is photogenerated. The tuning range is ultimately limited by the grating spectral bandwidth. A second configuration of the dual-wavelength DFB fiber laser is studied to further increase the tuning range. Implementing two DFB cavities with different Bragg wavelengths in the same erbium-doped fiber allows a more versatile control of the single longitudinal mode emission frequencies. A photogenerated millimeter signal of tunable frequency from 0.72 to 92 GHz is obtained from an extremely compact and simple fiber laser.

We also propose different mode-locked fiber lasers for photonic-assisted analog to digital conversion. Active and passive mode-locking techniques are studied in erbium-doped fiber cavities to satisfy target specifications in terms of pulse repetition frequency, pulse width and time jitter. The harmonically active mode-locking is carried out through high bandwidth optical Mach-Zehnder modulators inserted in the cavity, while semiconductor saturable absorbers were used for passive mode-locking. The use of intracavity polarizing fibers is also explored: control of the mode-locking operation regime is demonstrated via polarization state adjustment. Rep-

etition rates of tens of GHz, subpicosecond pulsewidths and time jitters below 180 fs have been accomplished through the different mode-locking approaches.

Apart from semiconductor saturable absorbers, single-walled carbon nanotubes have shown ultrafast optical nonlinearities suitable for passive mode-locking. Fiber lasers passively mode-locked using carbon nanotubes as saturable absorbers are being proposed in the last years, and great effort is dedicated to implement nanotubes saturable absorbers in fiber lasers. The thesis also deals with the study of a new approach to deposit carbon nanotubes in optical fibers, in which tilted fiber Bragg gratings are used to enable optical light to interact with the nanotubes. Ultrafast optical switching is demonstrated using such carbon nanotube-based fiber device.

Resumen

Esta tesis estudia los láseres de fibra óptica para su inclusión en aplicaciones de fotónica de microondas. Las prestaciones de la tecnología electrónica en estas aplicaciones están limitadas para frecuencias de trabajo de decenas de GHz. En este contexto, la tecnología óptica ha encontrado aplicaciones potenciales con el fin de extender las especificaciones de sistemas de microondas tradicionales. En particular, los láseres de fibra se presentan como fuentes ópticas fiables de coste reducido las cuales están ganando interés como soluciones compactas en comparación con láseres de estado sólido. El objetivo de esta tesis es el diseño, fabricación y caracterización de láseres de fibra como fuentes ópticas compactas con aplicaciones de fotónica de microondas, como son la generación de ondas en la banda de microondas-milimétricas y la conversión analógico-digital asistida ópticamente.

En esta tesis se presenta el desarrollo de un láser de fibra de realimentación distribuida capaz de emitir en dos longitudes de onda en régimen continuo para la generación de señales de microondas por fotomezclado. La cavidad óptica está constituida por una red de difracción de Bragg grabada en una fibra dopada con erbio, en la que se aplican dos desfases puntuales. La sintonización dinámica de la diferencia de frecuencia de los dos modos emitidos se lleva a cabo mediante el empleo de dos actuadores piezoeléctricos controlados por una fuente de tensión continua. Tras la fotodetección de la salida del láser se obtiene una señal de microondas con un rango de sintonización continuo de 0.12-7 GHz. La máxima frecuencia de sintonización viene limitada por el ancho de banda espectral de la red de difracción. Por ello, se ha estudiado una segunda configuración del láser con el fin de incrementar el rango de sintonización. La implementación de dos cavidades de realimentación distribuida con diferentes frecuencias de emisión en la misma fibra dopada permite un control más versátil de las frecuencias de emisión de ambos modos ópticos. Esta fuente altamente compacta y sencilla es capaz de proporcionar una señal fotogenerada con un rango de sintonización de 0.72 a 92 GHz.

También se proponen distintos láseres de fibra pulsados mode-locked para aplicaciones de conversión analógico-digital asistida ópticamente. Se han estudiado diferentes técnicas activas y pasivas de mode-locking en láseres de fibra dopadas con erbio orientadas a cumplir requerimientos

en términos de frecuencia de repetición, ancho temporal de pulso y ruido jitter. El diseño activo de mode-locking armónico se ha llevado a cabo mediante moduladores ópticos de gran ancho de banda en la cavidad óptica, mientras que para el mode-locking pasivo se han empleado absorbentes saturables de semiconductor. También se ha explorado el uso de fibras polarizadoras, y se ha demostrado la posibilidad de control del régimen mode-locking a través del ajuste de estado polarización. Los diferentes esquemas de mode-locking han permitido obtener frecuencias de repetición de decenas de GHz, anchos de pulso por debajo del picosegundo y ruidos jitter inferiores a 180 fs.

Aparte de los absorbentes saturables de semiconductor, nanotubos de carbono monocapa han mostrado unas propiedades no lineales ultrarrápidas adecuadas para láseres mode-locked pasivos. En los últimos años se han propuesto láseres de fibra mode-locked pasivos los cuales emplean nanotubos de carbono como absorbente saturable, invirtiendo un gran esfuerzo en la integración de estos nanotubos en cavidades de fibra óptica. La tesis también trata sobre el estudio de una nueva técnica para la inclusión de nanotubos de carbono en fibras ópticas, en la cual se hace uso de redes de difracción de Bragg inclinadas para posibilitar la interacción de la luz con los nanotubos. Empleando este dispositivo se ha demostrado efectos de conmutación óptica ultrarrápida gracias a la no linealidad de los nanotubos.

Resum

Esta tesi estudia els làsers de fibra òptica per a aplicacions de fotònica de microones. Les prestacions de la tecnologia electrònica en estes aplicacions estan limitades per a freqüències de treball de desenes de GHz. En este context, la tecnologia òptica ha trobat aplicacions potencials amb la finalitat d'estendre les especificacions de sistemes de microones tradicionals. Particularment, els làsers de fibra es presenten com a fonts òptiques fiables de cost reduït, les quals estan guanyant interès com a solucions compactes en comparació amb els làsers d'estat sòlid. L'objectiu d'esta tesi es el disseny, fabricació i caracterització de làsers de fibra com a fonts òptiques compactes amb aplicacions de fotònica de microones, com son la generació d'ones a la banda de microones-mil·limètriques i la conversió analògic-digital assistida òpticament.

En esta tesi es presenta el desenvolupament d'un làser de fibra de realimentació distribuïda capaç d'emetre en dos longituds d'ona en règim continu per a la generació de senyals de microones per fotomesclat. La cavitat òptica està constituïda per una xarxa de difracció de Bragg gravada en una fibra dopada amb erbi, en la qual s'apliquen dos desfasaments puntuals. La sintonització dinàmica de la diferència de freqüència dels dos modes emesos es porta a terme mitjançant l'ús de dos actuadors piezoelèctrics controlats per una font de tensió contínua. Després de la fotodetecció de la eixida del làser s'obté un senyal de microones amb un rang de sintonització continu de 0.12 a 7 GHz. La màxima freqüència de sintonització ve limitada per l'ample de banda espectral de la xarxa de difracció. Per això s'ha estudiat una segona configuració del làser amb la finalitat d'incrementar el rang de sintonització. L' implementació de dos cavitats de realimentació distribuïda amb diferents freqüències d'emissió en la mateixa fibra dopada permet un control més versàtil de les freqüències d'emissió d'ambdós modes òptics. Aquesta font altament compacta i senzilla es capaç de proporcionar un senyal fotogenerat amb un rang de sintonització de 0.72 a 92 GHz.

També es proposen distints làsers de fibra polsats mode-locked per a aplicacions de conversió analògic-digital assistida òpticament. S'han estudiat diferents tècniques actives i passives de mode-locking en làsers de fibra dopada amb erbi orientades a complir requeriments en termes de freqüència de repetició, ample temporal dels pols i soroll jitter. El disseny

actiu de mode-locking harmònic s'ha portat a terme mitjançant moduladors òptics de gran ample de banda en la cavitat òptica, mentre que per al mode-locking passiu s'han utilitzat absorbents saturables de semiconductor. També s'ha explorat l'ús de fibres polaritzadores i s'ha demostrat la possibilitat de control del règim mode-locking a través de l'ajust de l'estat de polarització. Els diferents esquemes de mode-locking han permès obtenir freqüències de repetició de desenes de GHz, amples de pols per baix del pico segon i sorolls jitter inferiors a 180 fs.

Apart dels absorbents saturables de semiconductor, nanotubs de carboni monocapa han mostrat unes propietats no lineals ultra ràpides adequades per a làsers de fibra mode-locked passius. En els últims anys s'han proposat làsers de fibra mode-locked passius, els quals utilitzen nanotubs de carboni com absorbent saturable, invertint un gran esforç en la integració d'aquests nanotubs en cavitats de fibra òptica. La tesi també tracta sobre l'estudi d'una nova tècnica per a la inclusió de nanotubs de carboni en fibres òptiques, en la qual s'utilitzen xarxes de difracció de Bragg inclinades par a possibilitar la interacció de la llum amb els nanotubs. Utilitzant aquest dispositiu s'han demostrat efectes de commutació òptica ultra ràpida gràcies a la no linealitat dels nanotubs.

Contents

Chapter 1

Introduction

Optical fiber technology has revolutionized the telecommunications over the past decades, especially with the explosive growth of the Internet and the exponentially increasing bit rate demand [1]. In addition to optical communications, optical fiber finds manifold fields of applications like optical sensing [2], microwave photonics [3,4], medical imaging [5], material processing [6] and so on. Fiber lasers have gained great interest since they possess a number of physical attributes that distinguish them from other classes of lasers and that differentiate them in terms of functionality, performance, and practicality. This thesis studies some practical implementations of fiber lasers to be applied in microwave photonics applications, i. e., the combination of radiofrequency engineering and optoelectronics to make it possible to have functions in microwave systems that are complex or even not directly possible in the radiofrequency domain. Dual-wavelength continuous wave and pulsed mode-locked fiber lasers are designed, fabricated and characterized aimed to microwave and millimeter wave generation through photomixing and to photonic-assisted analog to digital conversion.

1.1 Fiber lasers

The fabrication of a laser was first proposed by Schawlow and Townes in 1958 [7], and the first experimental demonstration was realized by Theodore Maiman in 1960 [8]. In those days, his assistant Irnee D'Haenens called it *"A solution that is looking for a problem"* [9]. Since then, an intense scientific development of this device has been carried out. Very soon after the first laser proposal, the use of a waveguiding structure to provide guiding resonant structures in laser cavities was suggested [10]. The first demonstration of a fiber laser appeared in 1961 using a neodymium doped fiber with a large core [11]. Although fiber lasers were experimentally investigated during the 1960s [12, 13], 1970s [14, 15], and early 1980s [16], it is not until the appearance of low loss doped fibers [17] that practical fiber lasers were developed. The commercial

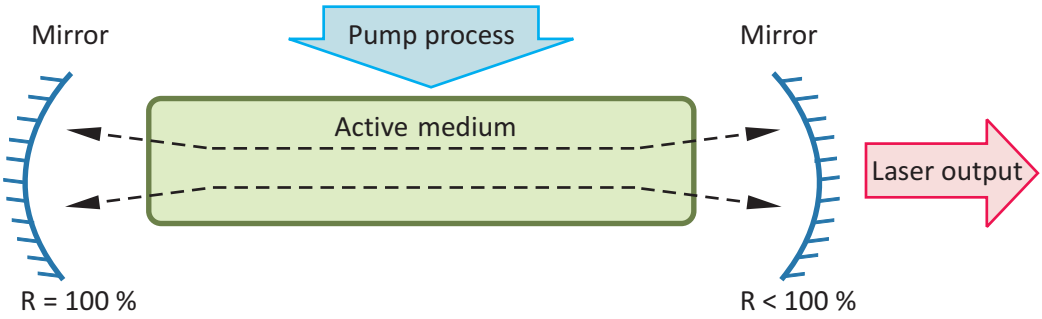

Figure 1.1: Elements of a typical laser oscillator.

market has been pioneered especially by one company, IMRA [18], but as the market has grown, more companies have joined the game and developed commercial fiber laser products. The development of fiber lasers has initially been driven by the massive development of telecommunication components, and for many years fiber lasers based on erbium technology have dominated the fiber laser market. Very recently companies like e.g. IMRA and Fianium [19] have also included fiber lasers based on ytterbium (Yb) doped fibers in their assortment. A major reason for this recent development of fiber lasers is that fiber lasers can now be directly pumped by laser diodes. The optical confinement provided by the fiber, combined with the excellent laser properties of trivalent rare earth ions, make fiber lasers extremely efficient. Erbium-doped fiber lasers can operate with exceptionally low thresholds, as low as 100 μW, and yet can be pumped extremely hard to produce output powers in excess of 100 W, with optical conversion efficiencies greater than 50%. Furthermore, the numerous laser transitions available from trivalent rare earth ions lend them the ability to generate light over a wide selection of wavelengths, from the ultraviolet (UV) to the midinfrared (mid-IR), with broad tuning ranges. Fiber lasers now compete directly in several domains with solid state and semiconductor sources, over which they present the advantage of high brightness, excellent mode quality, highly efficient coupling into a single-mode fiber, enhanced heat dissipation due to the larger surface-volume ratio of the active medium, and far superior wavelength stability with temperature [20].

To better understand how fiber lasers work, it is convenient to explain the basics of a fundamental laser structure. The word laser stands for Light Amplification by Stimulated Emission of Radiation. Lasers are devices that generate or amplify light, just as transistors and vacuum tubes generate and amplify electronic signals at audio, radio, or microwave frequencies. Here "light" must be understood broadly, since different kinds of lasers can amplify radiation at wavelengths ranging from the very long infrared region, merging with millimeter waves or microwaves, up through the visible region and extending now to the vacuum ultraviolet and even X-ray regions. Lasers come in a great variety of forms, using many different materials, many different atomic systems, and many different kinds of pumping or excitation techniques. Nevertheless, every laser comprises three essential elements, as shown in figure 1.1. These parts are:

- Active medium: medium consisting of an appropriate collection of atoms, molecules, ions, or in some instances a semiconducting crystal. This medium is susceptible of getting excited into a higher quantum-mechanical energy level, showing stimulated coherent amplification of electromagnetic radiation within a certain band of frequencies.

- Pumping process: mechanism to excite the active medium to higher quantum-mechanical energy levels. This process is not only responsible for producing merely excited atoms, but for providing population inversion, in which more atoms are excited into some higher quantum energy level than are in some lower energy level in the laser medium.

- Optical feedback: commonly implemented by an optical cavity. In combination with coherent amplification, this feedback yields laser oscillation. Optical feedback is usually supplied by mirrors at each end of the amplifying laser medium, carefully aligned so that waves can bounce back and forth between these mirrors with very small loss per bounce.

As can be observed in figure 1.1, the output signal is coupled out from the laser in this case through a partially transmitting mirror. This output beam is both highly directional and highly monochromatic. The structure of figure 1.1 is a linear or "standing-wave" cavity, since light propagates in both directions (backward and forward), creating a longitudinal standing wave. Another well-known cavity model for laser oscillation is the ring cavity, where light propagates in only one direction avoiding the standing wave phenomenon.

The emitting frequency features of lasers are conditioned to the emission cross section of the active medium and the cavity frequency response. On the one hand, the first parameter sets the spectral range of optical components that experience amplification in the active medium, and depends directly on the energetic level structure of the host particles. On the other hand, the cavity frequency response sets the spectral frequencies that can experience coherent feedback in the cavity, therefore being amplified further over other spectral components and oscillating in the laser. For the linear cavity shown in figure 1.1, also known as Fabry-Pérot resonator, the transmittance function has the expression

$$T = \frac{(1-R)^2}{1+R^2-2R\cos(k_0 2nl)}. \tag{1.1}$$

In equation (1.1), R denotes the reflectivity of the mirrors (considering both mirrors equal), k_0 the wavenumber of light in vacuum, and n and l the refractive index and length of the cavity respectively. Figure 1.2 shows a Fabry-Pérot response for two different values of mirrors reflectivity. It is worth explaining some important properties of Fabry-Pérot response, as they are common to many other cavity structures.

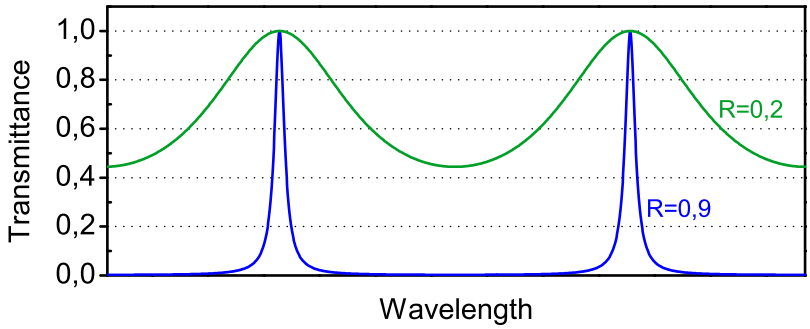

Figure 1.2: Transmittance response of a Fabry-Pérot resonator with mirrors of reflectivities 0.2 (green) and 0.9 (blue), respectively.

First of all, it shows a periodic response with wavelength. In a linear resonator, infinite discrete frequencies can interfere constructively keeping the relation

$$\lambda_m = \frac{2nl}{m} \quad \text{for } m = 1, 2, \ldots \tag{1.2}$$

All these resonant wavelengths λ_m appear as transmission peaks in the transmittance response of fig. 2. Their spectral separation is called Free Spectral Range (FSR), and is related with the effective length $2nl$ of the cavity through the relation

$$FSR = \frac{c_0}{2nl}, \tag{1.3}$$

where c_0 denotes the light speed in vacuum. Another feature of Fabry-Pérot resonances is the finesse F, dependent on the mirrors reflectivity. The more reflective the mirrors are, the higher the finesse is. The effect of a high finesse, as can be noticed in fig. 2, is the sharpening of the resonances. The finesse parameter has the expression

$$F = \frac{4R}{(1-R)^2}. \tag{1.4}$$

Transmission longitudinal modes of a Fabry-Pérot resonator in conjunction with the emission spectrum of the active medium leads to a collection of simultaneously oscillating components in the cavity. Depending on the number of oscillating longitudinal modes emitted, the laser would produce a broadband or a narrow band emission.

A fiber laser is a particular kind of laser in which the active medium is an optical fiber doped with a rare earth element. Optical fibers are cylindrical structures that enable waveguiding of light. They are usually based on a core surrounded by a cladding, with refractive indexes slightly lower for the cladding. Then, an electromagnetic signal injected to the core at a certain angle can propagate through the core

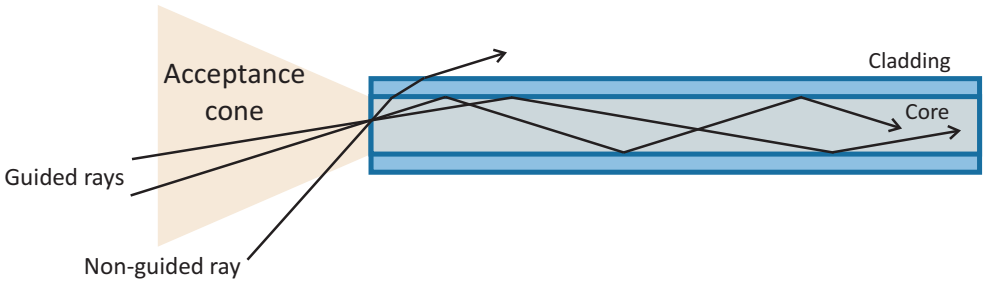

Figure 1.3: Total Internal Reflection of light rays in an optical fiber.

of the fiber via Total Internal Reflection (TIR), as shown in figure 1.3. Depending on the fiber profile (diameters and refractive indexes of cladding and core), the fiber allows the propagation of multiple transversal modes (multimode fiber, MMF) or a single transversal mode (singlemode fiber, SMF). The latter condition is desired for most practical applications, in particular for optical communications, as it avoids the intermodal dispersion that can severely degrade the communication capacity.

The fiber core can be doped with ions of rare earth elements, making up the active medium of a fiber laser. Such rare earth ions are erbium (Er^{3+}), neodymium (Nd^{3+}), ytterbium (Yb^{3+}), thulium (Th^{3+}) or praseodymium (Pr^{3+}) among others. These ions show absorption and emission lineshapes associated with transitions between states of energy. The common principle of optical amplification comprises a pump process, where an ion with an initial ground state reaches a metastable excited state by the absorption of a pump photon, and a radiative decay, where the excited ion comes back to the ground state, transferring the difference of energy in the form of an emitted photon. This last emission can be spontaneous or stimulated by other photon with the same energy. In the latter case, the stimulated emission contributes to the amplification of the incoming signal. Furthermore, the stimulated emitted photon is coherent with the incoming photon, building up in phase the propagating intensity. Figure 1.4 illustrates the stimulated emission process. The wavelengths of pump absorption and signal emission depend on the energy levels of each rare earth element. Table I compiles the main rare earth ions with their common host glasses and their wavelength emission ranges. Fiber laser pump sources are usually laser diodes emitting light with low-quality output mode with a suitable wavelength for the excitation of the dopant of the laser.

For standard single mode fiber, the core diameter ranges from 3 to 10 μm, so that a significant intensity can be obtained with a modest average power. A signal with an average power of 10 mW coupled into a fiber with a core diameter of 6 μm will result in an intensity of 35 kW/cm^2. A consequence is that the intensities necessary to reach the continuous-wave oscillation threshold can be achieved with modest input powers. This property has been exploited extensively in the design of short-cavity diode-pumped single-frequency neodymium, erbium, and ytterbium doped fiber lasers [21–23]. The inherent waveguiding property associated with the fiber ensures that the intensity is maintained over long distances, thereby providing

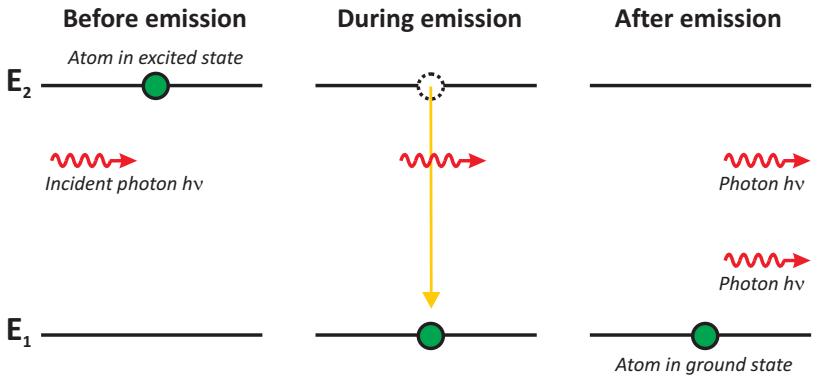

Figure 1.4: Stimulated emission amplification process.

long interaction lengths between the rare earth dopant and the pump field. Hence, a significant intracavity gain can be developed, and a small-signal gain of 25 dB is not uncommon. A small-signal gain of this magnitude enables elements with a comparatively high insertion loss, such as optical isolators, intensity modulators, and integrated interference filters, to be inserted in the cavity of a fiber laser without significantly increasing the oscillation threshold or reducing the output power.

Another inherent property of fiber lasers is the compatibility with standard single mode fibers. As the laser oscillation is actually performed in the core of an optical fiber, the output signal is efficiently coupled to another fiber. The guided mode propagation of optical fiber also allows for a reduced or suppressed thermal distortion of the optical path, and diffraction-limited, high-quality optical beams are usually generated.

Table I: Common laser-active ions, host glasses and relevant emission wavelengths.

Ion	**Common host glasses**	**Relevant emission wavelength (μm)**
Neodymium (Nd^{3+})	Silicate and phosphate glasses	1.03-1.1, 0.9-0.95, 1.32-1.35
Ytterbium (Yb^{3+})	Silicate glass	1.0-1.1
Erbium (Er^{3+})	Silicate, phosphate and fluoride glasses	1.5-1.6, 2.7, 0.55
Thulium (Tm^{3+})	Silicate, germanate and fluoride glasses	1.7-2.1, 1.45-1.53, 0.48, 0.8
Praseodymium (Pr^{3+})	Silicate and fluoride glasses	1.3, 0.635, 0.6, 0.52, 0.49
Holmium (Ho^{3+})	Silicate, and fluorozirconate glasses	2.1, 2.9

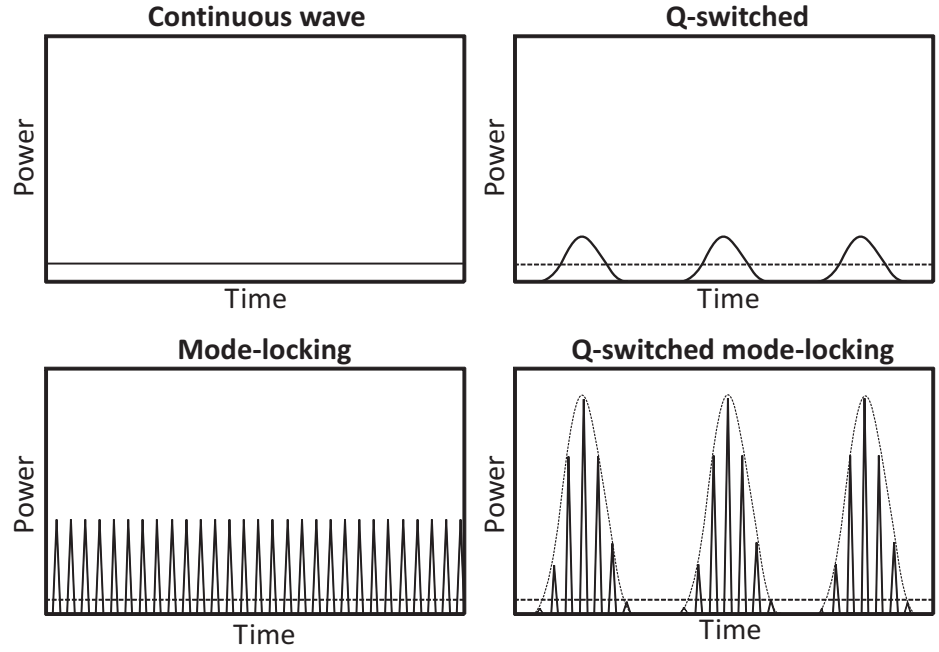

Figure 1.5: Temporal regimes of laser operations. In the pulsed regimes, the dotted lines represent the average power levels, which for comparison are equal in all four graphs [24].

Compared to gas and solid state lasers, fiber lasers are more compact as fibers can be easily bent and coiled.

In a broad sense, a fiber laser is capable of converting the poor quality output of a pump laser diode into a high-brightness coherent light. While the pumping supply is a continuous process, the output of the fiber laser can take several temporal formats, depending on the operation regime. Lasers in general can be classified, according to their temporal dynamics, into four principle modes of operation, namely continuous-wave (CW), Q-switched, mode-locked (ML) and Q-switched mode-locked (QML). The temporal characteristics of these different modes are depicted in figure 1.5. As can be seen from this graphic, a CW laser generates an output optical signal with constant power. In this case, instantaneous and average powers are equal. For the other cases of operation regimes, the emitted signal has a pulsed profile, characterized by parameters as pulse duration, frequency repetition rate, pulse energy and instantaneous peak power. In figure 1.5, the average power for the pulsed regimes is plotted, being equal for comparison in all four regimes.

Lasers with high average output power usually operate in CW mode irrespective of their specific architecture. In CW operation, lasers can run with a single longitudinal mode of the optical resonator, providing a narrow linewidth emission with good coherence, which is interesting for spectroscopy and interferometry. In other cases of CW operation, the laser can emit a signal with a broad bandwidth, suitable for fiber-optic gyroscope (FOG) applications [25].

In a Q-switched laser, the quality factor of the resonant cavity is changed with time. When the quality factor is low, the laser is unable to oscillate, and the active medium stores energy from the pump source in form of population inversion. Then, when the quality factor is deliberately enhanced, all the stored energy is released in the form of a powerful optical pulse. The upper lifetime of the active medium should be long enough to reach high energy storage rather than losing the energy as fluorescence. Depending on the way of modulating the Q factor, Q-switching is named passive or active. Typical applications of such lasers are material processing (e.g. cutting, drilling, and laser marking), pumping nonlinear frequency conversion devices, range finding, and remote sensing. This kind of lasers delivers pulses with durations of nanoseconds, and pulse energies of miliJoules. For fiber lasers, the use of multimode fibers can supply pulse energies above miliJoule level [26].

In the case of mode-locked lasers, the mechanism of pulse shaping is different from Q-switching lasers. In a laser cavity, multiple longitudinal modes can oscillate as discussed previously (see eq. (1.2)). The output of this multi-line source, when all modes oscillate independently from the others, is a composition of random phase related optical components, giving an averaged constant power output. If we are able to set a common phase reference to all longitudinal modes, the coherent sum of all longitudinal modes leads to an optical train of pulses, with a period equal to the cavity roundtrip time. Mode-locked single mode fiber lasers can deliver pulses with durations of 100 fs and energies of 3 nJ [27], only about one order of magnitude lower than the energy outputs of bulk femtosecond lasers [28]. Furthermore, single mode fiber lasers can have very low timing jitter compared with bulk lasers [29] and also the capability for a high degree of integration. Thus, in applications sensitive to timing jitter and laser size with reduced power requirements, fiber lasers hold an advantage over bulk femtosecond lasers.

This thesis studies new schemes of fiber lasers for applications in optoelectronics applications such as microwave signal processing, photonic analog-to-digital conversion, millimeter and THz optical generation and beamforming [4]. All the addressed structures are based on optical communication technologies, so the wavelength of emission will be centered at 1.55 μm. Consequently, erbium-doped fibers have been chosen as active section of the lasers to be developed. The main cavity structures studied in this thesis are continuous wave distributed feedback (DFB) fiber lasers and ring-cavity mode-locked fiber lasers. The following sections introduce these configurations.

1.2 Distributed feedback fiber lasers

As we have described previously, in addition to an active medium and a pumping process, a laser needs a feedback mechanism to allow coherent oscillation. In a distributed feedback (DFB) laser, the optical feedback is not induced by punctual mirrors

as in the case of Fabry-Pérot lasers, but it is provided from diffraction gratings. Distributed feedback has been implemented in laser diodes, quantum cascade lasers and fiber lasers. One of its most important properties is the flexibility in controlling the emission wavelength, which is dictated by the frequency-dependent reflectance of the diffraction grating.

The erbium-doped fiber Bragg grating laser was first demonstrated around 20 years ago [22] and has since found a number of potentially useful applications. It consists of a short length of high-concentration erbium-doped fiber with either two discrete Bragg grating reflectors forming a distributed Bragg reflector (DBR) structure [22] or a single phase-shifted grating forming a distributed feedback (DFB) structure [30]. Cavity length between the two Bragg gratings determines the free spectral range, and single-longitudinal-mode operation is ensured with a sufficiently short cavity in a DBR laser. To obtain single-frequency operation in a DFB laser one can either use an end reflector to change the round-trip phase shift in the cavity or introduce into the grating a single-pass optical phase shift (a local defect of the grating structure) [30, 31]. The phase shift of these DFB fiber lasers is static, and they usually operate in a continuous wave regime. However, unavoidable birefringence in DFB lasers results in the possible existence of two orthogonal polarization modes of slightly different frequency oscillating in the cavity. By controlling the degree of linear birefringence in the grating, which induces a polarization-dependent grating reflectance [32] or by inducing a birefringent phase shift in the center of the grating [33], the thresholds of each polarization mode can be controlled and hence the laser can be made to exhibit either a single polarization mode or two orthogonal polarization modes. The polarization mode thresholds can also be altered by applying twist to the laser, thus inducing circular birefringence, which under certain circumstances can be used to force single-polarization-mode operation [34]. In single-polarization-mode operation, the threshold of one of the polarization modes is never reached with practical pump powers.

The DFB fiber laser is found to be a more environmentally stable configuration than the DBR laser. Other favorable attributes of the DFB fiber laser are its small size, simplicity in design, the ability to accurately set the wavelength during manufacture, an intrinsically narrow emission linewidth, compatibility with the transmission medium, and low sensitivity of the emission frequency to temperature ($\sim$10 pm/K) compared with the semiconductor laser. Consequently, a number of potential applications of DFB lasers have been demonstrated; for example, as a coherent source to interrogate fiber-optic interferometric sensor arrays [35], as a high-resolution strain sensor [36], and as a low and high-frequency hydrophone [37, 38].

The single mode emission of DFBs with a phase shift written in the grating comes from the spectral response of the cavity. A fiber Bragg grating (FBG) is basically a periodic modulation of the refractive index of the core of an optical fiber along its longitudinal axis. Propagating light through the periodically disturbed core results in numerous Fresnel reflections, coupling co-propagating light into counter-propagating

light and vice-versa. When the wavelength of the optical signal matches the Bragg wavelength, λ_{Bragg}, all counter-propagating reflections sum constructively, reflecting the signal backwards. This frequency-selective reflectivity has a finite bandwidth, given by the length and strength of the grating [39]. An FBG behaves as a stop-band optical filter for the transmitted signal, and as a band-pass filter for the reflected signal. FBGs have found to be versatile devices not only for optical spectral filtering application [40], but e. g. for dispersion compensation [41], mode-locking stabilization [42] and sensing [39, 43] among others.

Figure 1.6 shows the scheme of a grating with a $\lambda/4$ phase shift, and its spectral transmittance. The phase shift induces a narrow-width transmission peak in the stop-band of the uniform grating. The structure can be understood as two gratings out of phase with each other, which act as a wavelength selective Fabry-Pérot resonator, allowing light at the resonance to penetrate the reflection band of the original grating. The Bragg wavelength is directly proportional to the grating period, so great flexibility in setting the wavelength emission of a DFB laser is accomplished when writing Bragg gratings. The most widespread methods to inscribe Bragg gratings in optical fibers are the two-beam interferometric method [44] and the phase mask method [45, 46], both based on the irradiation of periodic patterns of UV light upon photosensitive fibers.

One interesting feature of the DFB resonant structure is wavelength tunability. By means of adjusting the phase shift, it is possible to continuously tune the frequency of the transmission peak within the stop-band. It results in a tunable single mode emission fiber laser. This tunability has been exploited for CW fiber lasers [47] and fiber laser Q-switching mechanism [48].

1.3 Mode-locked fiber lasers

Classical solid-state mode-locked lasers, i.e., lasers based on crystals, have traditionally dominated the market, like the Ti:Sapphire and the Nd:YAG lasers. In terms of reliability and long term stability compared with the Gas lasers and Dye lasers,

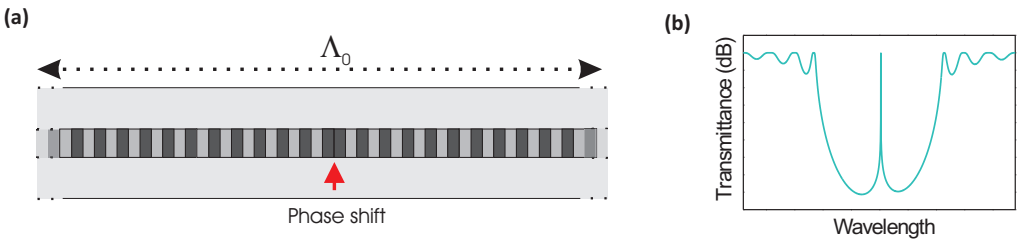

Figure 1.6: DFB cavity. (a) $\lambda/4$-Phase shifted uniform grating structure. (b) Passive transmission response of a $\lambda/4$-phase shifted uniform grating.

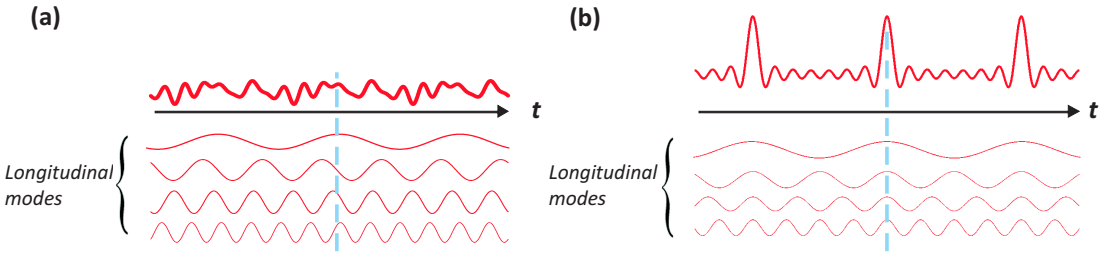

Figure 1.7: Mode locking mechanism. (a) Longitudinal oscillating modes with no shared phase reference, leading to a chaotic optical output. (b) Longitudinal oscillating modes with common phase reference or mode-locking, resulting in a pulsed optical signal.

the solid-state lasers are still the preferred choice. However, solid-state lasers require stable laboratory-like working environments such as optical table and constant room temperature. Furthermore, the solid-state lasers are really expensive and need often maintenance which is also a high consumption. The potential of making compact, cost-effective and stable fiber lasers with low price makes mode-locked fiber lasers a very promising alternative to classical solid-state lasers. High gain rare-earth doped fiber with broad gain bandwidth, excellent quality beam, optical fiber compatibility and efficient heat dissipation are some of the fiber lasers key properties.

Mode-locking operation regime has been introduced in section 1.1, among other laser regimes. It consists of the phase locking of longitudinal modes of a laser resonant cavity. In this way, the temporal summation of modes provides a pulsed pattern, with temporal period equal to the cavity roundtrip time. The higher the number of modes involved, the shorter the pulse duration is. This scenario is illustrated in figure 1.7. The concept can be associated with the Fourier decomposition of a Dirac delta comb function, where an infinite summation of sinusoids with equal phase constant results in a periodic delta train. As for Q-switching, mode-locking mechanisms are active or passive.

Active mode-locking of fiber lasers is very attractive for high-bit-rate communications systems, because active mode-locked lasers produce pulses in synchronism to a well-defined radio-frequency clock signal. The clock signal can be obtained directly from the circuitry of an optical communication network, or it can be generated by clock-recovery from an existing data stream.

A classic explanation of the principles of active mode-locking can be found in [49]. Amplitude modulation (AM) [50] and frequency modulation (FM) [51] active mode-locking are generally distinguished. In AM mode-locking the cavity loss is periodically modulated with a modulation frequency exactly matched to the fundamental frequency of the cavity or a multiple of it. In the mode-locking master equation, this modulated loss is expressed as [52]

$$L_{AM} = M\left(1 - \cos(\omega_M t)\right), \tag{1.5}$$

where M is the modulation depth and ω_M is the modulation angular frequency. A pulse can then build up synchronously thanks to the exerted modulator, being centered in the middle of the modulation temporal function and successively shortened in each roundtrip. Eventually, pulse shortening is limited by the finite gain bandwidth of the optical laser medium, and a steady-state pulse, with a width very much smaller than the modulation window, is obtained. An illustration of the modulation function and temporal steady-state pulse is given in figure 1.8 (a).

In the frequency domain it is assumed that the modulator produces sidebands to each of the oscillating axial modes at the axial mode spacing defined by the modulation frequency. An axial mode at the frequency ω_n that passes through the amplitude modulator with losses given by equation (1.5) results in three spectral components as follows:

$$\begin{aligned} & M\left[1-\cos(\omega_M t)\right]\exp(j\omega_n t) \\ & = M\left[1-\frac{1}{2}\exp(j\omega_M t)-\frac{1}{2}\exp(-j\omega_M t)\right]\exp(j\omega_n t) \\ & = M\left[\exp(j\omega_n t)-\frac{1}{2}\exp(j(\omega_n+\omega_M)t)-\frac{1}{2}\exp(j(\omega_n-\omega_M)t)\right]. \end{aligned} \tag{1.6}$$

Figure 1.8 (b) shows this sideband generation. All these new sidebands tend to lock the modes of the laser in phase. In FM mode-locking the phase, instead of the cavity losses, is modulated at a multiple of the fundamental frequency of the cavity roundtrip time, which also leads to pulses very much shorter than the modulation period. In contrast to amplitude modulation, generated sidebands are out of phase with the carrier, which leads to a chirp on the steady state pulse. Then pulse shortening in FM mode-locking comes from the gain spectral filtering of chirped pulses.

Active mode-locking is of special interest for the generation of high repetition rates, since modulation frequency can be set to a multiple of the fundamental roundtrip time of the cavity. Using cavities with fundamental roundtrips of the order of MHz, it is feasible to obtain pulse repetition rates of the order of tens of GHz [53]. For applications in telecommunications, integrated $LiNbO_3$ amplitude or phase modulators with typical bandwidths over 40 GHz are the most common active mode-lockers.

The other way to mode-lock a fiber laser is passive mode-locking. In contrast to the active case, passive mode-locking manages to phase lock the longitudinal modes of the cavity without an external reference signal. Therefore, passive mode-locking permits a reduction of the laser complexity, since there is no need for electronic synthesizers and optoelectronics modulators. Since the early works in 1991 [49, 54], traditionally two passive mode-locking techniques have been developed. We can distinguish (1) passive mode-locking with an all-optical switch based on the Kerr nonlinearity of the optical fiber, and (2) passive mode-locking with a saturable absorber.

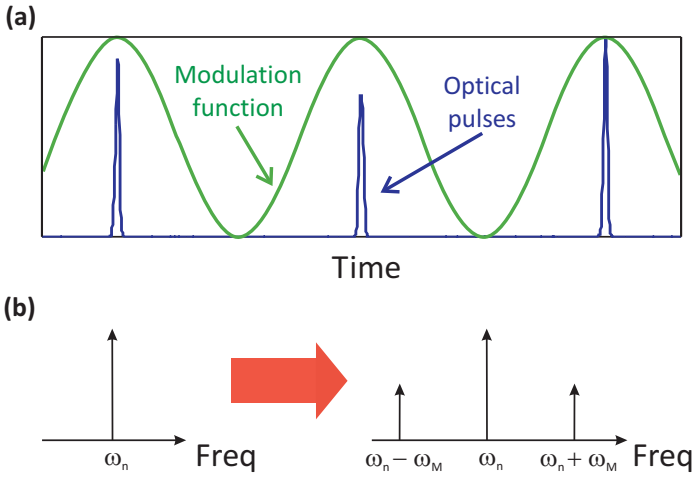

Figure 1.8: Active AM mode-locking. (a) Temporal loss modulation and pulse formation. (b) Spectral sideband generation in AM mode-locking

Kerr nonlinearity is a nonlinear effect, consisting of a change in the refractive index of the material when an external electric field is applied. It is a third order nonlinear effect, as the change of the refractive index is proportional to the square of the applied field. Basically, an intense electromagnetic field can alter its own propagation medium by changing the refractive index. The index change yields to Self Phase Modulation (SPM), or Cross Phase Modulation (XPM) (when two or more signals are involved in the interaction). Considering the state of polarization of an optical signal, Kerr effect induces Nonlinear Polarization Rotation (NLPR) [55]. Kerr passive mode-locked fiber lasers exploit NLPR to obtain pulse intensity-dependent losses [56]. An intensity-dependent loss element in the cavity allows longitudinal modes to lock in phase, in order to build up a pulsed regime in which high signal peak values are less attenuated than low level signal values. In addition, as the Kerr response is in practice an instantaneous phenomenon (in comparison with typical pulse durations), the intensity-dependent losses are not limited by a temporal response.

The use of external saturable absorbers (SA) is another approach to obtain an intensity-dependent loss element. Saturable absorber mode-locking is compatible with all-polarization-maintaining cavity designs and can produce stable pulses with no need for nonlinear effects in the cavity in comparison with NLPR mode-locking techniques. A saturable absorber is an optical element which induces decreasing losses in the cavity with increasing intensity of the incident optical signal, and can operate in reflection or transmission. The most common saturable absorber employed in mode-locked lasers is the semiconductor-based saturable absorber [57]. The semiconductor saturable absorption is related to an interband transition: the energy of absorbed photons is transferred to electrons, which are brought from the valence band to the conduction band. There is first some fairly rapid thermalization relaxation within the conduction and valence band within e.g. 50–100 fs, and later (often on a time scale of tens or hundreds of picoseconds) the carriers recombine, often with the aid of crystal defects. Other saturable absorber alternatives for fiber lasers are optical fibers

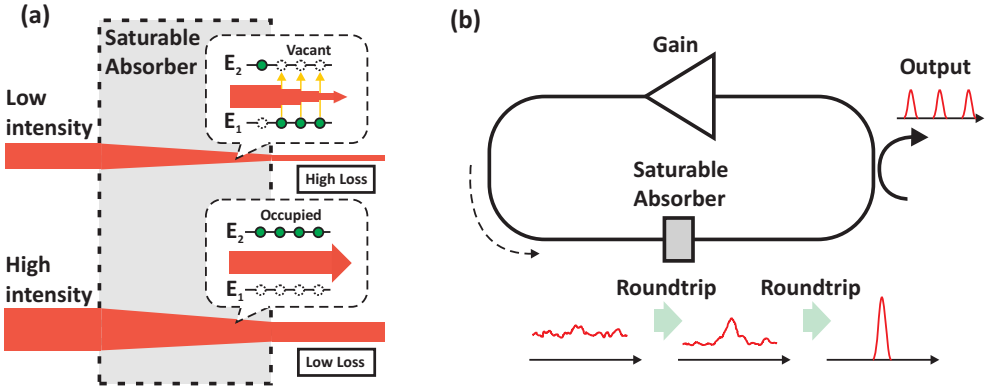

Figure 1.9: (a) Working concept of a saturable absorber. (b) Pulse shaping in a ring cavity fiber laser.

doped with chromium, samarium or bismuth [58], carbon nanotubes [59] or simply not pumped rare-earth doped fiber sections [60]. Figure 1.9 (a) shows the mechanism of a SA for a low and high incoming power. The insertion loss of a SA follows the expression

$$\alpha(t) = \frac{\alpha_0}{1 + \dfrac{|A(t)|^2}{|A_{SA}|^2}} + \alpha_{ns}, \tag{1.7}$$

where α_0 is the saturation absorption, $A(t)$ is the instantaneous amplitude of the incoming pulse, A_{SA} is the saturation amplitude of the absorber, and α_{ns} is the non-saturable absorption. This expression assumes an instantaneous response, without considering the recovery time of the absorber. In a fiber laser cavity, when the pump process is activated, amplified spontaneous noise is generated from the active medium. This noise passes through the SA, and random intensity peaks are less attenuated than lower level noise. This process is repeated each roundtrip, shaping the optical pulse, and attenuating the surrounding noise, as illustrated in figure 1.9 (b).

Nonlinear pulse propagation in optical fibers can be accurately modeled by one or more coupled partial differential equations which, for historical reasons, are called the nonlinear Schrödinger equations (NLSE) (not related to the quantum mechanical Schrödinger equation). The NLSE have been applied in fiber optics since the beginning of the eighties, where it was used to describe Mollenauer's first experimental observations of solitons in optical fibers [61]. The NLSE have also been applied in numerous other fields [62–64]. Today it is used extensively to model pulse propagation in optical fibers [65–67]. When dispersion in the NLSE has a negative sign, which corresponds to optical fibers with anomalous chromatic dispersion, NLSE yield a solution preserving its temporal and spectral profile through propagation. The invariable propagation is accomplished when nonlinear SPM balances the dispersion effects. This kind of optical signal is known as soliton.

The soliton phenomenon was first described by the naval engineer John Scott Russell, who observed a solitary wave in the Union Canal in Scotland propagating without distortion and named it the *"Wave of Translation"* [68]. His discovery aroused scientific community's interest like Lord Rayleigh, who contributed actively to the solitary wave theory. Since then, numerous works about optical solitons have been published due to their important applications in optical communications and lasers[1] [69]. In mode-locked fiber lasers, optical solitons play an important role in pulse shaping within the cavity. When the fiber cavity shows an anomalous net dispersion, then solitonic propagation is allowed. An intriguing property of optical solitons is their stability: although the initial pulse differs from the exact soliton solution, the pulse automatically evolves to the ideal soliton shape while shedding part of its energy into a weak background. Solitons are also very stable against changes of the properties of the medium, provided that these changes occur over distances which are long compared with the soliton period. This means that solitons can adiabatically adapt their shape to slowly varying parameters of the medium. Also, solitons can accommodate to some amount of higher-order dispersion; they then automatically adjust their shape to achieve the mentioned balance under the given conditions.

1.4 Objectives

The main objective of the thesis is the development of erbium-doped fiber lasers for applications in microwave photonics. The thesis is divided into two thematic blocks. On the one hand, continuous wave DFB fiber lasers are considered for microwave signal photogeneration. A high frequency sinusoid is generated in a photodetector via photomixing two optical continuous wave tones [70]. The photocurrent generated in a photodetector is proportional to the received optical power. Then, an optical signal composed of two optical tones results in a photodetected microwave signal with a frequency equal to the tones spectral separation. The thesis will focus on the design of optical sources able to emit two CW wavelengths for photomixing. Our laser will be based on a two phase-shifted DFB fiber laser. Conventional DFB with one phase shift applied to the Bragg grating emits a single longitudinal mode. When a second phase shift is added, the laser is able to emit two longitudinal modes, with a spectral separation determined by the grating response and the phase shifts characteristics. Our design also deals with dynamic tunability of the two modes spectral difference, which is transferred to a frequency tunability of the photogenerated microwave signal.

[1] Before the Russell's observation, this kind of hydrodynamic solitary waves had been already observed. Spaniard sailors found waves like these during their American conquest travels. For example, Diego de Aguirre noticed these waves in the Orinoco River mouth. The Indians who lived in the region called this phenomenon "Macareo". Previously, Vicente Yañez Pinzón (in 1500) found the same waves over the Amazonas River where native people called them "Pororoco" ("great crash" in the Tupiguaraní language). The interaction of both conquerors with the waves had the same results, the sinking of several vessels. In 1999, the Brazilian surfer Picuruta Salazar rode the "Pororoco" during 35 minutes, covering a distance of 12.5 kilometres. The "Macareo" wave at the Amazonas goes upriver and carries out its effects up to 800 Km from the river mouth.

Tunability is obtained by a control of the induced phase shifts in the grating, in such a way that phase shift values are adjusted independently. For this purpose, piezoelectric actuators are used. Our work aims for compact and simple fiber lasers, with the maximum tuning range achievable. The maximum tuning range is ultimately limited by the spectral response of the Bragg grating. Different approaches are studied to further increase the tuning range with no need for replacing the written grating.

On the other hand, pulsed fiber lasers are proposed for high-sampling-rate applications such as photonic-assisted analog to digital conversion (PADC) [71]. When the sampling process in a PADC is carried out in the photonic domain, low-temporal-noise high-repetition-rate pulsed optical sources are required. Fiber lasers can make a difference for the pulsed source implementation, as they can provide low time jitters, high pulse repetition frequencies and compact cost-effective implementations. One of the targets of the thesis is the study of different mode-locked fiber laser structures to fulfill objective specifications. Active mode-locking using commercial Mach-Zehnder modulators and passive mode-locked fiber lasers based on semiconductor saturable absorbers are designed, fabricated and characterized. The use of intracavity polarizing fibers in a ring fiber laser is explored, which will allow us to control the mode-locked operation regime dynamically through polarization state adjustment. Another solution for passive mode-locking is the use of single walled carbon nanotubes. Carbon nanotubes have shown ultrafast optical nonlinearities suitable for passive mode-locking as saturable absorber. One challenge of mode-locked fiber lasers with carbon nanotubes is the proper deposition of nanotubes in the optical fiber. The thesis also deals with the study of a new approach to deposit carbon nanotubes in optical fibers, in which tilted fiber Bragg grating are used to enable optical light to interact with the nanotubes. Ultrafast optical switching is demonstrated using a carbon nanotube-coated fiber in a phase-sensitive pump-probe experiment.

The format for this thesis is based on article compilation. Relevant articles published in specialized scientific journals elaborated by the PhD student are attached to constitute different thesis chapters. The thesis is organized as follows. Chapter 1 has presented an introduction to the fiber laser fundaments and the pursued objectives. Chapter 2 deals with tunable dual-wavelength distributed feedback fiber lasers. An initial description of the working principles precedes the two main published contributions; the first one presenting the tunable two-shifted dual-wavelength fiber laser obtained, and the second one addressing the extension of the tuning range with a cascaded DFB structure. Chapter 3 focuses on pulsed mode-locked fiber laser, in which three publications are enclosed. Different mode-locking fiber laser structures are presented for PADC applications, and an innovative use of tilted Bragg grating for light interaction with carbon nanotubes is treated. Chapter 4 presents the general discussion extracted from the results. Finally, Chapter 5 sums up the main conclusions of the thesis.

Bibliography

[1] R. Ramaswami and K. Sivarajan, *Optical Networks: A Practical Perspective*. San Francisco, CA: Morgan Kaufmann, 2001.

[2] A. Kersey, M. Davis, H. Patrick, M. LeBlanc, K. Koo, C. Askins, M. Putnam, and E. Friebele, "Fiber grating sensors," *Lightwave Technology, Journal of*, vol. 15, no. 8, pp. 1442 –1463, Aug. 1997.

[3] A. J. Seeds, "Microwave photonics," *IEEE Transactions on Microwave Theory and Techniques*, vol. 50, no. 3, pp. 877–887, Mar. 2002.

[4] J. Capmany and D. Novak, "Microwave photonics combines two worlds," *Nature Photonics*, vol. 1, pp. 319–330, 2007.

[5] A. Katzir, Ed., *Lasers and Optical Fibers in Medicine (Physical Techniques in Biology and Medicine)*. San Diego, CA: Academic Press, 1993.

[6] A. Arai, J. Xu, J. Sohn, and G. Cho, "Applications of femtosecond fiber lasers in material processing," in *Lasers and Electro-Optics Europe (CLEO EUROPE/EQEC), 2011 Conference on and 12th European Quantum Electronics Conference*, May 2011, p. 1.

[7] A. L. Schawlow and C. H. Townes, "Infrared and Optical Masers," *Physical Review*, vol. 112, pp. 1940–1949, 1958.

[8] T. H. Maiman, "Stimulated optical radiation in ruby masers," *Nature*, vol. 187, pp. 493–494, 1960.

[9] J. Hecht, *Laser pioneers*. Academic Press, 1992. [Online]. Available: http://books.google.dk/books?id=IuVRAAAAMAAJ

[10] E. Snitzer, "Proposed Fiber Cavities for Optical Masers," *Journal of Applied Physics*, vol. 32, no. 1, pp. 36–39, Jan. 1961.

[11] E. Snitzer, "Optical maser action of Nd^{+3} in a barium crown glass," *Physical Review Letters*, vol. 7, pp. 444–446, Dec. 1961.

[12] C. J. Koester and E. Snitzer, "Amplification in a fiber laser," *Applied Optics*, vol. 3, no. 10, pp. 1182–1186, Oct. 1964.

[13] G. Holst, E. Snitzer, and R. Wallace, "High-coherence high-power laser system at 1.0621 μm," *IEEE Journal of Quantum Electronics*, vol. 5, no. 6, p. 342, June 1969.

[14] J. Stone and C. Burrus, "Neodymium-doped silica lasers in end-pumped fiber geometry," *Applied Physics Letters*, vol. 23, no. 7, pp. 388 –389, Oct. 1973.

[15] J. Stone and C. A. Burrus, "Neodymium-doped fiber lasers: Room temperature cw operation with an injection laser pump," *Applied Optics*, vol. 13, no. 6, pp. 1256–1258, June 1974.

[16] M. Digonnet, C. Gaeta, and H. Shaw, "1.064- and 1.32- μm Nd:YAG single crystal fiber lasers," *Lightwave Technology, Journal of*, vol. 4, no. 4, pp. 454 – 460, Apr. 1986.

[17] S. B. Poole, J. E. Townsend, D. N. Payne, M. E. Fermann, G. J. Cowle, R. I. Laming, and P. R. Morkel, "Characterization of special fibers and fiber devices," *IEEE/OSA Journal of Lightwave Technology*, vol. 7, no. 8, pp. 1242–1255, Aug. 1989.

[18] http://www.imra.com.

[19] http://www.fianium.com.

[20] A. Tünnermann, T. Schreiber, F. Röser, A. Liem, S. Höfer, H. Zellmer, S. Nolte, and J. Limpert, "The renaissance and bright future of fibre lasers," *Journal of Physics B: Atomic, Molecular and Optical Physics*, vol. 38, no. 9, p. S681, 2005.

[21] I. Jauncey, L. Reekie, J. Townsend, C. Rowe, and D. Payne, "Single-longitudinal-mode operation of an Nd^{3+}-doped fibre laser," *Electronics Letters*, vol. 24, no. 1, pp. 24 –26, Jan. 1988.

[22] G. A. Ball, W. W. Morey, and W. H. Glenn, "Standing-wave monomode erbium fiber laser," *Photonics Technology Letters, IEEE*, vol. 3, no. 7, pp. 613–615, July 1991.

[23] A. Asseh, H. Storoy, J. Kringlebotn, W. Margulis, B. Sahlgren, S. Sandgren, R. Stubbe, and G. Edwall, "10 cm Yb^{3+} dfb fibre laser with permanent phase shifted grating," *Electronics Letters*, vol. 31, no. 12, pp. 969 –970, June 1995.

[24] A. E. H. Oehler, "Multiwave-mode-locked solid-state lasers with up to 100 GHz, applied in a novel broadband telecom source," Ph.D. dissertation, ETH, 2009.

[25] R. A. Bergh, B. Culshaw, C. C. Cutler, H. C. Lefevre, and H. J. Shaw, "Source statistics and the kerr effect in fiber-optic gyroscopes," *Optics Letters*, vol. 7, no. 11, pp. 563–565, Nov. 1982.

[26] D. Richardson, H. Offerhaus, J. Nilsson, and A. Grudinin, "New fibers portend a bright future for high-power lasers," *Laser Focus World*, vol. 35, no. 6, pp. 92–94, 1999.

[27] L. E. Nelson, S. B. Fleischer, G. Lenz, and E. P. Ippen, "Efficient frequency doubling of a femtosecond fiber laser," *Optics Letters*, vol. 21, no. 21, pp. 1759–1761, Nov. 1996.

[28] K. Lamb, D. E. Spence, J. Hong, C. Yelland, and W. Sibbett, "All-solid-state self-mode-locked Ti:sapphire laser," *Optics Letters*, vol. 19, no. 22, pp. 1864–1866, Nov. 1994.

[29] F. Haberl, M. Ober, M. Hofer, M. Fermann, E. Wintner, and A. Schmidt, "Low-noise operation modes of a passively mode-locked fiber laser," *Photonics Technology Letters, IEEE*, vol. 3, no. 12, pp. 1071 –1073, Dec. 1991.

[30] J. T. Kringlebotn, J. L. Archambault, L. Reekie, and D. N. Payne, "Er^{3+}:Yb^{3+} codoped fiber distributed-feedback laser," *Optics Letters*, vol. 19, no. 24, pp. 2101–2103, 1994.

[31] W. H. Loh and R. I. Laming, "1.55 μm phase-shifted distributed feedback fibre laser," *Electronics Letters*, vol. 31, no. 17, pp. 1440–1442, 1995.

[32] M. Ibsen, E. Ronnekieiv, G. Cowle, M. Berendt, O. Hadeler, M. Zervas, and R. Laming, "Robust high power (>20 mW) all-fibre DFB lasers with unidirectional and truly single polarisation outputs," in *Lasers and Electro-Optics, 1999. CLEO '99. Summaries of Papers Presented at the Conference on*, May 1999, pp. 245 –246.

[33] J. Philipsen, M. Berendt, P. Varming, V. Lauridsen, J. Povlsen, J. Hubner, M. Kristensen, and B. Palsdottir, "Polarisation control of DFB fibre laser using UV-induced birefringent phase-shift," *Electronics Letters*, vol. 34, no. 7, pp. 678 –679, Apr. 1998.

[34] Z. Harutjunian, W. Loh, R. Laming, and D. Payne, "Single polarisation twisted distributed feedback fibre laser," *Electronics Letters*, vol. 32, no. 4, p. 346, Feb. 1996.

[35] G. A. Cranch, "Frequency noise reduction in erbium-doped fiber distributed-feedback lasers by electronic feedback," *Optics Letters*, vol. 27, no. 13, pp. 1114–1116, July 2002.

[36] K. Koo and A. Kersey, "Bragg grating-based laser sensors systems with interferometric interrogation and wavelength division multiplexing," *Lightwave Technology, Journal of*, vol. 13, no. 7, pp. 1243 –1249, July 1995.

[37] D. J. Hill, P. J. Nash, D. A. Jackson, D. J. Webb, S. F. O'Neill, I. Bennion, and L. Zhang, "Fiber laser hydrophone array," M. A. Marcus and B. Culshaw, Eds., vol. 3860, no. 1. SPIE, 1999, pp. 55–66.

[38] D. Thingbø, E. Rønnekleiv, J. Thomas, and J. T. Kringlebotn, "Intrinsic distributed feedback fibre laser high frequency hydrophone," in *Bragg Gratings,*

Photosensitivity, and Poling in Glass Waveguides. Optical Society of America, 1999, p. AC6.

[39] A. Othonos and K. Kalli, *Fiber Bragg Gratings: Fundamentals and Applications in Telecommunications and Sensing*. Boston-London: Artech House, 1999.

[40] I. Baumann, J. Seifert, W. Nowak, and M. Sauer, "Compact all-fiber add-drop-multiplexer using fiber Bragg gratings," *Photonics Technology Letters, IEEE*, vol. 8, no. 10, pp. 1331 –1333, Oct. 1996.

[41] K. O. Hill, F. Bilodeau, B. Malo, T. Kitagawa, S. Thériault, D. C. Johnson, J. Albert, and K. Takiguchi, "Chirped in-fiber Bragg gratings for compensation of optical-fiber dispersion," *Optics Letters*, vol. 19, no. 17, pp. 1314–1316, Sept. 1994.

[42] D. Turchinovich, X. Liu, and J. Lægsgaard, "Monolithic all-PM femtosecond Yb-fiber laser stabilized with a narrow-band fiber Bragg grating and pulse-compressed in a hollow-core photonic crystal fiber," *Optics Express*, vol. 16, no. 18, pp. 14 004–14 014, Sept. 2008.

[43] J. Albert, "Tilted fiber Bragg gratings as multi-sensors," *Optics and Photonics News*, vol. 22, no. 10, pp. 28–33, Oct. 2011.

[44] G. Meltz, W. W. Morey, and W. H. Glenn, "Formation of Bragg gratings in optical fibers by a transverse holographic method," *Optics Letters*, vol. 14, no. 15, pp. 823–825, Aug. 1989.

[45] K. O. Hill, B. Malo, F. Bilodeau, D. C. Johnson, and J. Albert, "Bragg gratings fabricated in monomode photosensitive optical fiber by UV exposure through a phase mask," *Applied Physics Letters*, vol. 62, no. 10, pp. 1035–1037, Mar. 1993.

[46] D. Z. Anderson, V. Mizrahi, T. Erdogan, and A. E. White, "Production of in-fibre gratings using a diffractive optical element," *Electronics Letters*, vol. 29, no. 6, pp. 566–568, 1993.

[47] H. Yoon, K. M. Cho, S. B. Lee, S. S. Choi, and D. Park, "Tunable Er^{3+}-doped fiber distributed-feedback laser," in *Lasers and Electro-Optics Society 2000 Annual Meeting. LEOS 2000. 13th Annual Meeting. IEEE*, vol. 2, 2000, pp. 401 –402 vol.2.

[48] P. Pérez-Millán, J. L. Cruz, and M. V. Andrés, "Active Q-switched distributed feedback erbium-doped fiber lasers," *Applied Physics Letters*, vol. 87, no. 1, p. art. no. 011104, July 2005.

[49] M. E. Fermann, M. Hofer, F. Haberl, A. J. Schmidt, and L. Turi, "Additive-pulse-compression mode locking of a neodymium fiber laser," *Optics Letters*, vol. 16, no. 4, pp. 244–246, Feb. 1991.

[50] J. D. Kafka, T. Baer, and D. W. Hall, "Mode-locked erbium-doped fiber laser with soliton pulse shaping," *Optics Letters*, vol. 14, no. 22, pp. 1269–1271, Nov. 1989.

[51] M. W. Phillips, A. I. Ferguson, and D. C. Hanna, "Frequency-modulation mode locking of a Nd^{3+}-doped fiber laser," *Optics Letters*, vol. 14, no. 4, pp. 219–221, Feb. 1989.

[52] H. Haus, "A theory of forced mode locking," *Quantum Electronics, IEEE Journal of*, vol. 11, no. 7, pp. 323 –330, Jul. 1975.

[53] L. Schares, R. Paschotta, L. Occhi, and G. Guekos, "40-GHz mode-locked fiber-ring laser using a Mach-Zehnder interferometer with integrated SOAs," *Lightwave Technology, Journal of*, vol. 22, no. 3, p. 859, Mar. 2004.

[54] I. N. Duling, "All-fiber ring soliton laser mode locked with a nonlinear mirror," *Optics Letters*, vol. 16, no. 8, pp. 539–541, Apr. 1991.

[55] R. W. Boyd, *Nonlinear Optics, Third Edition*, 3rd ed. Academic Press, Apr. 2008.

[56] V. Matsas, T. Newson, D. Richardson, and D. Payne, "Selfstarting passively mode-locked fibre ring soliton laser exploiting nonlinear polarisation rotation," *Electronics Letters*, vol. 28, no. 15, pp. 1391 –1393, Jul. 1992.

[57] U. Keller, K. Weingarten, F. Kartner, D. Kopf, B. Braun, I. Jung, R. Fluck, C. Honninger, N. Matuschek, and J. Aus der Au, "Semiconductor saturable absorber mirrors (SESAM's) for femtosecond to nanosecond pulse generation in solid-state lasers," *Selected Topics in Quantum Electronics, IEEE Journal of*, vol. 2, no. 3, pp. 435 –453, Sept. 1996.

[58] V. V. Dvoyrin, V. M. Mashinsky, and E. M. Dianov, "Yb-Bi pulsed fiber lasers," *Optics Letters*, vol. 32, no. 5, pp. 451–453, Mar. 2007.

[59] S. Yamashita, "A tutorial on nonlinear photonic applications of carbon nanotube and graphene," *Lightwave Technology, Journal of*, vol. 30, no. 4, pp. 427 –447, Feb. 2012.

[60] S. Colin, E. Contesse, P. Le-Boudec, G. Stephan, and F. Sanchez, "Evidence of a saturable-absorption effect in heavily erbium-doped fibers," *Optics Letters*, vol. 21, no. 24, pp. 1987–1989, Dec. 1996.

[61] L. F. Mollenauer, R. H. Stolen, and J. P. Gordon, "Experimental observation of picosecond pulse narrowing and solitons in optical fibers," *Physical Review Letters*, vol. 45, pp. 1095–1098, Sept. 1980.

[62] T. R. Taha and M. I. Ablowitz, "Analytical and numerical aspects of certain nonlinear evolution equations. II. Numerical, nonlinear Schrödinger equation," *Journal of Computational Physics*, vol. 55, no. 2, pp. 203 – 230, 1984.

[63] N. Yajima, M. Oikawa, J. Satsuma, and C. Namba, "Modulated Langmuir waves and nonlinear Landau damping," *Journal of the Physical Society of Japan*, vol. 45, no. 2, pp. 643–651, 1978.

[64] K. E. Strecker, G. B. Patridge, A. G. Truscott, and R. G. Hulet, "Formation and propagation of matter-wave soliton trains," *Nature*, vol. 417, pp. 150–153, 2002.

[65] J. Limpert, T. Schreiber, T. Clausnitzer, K. Zöllner, H. Fuchs, E. Kley, H. Zellmer, and A. Tünnermann, "High-power femtosecond Yb-doped fiber amplifier," *Optics Express*, vol. 10, no. 14, pp. 628–638, July 2002.

[66] F. O. Ilday, J. R. Buckley, W. G. Clark, and F. W. Wise, "Self-similar evolution of parabolic pulses in a laser," *Physical Review Letters*, vol. 92, p. 213902, May 2004.

[67] T. Geisler, K. A. Shore, M. P. Soerensen, P. L. Christiansen, J. Mørk, and J. Mark, "Nonlinear fiber external cavity mode locking of erbium-doped fiber lasers," *Journal of the Optical Society of America B*, vol. 10, no. 7, pp. 1166–1174, July 1993.

[68] J. Russell, *Report on waves: made to the meetings of the British Association in 1842-43*, 1845.

[69] A. Hasegawa, "Optical soliton theory and its applications in communication," in *Optical Solitons*, ser. Lecture Notes in Physics, K. Porsezian and V. Kuriakose, Eds. Springer Berlin / Heidelberg, 2003, vol. 613, pp. 9–31.

[70] A. Garcia-Juarez, C. Gutierrez-Martinez, A. Torrez-Fortiz, and J. Meza-Perez, "Photomixing of two laser diodes for generating tunable microwave signals (1- to 25-GHz) with applications to high-speed telecommunication systems," A. M. O. and J. L. Paz, Eds., vol. 5622, no. 1. SPIE, 2004, pp. 917–921.

[71] G. C. Valley, "Photonic analog-to-digital converters," *Optics Express*, vol. 15, no. 5, pp. 1955–1982, Mar. 2007.

Chapter 2

Dual-wavelength distributed feedback fiber lasers

2.1 Introduction

The laser oscillator proposed for the microwave photogenerated signal system is a distributed feedback (DFB) fiber laser. The fiber laser consists of a Bragg grating UV-written into a piece of silica fiber doped with active rare-earth ions. In section 1.2, the fundamentals of DFB fiber lasers were introduced, showing how this kind of structures can be used to build lasers with short cavities of few centimetres long. DFB fiber lasers are intrinsically continuous wave (CW) sources of single-longitudinal-mode emission. Single frequency lasers are required for a wide range of applications in optical communications (such as wavelength-division multiplexing and CATV) [1, 2], lidar [3], fiber-optic sensors and spectroscopy [4]. To obtain single-frequency operation of a DFB laser one can either use an end reflector to change the round-trip phase shift in the cavity or introduce a single-pass optical phase shift in the grating (a local defect of the grating structure) [5, 6]. In this chapter we will study the application of DFB lasers in microwave signal generation. For this purpose, a DFB fiber laser able to emit two longitudinal modes is implemented.

The dual longitudinal mode emission comes from the application of two local phase shifts in the fiber grating. The insertion of phase shifts in the optical grating is performed by stretching short sections of the fiber grating through piezoelectric actuators. This technique provides a greater versatility than fixed phase shifts induced in the grating writing process [7, 8]. Control of the driving voltage of the piezoelectric actuators allows direct tuning of the optical frequency separation between the two emitted modes, thus making possible the tunability of the photomixed microwave signal. The maximum achievable microwave frequency is limited by the Bragg stopband bandwidth, usually below 10 GHz for typical uniform gratings. In this chapter, we also present an alternative technique to further extend the maximum photogenerated

frequency beyond the stopband bandwidth.

2.2 Dual-wavelength distributed feedback fiber laser

The operation principle of our dual-wavelength fiber laser is based on the application of two phase shifts in the grating written in a rare earth doped fiber. To better understand this concept, firstly the basics of conventional DFB with only one phase shift are explained. The generalized expression of the index modulation $\Delta n_{eff}(z)$ of a fiber Bragg grating is

$$\Delta n_{eff}(z) = \Delta n(z) \left(1 + \cos\left(\frac{2\pi}{\Lambda(z)} z + \phi(z)\right)\right), \tag{2.1}$$

where $\Delta n(z)$ is the refractive index modulation amplitude, $\Lambda(z)$ is the grating period and $\phi(z)$ is the phase of the periodical structure. The simplest grating design is known as uniform grating, and it involves the parameters $\Delta n(z)$, $\Lambda(z)$ and $\phi(z)$ to be z-independent. Different grating designs depend on the control of these parameters, and interesting spectral responses are exploited from, e. g., chirped gratings, where the grating period is linearly increased with z, apodized gratings, in which the modulation amplitude follows a particular profile to shape the spectral response, and so on [9]. One fundamental parameter in fiber Bragg gratings is the resonant Bragg wavelength, which is determined by the grating period through

$$\lambda_{Bragg} = 2 n_{eff} \Lambda, \tag{2.2}$$

being n_{eff} the effective index of the core mode. For grating responses centered at 1.5 μm, typical values of grating periods are about 540 nm, for an effective index of 1.44.

For a DFB laser in which a phase shift is induced in the grating, the $\phi(z)$ parameter takes the form

$$\phi(z) = \begin{cases} 0, & z < z_0 \\ \phi_0, & z \geq z_0 \end{cases} . \tag{2.3}$$

Equation (2.3) establishes a local phase change in the point $z = z_0$ of ϕ_0 radians. The discrete phase shift changes the resonance conditions in the cavity, creating a narrow transmission peak in the Bragg stop-band of the uniform grating (see figure 1.6 on page 10). The transmission peak response can be understood as a Fabry-Pérot cavity with FBGs as reflective mirrors. Figure 2.1 (a) illustrates this approach. In

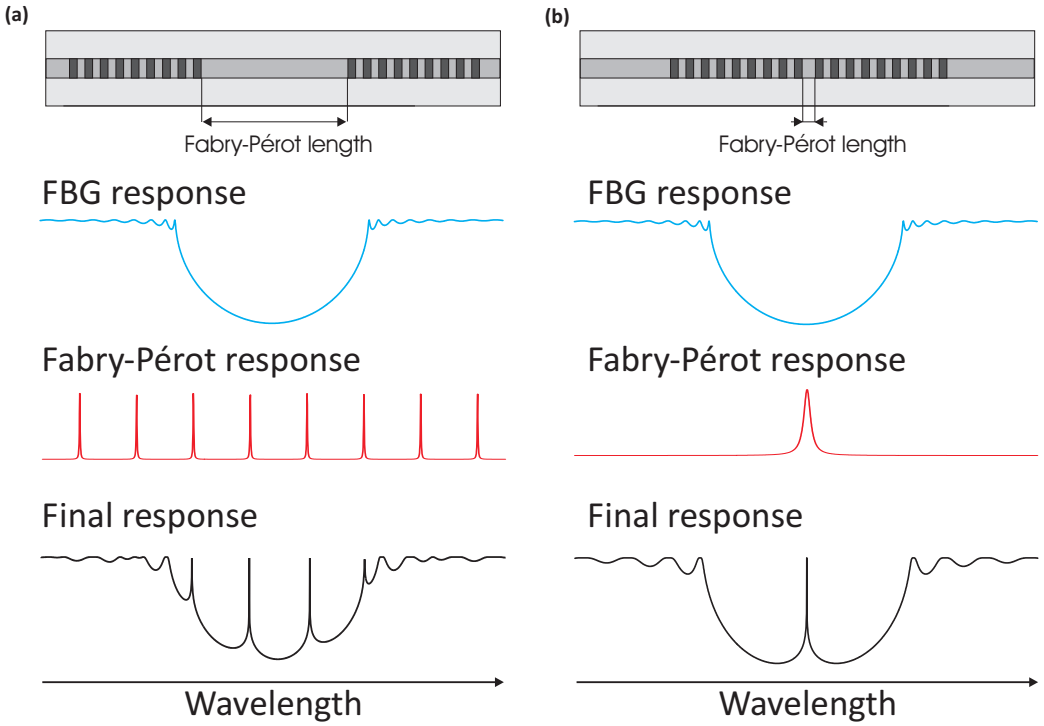

Figure 2.1: Fabry-Pérot fiber cavities with FBG mirrors for (a) long separation between mirrors and (b) short separation between mirrors. Transmission spectral responses of gratings, Fabry-Pérot cavities and resulting final structure are shown.

addition to the inherent multi-wavelength response defined by the Fabry-Pérot cavity length (see equations (1.1) and (1.3) on page 3), the FBG mirrors produce a reflective frequency-dependent response. Figure 2.1 (a) shows how both spectral responses combine to perform an overall passive response of multiple transmission wavelengths within the FBG transmission spectral stopband. When pumped, this fiber laser will be able to emit longitudinal modes in these transmission wavelengths. If we reduce the cavity length, i. e., the distance between gratings, the free spectral range of the Fabry-Pérot response increases, while FBG stopband response keeps unaltered. For a certain separation, the FSR is such that only one Fabry-Pérot resonance falls into the FBG response. This single longitudinal mode cavity is the so-called distributed Bragg reflector (DBR) laser. If we keep bringing closer both gratings, up to a distance comparable to the FBG period Λ_0, then a distributed feedback cavity is obtained, since this small distance between gratings is equivalent to a phase shift induced in a single grating, as equation (2.3) describes. The spectral response of both FBG mirrors and Fabry-Pérot cavity, as well as the overall response are shown in figure 2.1 (b). Indeed, the optical fiber cavity with the two FBGs mirrors close enough can be seen as a single FBG with a phase shift in the middle point.

In DFB cavities, the resonance occurs when the round-trip phase shift of the wave travelling through the grating is equal to 2π. The wavelength of the resonance is equal to the one which satisfies the relation

$$2\varphi_{FBG} + 2\varphi = 2\pi, \tag{2.4}$$

where φ_{FBG} is the phase of the FBG complex reflectance $r(\lambda)$, being $r(\lambda) = |r(\lambda)| \exp(\varphi_{FBG}(\lambda))$, while φ is the phase shift introduced to the travelling waves by the spatial phase shift: $\varphi = \phi_0/2$. Different values of the spatial phase shift set the resonance wavelength in different spectral position within the FBG stopband bandwidth. The narrow transmission peak has been exploited in filtering applications [10] and fabricating DFB lasers [5,6]. If the phase shift is tuned somehow, the resonance wavelength can be controlled, having been exploited for CW fiber lasers [11] and fiber laser Q-switching mechanism [12].

The passive responses of FBGs are calculated using the Transfer Matrix Method (TMM) [13]: a given fiber Bragg grating is divided into short sections which can be locally considered as uniform gratings. TMM makes use of these unit cells, each having its own response in form of a transfer matrix. The transfer matrix of a device relates the co- and counter-propagating fields at the output with the co- and counter-propagation input fields. When multiple devices are connected in cascade, the transfer matrix definition allows the total response to be calculated as a simple multiplication of the devices' matrixes. In the case of optical gratings, the final transfer matrix is obtained from the multiplication of individual transfer matrixes of uniform sections. The expression of the transfer matrix of a uniform grating can be calculated using the coupled-mode theory [9]. An example of the TMM application is the modelling of a chirped Bragg grating, in which the main grating is divided into small uniform sections with monotonically increasing grating periods.

Two resonances appear in a fiber Bragg grating when two phase shifts are applied. This two transmission peak operation, from now referred as dual-wavelength, is an extension of the phenomenon occurring with one single phase shift. The inclusion of two or more phase shifts allows the resonances to appear in two or more frequencies [14, 15]. Figure 2.2 shows a grating with two phase shifts. Similar to the conventional DFB structure, the spectral position of the transmission peaks is conditioned to the phase shifts values. Also the transmission peak shapes, in terms of linewidth and amplitude, are dependent on the phase shifts spatial positions. In order to get symmetrical peaks, the phase shifts are applied equidistant to the grating centre. For two π-phase shifts, the frequency separation between modes is [16]

$$\Delta\lambda = \frac{\lambda^2}{8n_{eff}\left(\Delta L + \frac{\pi}{2\kappa}\right)}, \tag{2.5}$$

in which n_{eff} is the effective refractive index, ΔL is the separation between phase shifts and κ is the FBG coupling coefficient. Other dual-wavelength fiber laser cavity structures have been proposed [8, 14, 17, 18], where the spacing between lasing wavelengths is fixed. The key innovation of our work is the implementation of a dynamic

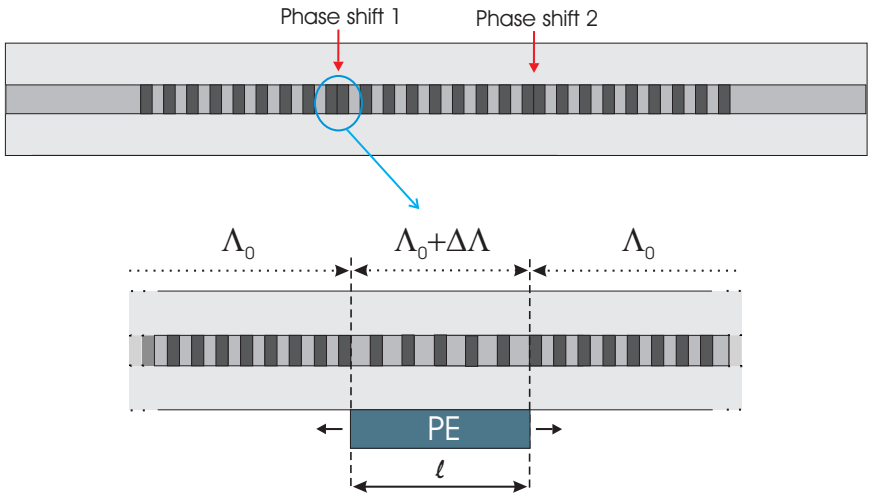

Figure 2.2: Dual-wavelength DFB cavity. Two $\pi/2$ phase shifts are applied to a uniform fiber Bragg grating (up). In practice, the phase shift is induced by a piezoelectric actuator (PE) glued to the fiber, producing an accumulated phase shift by stretching a short fiber section of length l (down).

control of these phase shifts to effectively tune the spectral separation between the two transmission peaks, hence to effectively tune the spectral separation of the laser emission wavelengths.

Simulations of passive transmission response for two phase-shifted gratings provide us with spectral resonance characterization. Real phase shifts induced in gratings are not ideally discrete as equation (2.3) represents. Particularly, the local phase shifts of our dual-wavelength DFB fiber laser are performed via piezoelectric actuators glued to the fiber, as figure 2.2 illustrates. Then, each phase shift is equivalent to a short section of grating with a slightly different grating period. Therefore, the length of this short section and the difference in the grating period determine the accumulated phase shift. This value is related to the modified period and the length of the perturbed section following the equation

$$\phi = 2\pi \left(\frac{\Delta\Lambda}{(\Lambda_0 + \Delta\Lambda)\Lambda_0} \right) l, \tag{2.6}$$

where Λ_0 is the original grating period, $\Delta\Lambda$ is the period variation and l is the length of the perturbed fiber section. This accumulated phase shift model is used in the passive response calculations to properly simulate our fiber laser.

The next step is the calculation of transmission spectral responses for different values of the phase shifts. We observed that a symmetrical wavelength displacement of both transmission peaks from the Bragg wavelength occurs under a symmetric change of phase shift around $\pi/2$ radians. In other words, when the phase shifts have a value of $\pi/2 \pm \Delta\phi$, then the wavelengths of the transmission peaks separate symmetrically from each other with respect to the Bragg wavelength of the FBG and

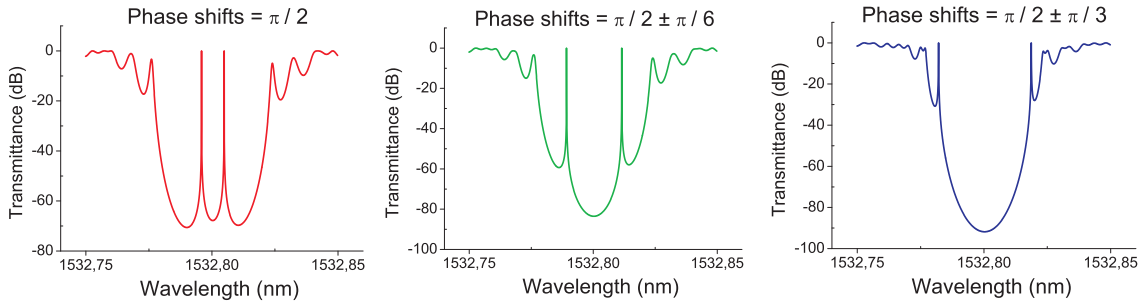

Figure 2.3: Transmission spectral responses of a dual-wavelength DFB cavity with phase shift values of $\pi/2$, $\pi/2 \pm \pi/6$, and $\pi/2 \pm \pi/3$.

the transmission peaks are equivalent in terms of amplitude and linewidth. Figure 2.3 shows the transmission response of a dual-wavelength DFB cavity for different values of grating phase shifts obeying the symmetry $\pi/2 \pm \Delta\phi$. For the simulations of figure 2.3, the grating length was 15 cm, the index modulation $5 * 10^{-5}$, the grating period 529.3 nm and the effective length of both phase shifts 1.5 mm.

Local phase shifts in the grating fiber are induced by piezoelectric actuators as discussed above. Piezoelectric materials exhibit internal generation of a mechanical strain resulting from an applied electrical field. The actuators used in our laser are plumbum (lead) zirconate titanate (PZT) ceramic components, and they are controlled by DC voltages of 0-100 Volts. In order to apply punctual phase shifts in a fiber grating, actuators with 2x2x2 mm dimensions are employed. When one of these PZT actuators is glued to the optical fiber, we are able to induce a grating phase shift by stretching the 2mm fiber short section. A maximum stretching displacement of 2.2 μm is obtained in the piezoelectric axis of the PZT cube. The new grating period induced in the short stretched length is obtained from the relation

$$\frac{l_0}{\Lambda_0} = \frac{l_0 + \Delta l}{\Lambda_0 + \Delta\Lambda}, \tag{2.7}$$

where l_0 is the PZT actuator length, Δl is the piezoelectric displacement, Λ_0 is the original grating period and $\Delta\Lambda$ the grating period variation. For the PZT values given above, and a grating original period of 529.3 nm, a grating variation of 0.58 nm is obtained. Turning to equation (2.6), the PZT actuator is able to induce a maximum accumulated phase shift of 8.3π radians, much more than enough for our purposes.

The dual-wavelength fiber laser with the cavity of figure 2.2 emits two single longitudinal modes at the transmission peaks of the passive response when the pumping level exceeds lasing threshold. Effective tunability of the spectral difference between modes is achieved through the control of both PZT actuators. The optical output is launched to a photodiode to generate a microwave signal with a frequency equal to the mode frequency difference. From figure 2.3, the maximum microwave frequency that can be achieved is limited by the grating stopband width, which ranges tens of pm.

The bandwidth of uniform gratings can be increased by shortening the total length for weakly modulated gratings, or inducing deeper change in the refractive index modulation for strongly modulated gratings. Nevertheless, a short weakly modulated grating with phase shifts results in wider transmission peaks which deteriorates the lasing mode linewidth. On the other hand, the maximum refractive index modulation is determined by the capacity of inducing changes of the refractive index, which depends fundamentally on the fiber photosensitivity and on the diffraction efficiency of the phase mask utilized for the inscribing process.

In order to extend the maximum frequency of the photogenerated microwave signal, a new approach is considered in this thesis. It is based on the implementation of two in-line DFB cavities in the same grating.

2.3 Cascaded distributed feedback dual-wavelength fiber laser

We have seen in the previous section the operation principle of our dual-wavelength DFB fiber laser with two controllable phase shifts, and how it exhibits a maximum output frequency difference between modes limited by the grating spectral response. Modifications of the uniform grating design can increase the grating bandwidth to a limited extent. In this section, a new structure based on DFB cavities is proposed to raise significantly the generated microwave signal tuning range.

The idea is the implementation of two single frequency DFB cavities in the same erbium-doped fiber, in the same fiber Bragg grating. Each DFB cavity will emit a single longitudinal mode. The emission frequency of each longitudinal mode is defined by the grating period and the magnitude of the phase shift. The challenge comes up from the use of a single grating for both cavities. The new structure consists of two fiber grating sections, each one with a different period and with an induced phase shift. Both the grating periods and the induced phase shifts are controlled by a simple setup of piezoelectric actuators. Figure 2.4 depicts the cavity scheme. The first DFB cavity has a grating period of Λ_1, which is equal to the original grating period written in the fiber. The second DFB period Λ_2 is slightly larger than Λ_1, and it originates from stretching the second half of the fiber grating. Each section of fiber grating has its own phase shift to constitute single mode DFB cavities. In the structure proposed in figure 2.4, the new grating period Λ_2 has to be large enough to not show overlapping in the spectral FBG responses.

This new approach could be considered as a modified version of the dual-wavelength cavity presented in section 2.2, but the physical concept is quite different. In this approach, as shown in figure 2.4, the system is clearly equivalent to two DFB cavities, each tuned to different wavelength given by their grating period. On the other hand, the previous structure of a single FBG presenting two phase shifts acts as a single

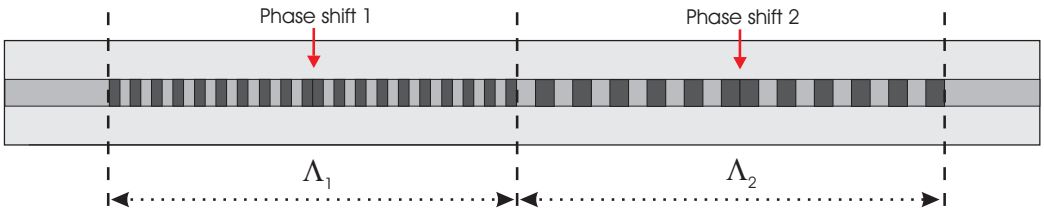

Figure 2.4: Two DFB cavities of different grating period in the same optical fiber.

cavity, where the two resonances are under the influence of each other. It is demonstrated by varying only one phase shift of the previous structure, as it affects to both resonances, in contrast to the two cascaded DFB cavities scheme of figure 2.4.

With the proposed structure, two DFB cavities lasing at different wavelengths are implemented using a single fiber Bragg grating. Figure 2.5 shows the calculated passive response of the cascaded phase-shifted gratings. The grating section with a higher grating period shows its spectral stopband centered at longer wavelengths. A narrow transmission peak appears in each stopband due to the grating phase shifts. In our laser setup, the half grating stretching as well as both local phase shifts are induced by PZT actuators, allowing a complete control on them. Other authors have proposed similar structures to achieve dual-wavelength optical emission. In reference [19] two different gratings written in the same fiber are used to induce two DFB cavities, and tunability of the modes frequency difference is demonstrated by heating up one of the DFB lasers. In comparison to our option, the work in [19] is based on writing two different gratings in the same fiber, and the tuning mechanism is thermal, with a much slower response than the PZT response. Other works employ more complicated fiber gratings than uniform gratings to reach dual-wavelength emission [7, 8], being the emission wavelengths fixed, without any tuning mechanism integrated in the laser.

The maximum wavelength separation reachable with the proposed scheme ranges hundreds of pm, which corresponds to photodetected signal frequencies of tens of GHz.

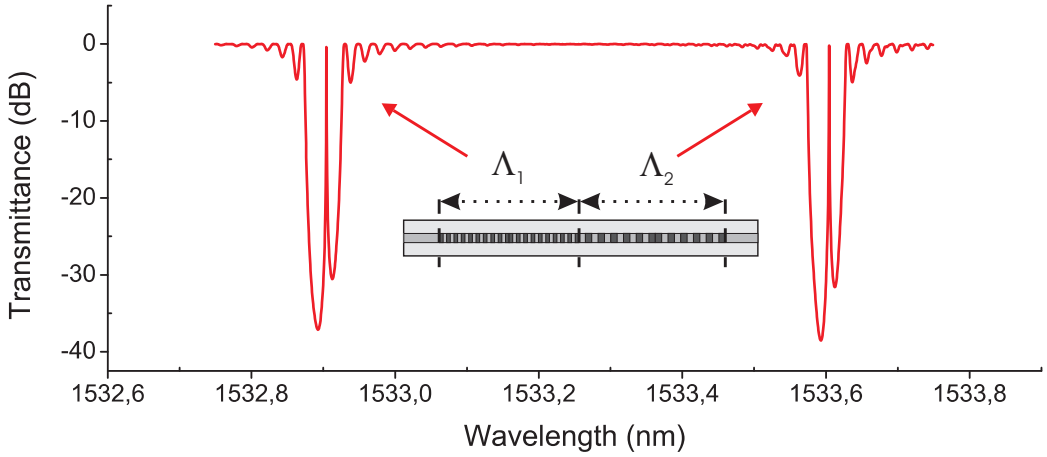

Figure 2.5: Spectral transmission response of two phase-shifted gratings with periods Λ_1 and Λ_2.

Such high frequencies signals have been measured in this thesis by means of external harmonic mixing in conjunction with the electrical spectrum analyzer. Spectra of up to 75 GHz photogenerated signals have been captured. Optical linewidths were also measured via Brillouin back-scattering amplification [20].

Bibliography

[1] N. Libatique, L. Wang, and R. Jain, "Single-longitudinal-mode tunable WDM-channel-selectable fiber laser," *Optics Express*, vol. 10, no. 25, pp. 1503–1507, Dec. 2002.

[2] C. C. Lee, Y. K. Chen, and S. K. Liaw, "Single-longitudinal-mode fiber laser with a passive multiple-ring cavity and its application for video transmission," *Optics Letters*, vol. 23, no. 5, pp. 358–360, Mar. 1998.

[3] K. Scholle, E. Heumann, and G. Huber, "Single mode Tm and Tm,Ho:LuAG lasers for LIDAR applications," *Laser Physics Letters*, vol. 1, no. 6, pp. 285–290, 2004.

[4] A. Astakhova, T. Danilova, A. Imenkov, N. Kolchanova, and Y. Yakovlev, "Single-mode fast-tunable lasers for laser-diode spectroscopy," *Semiconductors*, vol. 37, pp. 960–970, 2003.

[5] J. T. Kringlebotn, J. L. Archambault, L. Reekie, and D. N. Payne, "Er^{3+}:Yb^{3+} codoped fiber distributed-feedback laser," *Optics Letters*, vol. 19, no. 24, pp. 2101–2103, 1994.

[6] W. H. Loh and R. I. Laming, "1.55 μm phase-shifted distributed feedback fibre laser," *Electronics Letters*, vol. 31, no. 17, pp. 1440–1442, 1995.

[7] L. Jia, Z. Yin, L. Zhang, and X. Chen, "Dual-wavelength distributed feedback fiber laser based on double exposure and equivalent phase shift method," *Applied Optics*, vol. 50, no. 4, pp. 604–607, Feb. 2011.

[8] J. Sun, Y. Dai, X. Chen, Y. Zhang, and S. Xie, "Stable dual-wavelength DFB fiber laser with separate resonant cavities and its application in tunable microwave generation," *Photonics Technology Letters, IEEE*, vol. 18, no. 24, pp. 2587–2589, Dec. 2006.

[9] T. Erdogan, "Fiber grating spectra," *IEEE/OSA Journal of Lightwave Technology*, vol. 15, no. 8, pp. 1277–1294, Aug. 1997.

[10] J. Palací, P. Pérez-Millán, G. E. Villanueva, J. L. Cruz, M. V. Andrés, J. Martí, and B. Vidal, "Tunable photonic microwave filter with single bandpass based

on a phase-shifted fiber Bragg grating," *Photonics Technology Letters, IEEE*, vol. 22, no. 19, pp. 1467 –1469, Oct. 2010.

[11] H. Yoon, K. M. Cho, S. B. Lee, S. S. Choi, and D. Park, "Tunable Er^{3+}-doped fiber distributed-feedback laser," in *Lasers and Electro-Optics Society 2000 Annual Meeting. LEOS 2000. 13th Annual Meeting. IEEE*, vol. 2, 2000, pp. 401 –402 vol.2.

[12] P. Pérez-Millán, J. L. Cruz, and M. V. Andrés, "Active Q-switched distributed feedback erbium-doped fiber lasers," *Applied Physics Letters*, vol. 87, no. 1, p. art. no. 011104, July 2005.

[13] M. Born and E. Wolf, *Principles of Optics*. New York: Pergamon, 1980.

[14] Y. Dai, X. Chen, J. Sun, Y. Yao, and S. Xie, "Dual-Wavelength DFB fiber laser based on a chirped structure and the equivalent phase shift method," *Photonics Technology Letters, IEEE*, vol. 18, no. 18, pp. 1964–1966, Sept. 2006.

[15] S. Lovseth and D. Stepanov, "Analysis of multiple wavelength DFB fiber lasers," *Quantum Electronics, IEEE Journal of*, vol. 37, no. 6, pp. 770 –780, Jun. 2001.

[16] L. Xia, P. Shum, and T. Cheng, "Photonic generation of microwave signals using a dual-transmission-band FBG filter with controllable wavelength spacing," *Applied Physics Review B.*, vol. 86, pp. 61–64, 2007.

[17] X. Liu, "A novel dual-wavelength DFB fiber laser based on symmetrical FBG structure," *Photonics Technology Letters, IEEE*, vol. 19, no. 9, pp. 632–634, May 2007.

[18] S. Pradhan, G. E. Town, and K. J. Grant, "Dual-wavelength DBR fiber laser," *Photonics Technology Letters, IEEE*, vol. 18, no. 16, pp. 1741–1743, Aug. 2006.

[19] L. Li, A. Schulzgen, X. Zhu, J. V. Moloney, J. Albert, and N. Peyghambarian, "1 W tunable dual-wavelength emission from cascaded distributed feedback fiber lasers," *Applied Physics Letters*, vol. 92, no. 5, p. 051111, 2008.

[20] J. M. S. Domingo, J. Pelayo, F. Villuendas, C. D. Heras, and E. Pellejer, "Very high resolution optical spectrometry by stimulated Brillouin scattering," *Photonics Technology Letters, IEEE*, vol. 17, no. 4, pp. 855–857, Apr. 2005.

Articles chapter 2

1. G. E. Villanueva, P. Pérez-Millán, J. Palací, J. L. Cruz, M. V. Andrés, and J. Martí, "Dual-wavelength DFB erbium-doped fiber laser with tunable wavelength spacing," *Photonics Technology Letters, IEEE*, vol. 22, no. 4, pp. 254–256, Feb. 2010.

2. G. E. Villanueva, J. Palací, J. L. Cruz, M. V. Andrés, J. Martí, and P. Pérez-Millán, "High frequency microwave signal generation using dual-wavelength emission of cascaded DFB fiber lasers with wavelength spacing tunability," *Optics Communications*, vol. 283, no. 24, pp. 5165–5168, Dec. 2010.

Dual-wavelength DFB erbium-doped fiber laser with tunable wavelength spacing

G. E. Villanueva,[1] P. Pérez-Millán,[1] J. Palací,[1] J. L. Cruz,[2] M. V. Andrés,[2] and J. Martí[1]

[1]Nanophotonics Technology Center, Universidad Politécnica de Valencia, Camino de Vera s/n, 46022 Valencia, Spain
[2]Departamento de Física Aplicada-ICMUV, Universitat de València, Dr. Moliner 50, 46100 Burjassot, Spain

ABSTRACT

A novel tunable dual-wavelength DFB fiber laser is presented. It is based on the optical resonances induced by two local phase shifts introduced in the periodic structure of an erbium-doped fiber Bragg grating. A dynamic control of the phase shifts, which are generated by piezoelectric transducers, permits the tunability of the wavelength spacing between the optical harmonics of the laser signal. The wavelength spacing is continuously tuned from 0.128 to 7 GHz. Moreover, a MW carrier is created within such frequency tuning range by the heterodyne photodetection of the dual-wavelength laser signal.

I. Introduction

Dual-wavelength lasers are used in a wide variety of applications in wavelength-division-multiplexing communications systems [1], sensing [2], lidar-radar systems [3], high-resolution interferometry [4], or microwave photonic generation [5]. Such applications can take advantage of the inherent properties of fiber lasers such as narrow linewidth, high signal-to-noise ratio and fiber compatibility. Thus, different alternatives for dual-wavelength operation of fiber lasers are being proposed in the last years: the use of filters to select the lasing modes within the laser cavity is a straightforward method to generate a dual-wavelength signal [1,6,7]. However, these lasers are built with relatively long cavities, hence they do not operate with a single longitudinal mode at each lasing wavelength. This drawback is overcome by distributed Bragg reflector (DBR) or distributed feedback (DFB) dual-wavelength fiber lasers which, in addition, have a very compact structure. Since the first demonstration of a dual-wavelength DFB fiber laser [8], several structures of the cavity of the dual-wavelength fiber laser have been proposed [9-12], where the spacing between lasing wavelengths is fixed. A tunable wavelength spacing is of high interest in applications such as microwave generation or high-resolution spectroscopy. Recently, Li et al. have demonstrated tunable dual-wavelength emission using two cascaded DFB fiber lasers [13], where the tunability is performed by temperature control of one of the lasers. In this paper a

single DFB fiber laser is used to generate a tunable dual-wavelength emission. The tunability is carried out by inducing two dynamic phase shifts superimposed locally in the FBG of the laser cavity. As shown in [14] the magnitude of an FBG phase shift can be controlled dinamycally with electromechanical actuators. In our case, the phase shifts are induced independently by two piezoelectric actuators (PZT), which allow for a faster tuning response than temperature control. The wavelength spacing between the lasing modes is adjusted by detuning both phase shifts symmetrically from a π-phase shift value, which ensures the emission of laser modes of equal amplitude. The wavelength spacing is continuously tuned from 0.128 to 7 GHz and a microwave (MW) carrier is created within such frequency tuning range by the heterodyne photodetection of the dual-wavelength laser signal.

II. Operating principles and experimental set-up

When two phase shifts are induced in the periodic structure of a uniform FBG, two transmission peaks appear in the transmission stop-band response. Fig. 1(a) shows the structure of an FBG with two π-phase shifts. The wavelength spacing between the transmission peaks depends on the spatial separation and the difference between the magnitudes of the two phase shifts. In particular, if both phase shifts vary symmetrically from a π-phase shift value, i.e., one of the phase shifts has a value of π+$\Delta\varphi$ and the other π-$\Delta\varphi$, then the wavelengths of the transmission peaks separate symmetrically from each other with respect to the Bragg wavelength of the FBG and the transmission peaks are equivalent in terms of amplitude and linewidth. This condition ensures a laser emission with two longitudinal modes of equal amplitude. Note that the working principle of the fiber laser is different from that of two cascaded single-wavelength lasers. For the last case the emitted wavelengths could be tuned independently since each resonance would oscillate in different cavities. In the presented laser, a variation of only one of the phase-shifts implies a variation of both wavelengths, as these resonances share a common cavity.

Fig. 2 illustrates the theoretical transmission spectra of a uniform 15 cm long FBG for the case of two π-phase shifts, 2.5π/3 and 3.5π/3 phase shifts and 2π/3 and 4π/3 phase shifts, respectively, which have been calculated using the coupled mode theory and the transfer matrix method. The inset of Fig. 2 gives the wavelength separation between transmission peaks as a function of the phase increment $\Delta\varphi$. The greater the value of the difference $\Delta\varphi$, the higher the wavelength spacing between transmission peaks. The phase shifts are induced by two PZTs stuck to the fiber. When a DC voltage drives the PZTs, a mechanical strain is applied on the fiber, and a phase shift is created by a local variation of the period and the refractive index of the FBG. Fig. 1(b) shows the theoretical profile of the amplitude of the electric field inside a uniform FBG as function of the position in the propagation axis. It has been calculated using the coupled mode theory and the transfer matrix method for the two resonant wavelengths and for the phase shift configurations considered in Fig. 2.

As illustrated in Fig. 1(b), when the difference $\Delta\varphi$ increases, the field of a given resonance wavelength tends to concentrate gradually in one of the locations where a phase

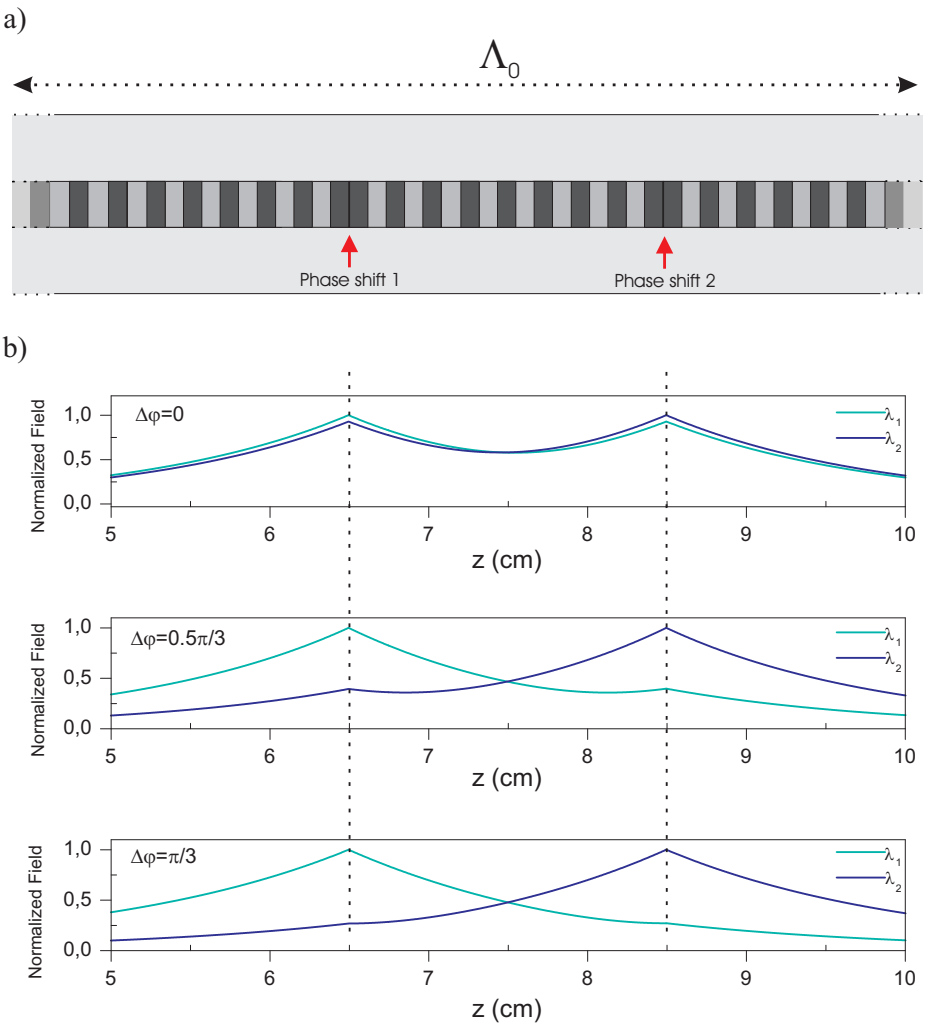

Figure 1: (a) Scheme of a uniform FBG of period Λ_0 with two spatial π-phase shifts. (b) Amplitude of the optical field as function of the position in the propagation axis for both resonance wavelengths in the cases of a phase difference $\Delta\varphi$=0 (up), $\Delta\varphi$=0.5π/3 (middle) and $\Delta\varphi$=π/3 (down).

shift has been performed, instead of concentrating at both locations at a time (as it happens when $\Delta\varphi$=0). This effect is exploited to reduce the mode competition in the laser emission dynamics, particularly at higher $\Delta\varphi$, since each single longitudinal mode is amplified by separate sections of the active medium.

Fig. 3 shows the experimental set-up. The DFB fiber laser consists of a 15-cm uniform grating written in an Er^{3+}-doped single-mode fiber. The absorption coefficient of the fiber at 979 nm and its peak absorption at 1530 nm are 13 and 20 dB/m, respectively. The two phase shifts are induced by two PZTs glued to the FBG and driven by a DC voltage source. The PZTs are cubes of 2x2x2 mm, and are situated symmetrically with respect to the center of the grating, separated 2 cm from each other. Besides the actuators, the fiber ends are fixed, and the FBG length (hence the Bragg wavelength) can be modified with a μm-precision

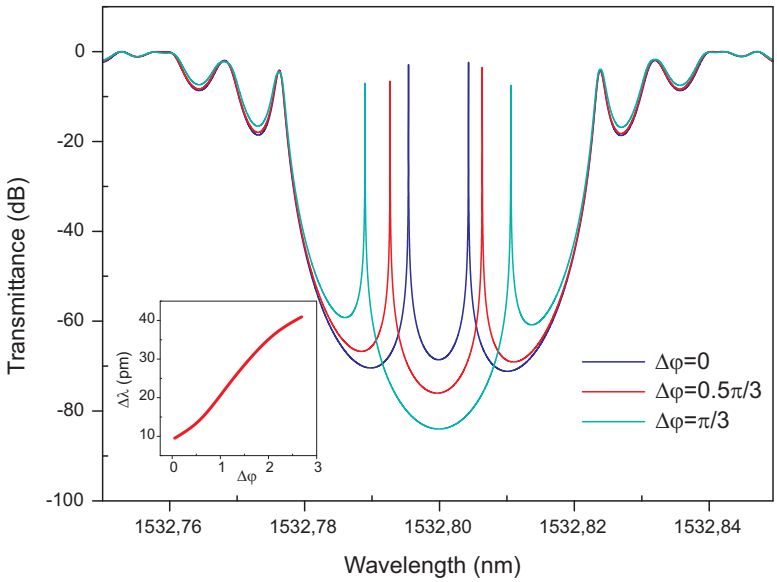

Figure 2: Transmittance spectra of a uniform FBG with two phase shifts for the cases of a phase difference $\Delta\varphi$ of 0, $0.5\pi/3$ and $\pi/3$. Inset shows the wavelength spacing for different phase increments $\Delta\varphi$.

positioner. A 980 nm diode laser pumps the fiber laser through a 980/1530 WDM, which extracts the output 1530 nm signal.

III. Results

We measured the optical spectrum of the laser output with a 10 pm resolution optical spectrum analyzer when pumping with 60 mW optical power. Dual-wavelength operation with equalized amplitudes of both laser modes is obtained by adjusting the μm-precision positioner and the DC driving voltage of the PZTs. Two single longitudinal modes with a power level of -13 dBm are emitted by the fiber laser. Fig. 4 shows the optical spectrum for different tuning values. CW operation with a wavelength spacing from 1 pm to 54 pm can be established. The maximum reachable value of 54 pm is limited by the bandwidth of the FBG. On the other hand, the minimum value of 1 pm is constrained by the spatial separation of the PZTs [15].

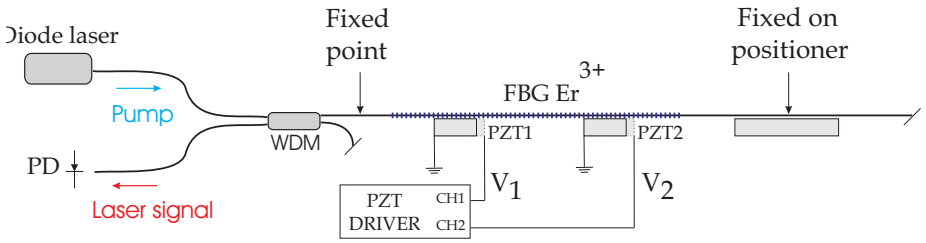

Figure 3: Configuration of the tunable dual-wavelength EDFL.

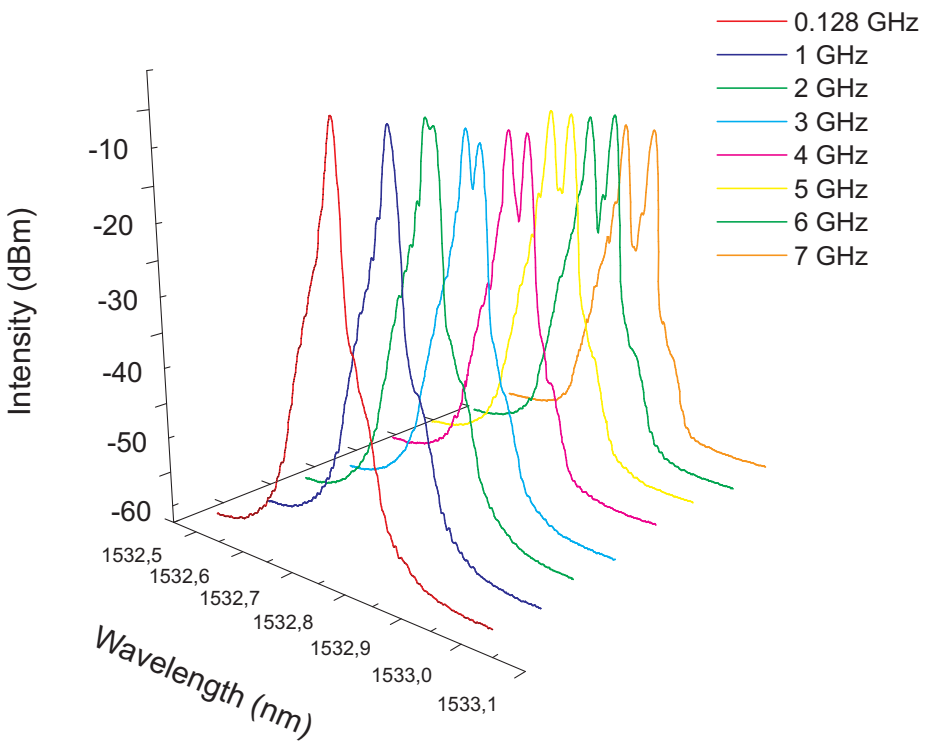

Figure 4: Optical spectra of the laser output for a wavelength spacing between both longitudinal modes in the range 0.128-7 GHz.

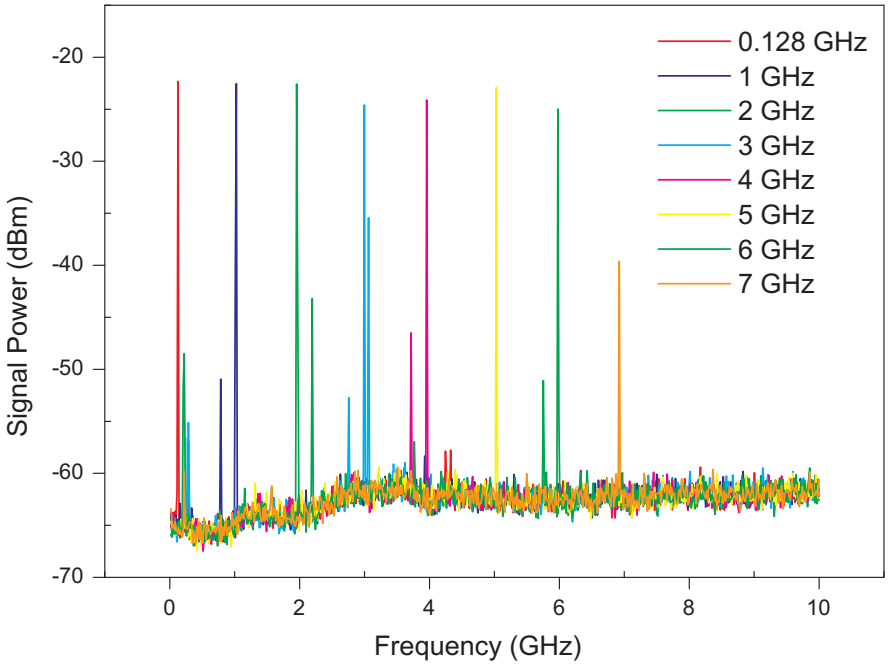

Figure 5: Electrical spectra of the photodetected signal for a wavelength spacing between the laser longitudinal modes in the range 0.128-7 GHz.

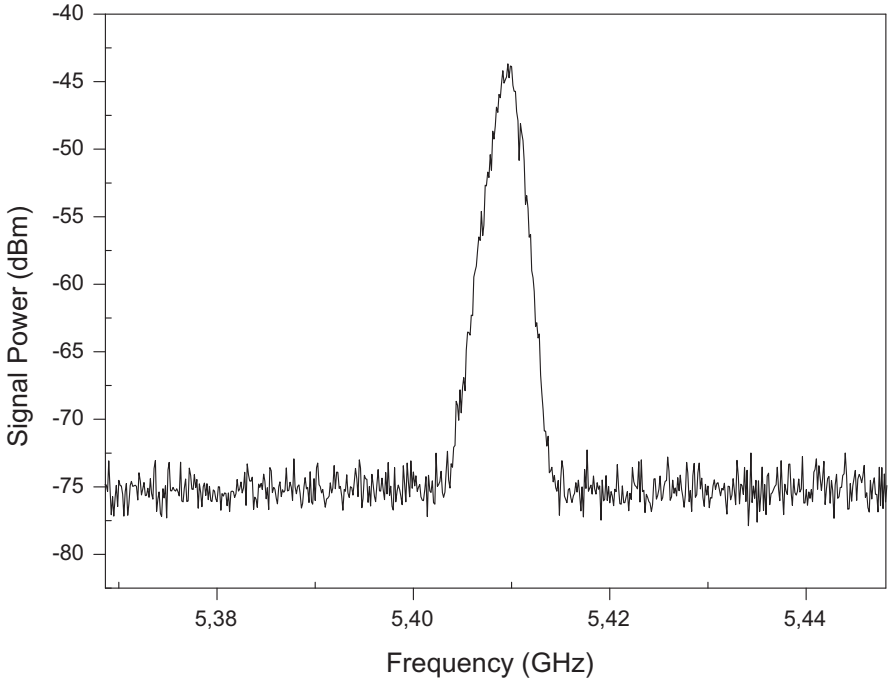

Figure 6: Electrical spectrum of a 5.41 GHz photogenerated signal.

The optical output can be photodetected in order to generate a microwave signal. Fig. 5 shows the electrical spectra of the photodetected signals corresponding with the optical spectra of Fig. 4. The frequency of the photogenerated carrier can be continuously tuned, and a sweep of 1 GHz step has been performed. The 1-54 pm optical tuning range corresponds with a 0.128-7 GHz electrical tuning range. The spectrum of a 5.41 GHz carrier is shown in Fig. 6, which exhibits a 3dB bandwidth of 3 MHz and a signal-to-noise ratio of 32 dB.

Fig. 5 shows an undesired harmonic close to the photogenerated main harmonic. Due to the birefringence of the erbium-doped fiber, the laser emission presents two eigen polarization modes for each wavelength. The typical birefringence of a single mode fiber is 10^{-6}, which results in a 135 MHz separation between orthogonal modes for a Bragg wavelength of 1530 nm. This value agrees satisfactorily with the separation observed experimentally in Fig. 5. In order to suppress this effect, an option could be exerting an external strain to the fiber, creating a suitable birefringence for single polarization emission. On the other hand, a polarization-dependent-loss fiber, instead of a standard fiber, could be used as active cavity of the laser. These fibers exhibit high losses in one of the orthogonal polarization, therefore only a single polarization state would be amplified appropriately for lasing.

The stability of the generated microwave signal is limited, with drifts of 100 MHz and considerable amplitude fluctuations due to gain mode competition. This problem is probably caused by a combination of effects. On the one hand, the existence of Er^{3+} ion pairs due to the high doping concentration of the fiber may cause optical self-pulsation

effects, which could be avoided by co-doping the erbium fiber with aluminum [16]. On the other hand, excited state absorption and concentration quenching due to interionic energy transfer in highly-doped erbium fibers may cause wavelength jitter of the laser signal.

IV. Conclusion

A novel dual-wavelength DFB fiber laser with tunable wavelength spacing has been proposed. Two PZTs are used to control dynamically the local phase shifts introduced in an erbium-doped FBG, permitting the tunability of the emitted modes. Single longitudinal mode operation of the two wavelengths is obtained, and a microwave signal is photodetected, achieving a continuous tuning frequency range from 0.128 to 7 GHz.

References

[1] J. Chow, G. Town, B. Eggleton, M. Ibsen, K. Sugden, and I. Bennion, "Multiwavelength generation in an erbium-doped fiber laser using in-fiber comb filters," IEEE Photon. Technol. Lett., vol. 8, pp. 60–62, 1996.

[2] S. Onoda, N. Tsukamoto, M. Ogino, K. Yamashita, O. Yumoto, K. Inoue, and Y. Komatsu, "A proposal of temperature sensing using a thin-film bandpass filter and dual-wavelength push–pull reflectometry," IEEE Photon. Technol. Lett., vol. 20, pp. 688–690, 2008.

[3] L. Morvan, N. D. Lai, D. Dolfi, J. P. Huignard, M. Brunel, F. Bretenaker, and A. L. Floch, "Building Blocks for a Two-Frequency Laser Lidar-Radar: A Preliminary Study," Appl. Optics, vol. 41, pp. 5702–5712, 2002.

[4] R. Onodera and Y. Ishii, "Two-wavelength laser-diode interferometer with fractional fringe techniques," Appl. Optics, vol. 34, pp. 4740–4746, 1995.

[5] C. Laperle, M. Svilans, M. Poirier, and M. Têtu, "Microwave Generation with Monolithic Dual-Wavelength DFB lasers," in 1997 Digest of the IEEE/LEOS Summer Topical Meetings, Montreal-Quebec, Canada, Aug. 1997, pp. 11–15.

[6] H. Okamura and K. Iwatsuki, "Simultaneous oscillation of wavelength-tunable, singlemode lasers using an Er-doped fibre amplifier," Electron. Lett., vol. 28, pp. 461–463, 1992.

[7] J. Nilsson, Y. W. Lee, and S. J. Kim, "Robust dual-wavelength ring-laser based on two spectrally different erbium-doped fiber amplifiers," IEEE Photon. Technol. Lett., vol. 8, pp. 1630–1632, 1996.

[8] M. Ibsen, E. Ronnekleiv, G. J. Cowle, M. N. Zervas, and R. I. Laming, "Multiple wavelength all-fibre DFB lasers," Electron. Lett., vol. 36, pp. 143–144, 2000.

[9] S. Pradhan, G. E. Town, and K. J. Grant, "Dual-Wavelength DBR Fiber Laser," IEEE Photon. Technol. Lett., vol. 18, pp. 1741–1743, 2006.

[10] J. Sun, Y. Dai, X. Chen, Y. Zhang, and S. Xie, "Stable dual-wavelength DFB fiber laser with separate resonant cavities and its application in tunable microwave generation," IEEE Photon. Technol. Lett., vol. 18, pp. 2587–2589, 2006.

[11] Y. Dai, X. Chen, J. Sun, Y. Yao, and S. Xie, "Dual-Wavelength DFB Fiber Laser Based on a Chirped Structure and the Equivalent Phase Shift Method," IEEE Photon. Technol. Lett., vol. 18, pp. 1964–1966, 2006.

[12] X. Liu, "A Novel Dual-Wavelength DFB Fiber Laser Based on Symmetrical FBG Structure," IEEE Photon. Technol. Lett., vol. 19, pp. 632–634, 2007.

[13] L. Li, A. Schülzgen, X. Zhu, J. V. Moloney, J. Albert, and N. Peyghambarian, "1 w tunable dual-wavelength emission from cascaded distributed feedback fiber lasers," Appl. Phys. Lett., vol. 92, n. 051111, 2008.

[14] P. Pérez-Millán, J. L. Cruz, and M. V. Andrés, "Active Q-switched distributed feedback erbium-doped fiber lasers," Appl. Phys. Lett., vol. 87, n. 011104, 2005.

[15] L. Xia, P. Shum, and T. Cheng, "Photonic generation of microwave signals using a dual-transmission-band FBG filter with controllable wavelength spacing," Applied Phys. Rev. B., vol. 86, pp. 61–64, 2007.

[16] A. Suzuki, Y. Takahashi, M. Yoshida, and M. Nakazawa, "A CW, polarization-maintaining $\lambda/4$-shifted DFB Er-doped fiber laser at 1.54 μm ," IEICE Electronics Express, vol. 4, pp. 251–257, 2007.

High frequency microwave signal generation using dual-wavelength emission of cascaded DFB fiber lasers with wavelength spacing tunability

G. E. Villanueva,[1] J. Palací,[1] J. L. Cruz,[2] M. V. Andrés,[2] J. Martí[1] and P. Pérez-Millán[1]

[1]Nanophotonics Technology Center, Universidad Politécnica de Valencia, Camino de Vera s/n, 46022 Valencia, Spain
[2]Departamento de Física Aplicada-ICMUV, Universitat de València, Dr. Moliner 50, 46100 Burjassot, Spain

ABSTRACT

A dual-wavelength fiber laser source based on two cascaded phase-shifted fiber Bragg gratings is presented. The gratings are written in an erbium-doped fiber, each configuring the cavity of a distributed feedback fiber laser. The spacing between lasing modes is controlled dynamically by the use of piezoelectric actuators. A continuous tuning range of 5-724 pm of the wavelength difference, which is equivalent to a photodetected 0.72-92 GHz range, is obtained. Efficient generation from the L to the W microwave and millimeter bands has been achieved by heterodyne photodetection of the dual-wavelength optical signal.

I. Introduction

The use of multi-wavelength fiber lasers has attracted a great research interest due to their applications in optical communications, sensing, radio astronomy or high resolution spectroscopy. Such fiber lasers offer interesting advantages such as narrow linewidths, fiber compatibility and high signal-to-noise ratio. Thus, different alternatives for dual-wavelength operation of fiber lasers are being proposed in the last years: the use of filters to select the lasing modes within the laser cavity is a straightforward method to generate a dual-wavelength signal [1, 2]. However, these lasers are built with relatively long cavities, hence they do not operate with a single longitudinal mode at each lasing wavelength. This drawback is overcome by distributed Bragg reflector (DBR) or distributed feedback (DFB) dual-wavelength fiber lasers which, in addition, have a very compact structure. Since the first demonstration of a dual-wavelength DFB fiber laser [3], several structures for the cavity of the dual-wavelength fiber laser have been proposed [4-7], where the spacing between lasing wavelengths is fixed. Tunable wavelength spacing is of high interest in applications such as microwave generation, high-resolution spectroscopy and reconfigurable

wavelength-division multiplexing (WDM) systems [8, 9]. Recently, Li et al. have demonstrated tunable dual-wavelength emission using two cascaded DFB fiber lasers [10], where the tunability was performed by temperature control of one of the lasers.

In this work a dual-wavelength room-temperature fiber laser based on two cascaded DFB sections implemented in a single fiber Bragg grating (FBG) is presented. Each section performs a single-wavelength laser emission with different grating period. A phase shift is induced in the center of each section in order to induce the lasing operation. These phase shifts can be controlled dynamically by electromechanical actuators [11]. The wavelength spacing between the two lasing modes is adjusted by stretching one of the sections and, therefore, shifting the stop-band spectral response of such grating section. The stretching is carried out dynamically by a piezoelectric actuator (plumbum zirconate titanate, PZT). Compared to a temperature-based option [10], this method allows a fast and continuous control of the wavelength spacing tunability. We demonstrate a continuous wavelength spacing tuning range from 5 to 724 pm, which corresponds to a millimeter signal frequency of 0.75 to 92 GHz when the dual-wavelength laser signal is photodetected. This frequency range covers bands of potential wireless communication applications, such as 38.6-40 GHz used for licensed high-speed microwave data links, 60 GHz short-range data links, and 71-76, 81-86 GHz point-to-point high-bandwidth communication links.

II. Dual-Wavelength Operating Principle

Single-frequency operation of DFB fiber laser is well-known currently [7, 10]. When two phase shifts are induced in the periodic structure of a uniform FBG, two transmission peaks appear in the transmission stop-band response. This phenomenon was exploited in a previous work to perform a tunable dual-wavelength fiber laser [12], where two phase shifts were induced in the grating using two PZT. The phase shifts could be controlled dynamically, thus allowing dynamic control of the wavelength difference. Nevertheless, the tunability was limited by the width of the stop-band response of the grating, of the order of 50 pm. In order to increase the tuning range of the wavelength spacing, a new approach is investigated. Fig. 1(a) illustrates the structure of the laser cavity: A single fiber grating is split in two sections with different grating periods. In this way, a dual-wavelength laser signal is obtained as the combined emission of two cascaded single-wavelength DFB fiber lasers. This scheme is conceptually different from the one presented in [12], which was based on one unique dual-wavelength DFB laser. Each section has a different grating period and a local phase shift in its center. These phase shifts create a single transmission peak in each of the stop-band response. The theoretical transmittance of the overall FBG is plotted in Fig. 1(b), where two stop-band responses corresponding with the two sections can be observed. The fiber where the FBG is written is doped with erbium. Hence, when pumping with a 980 nm diode laser, each cavity of the fiber laser oscillates at the wavelength corresponding to its transmission peak and, therefore, two single longitudinal modes are emitted.

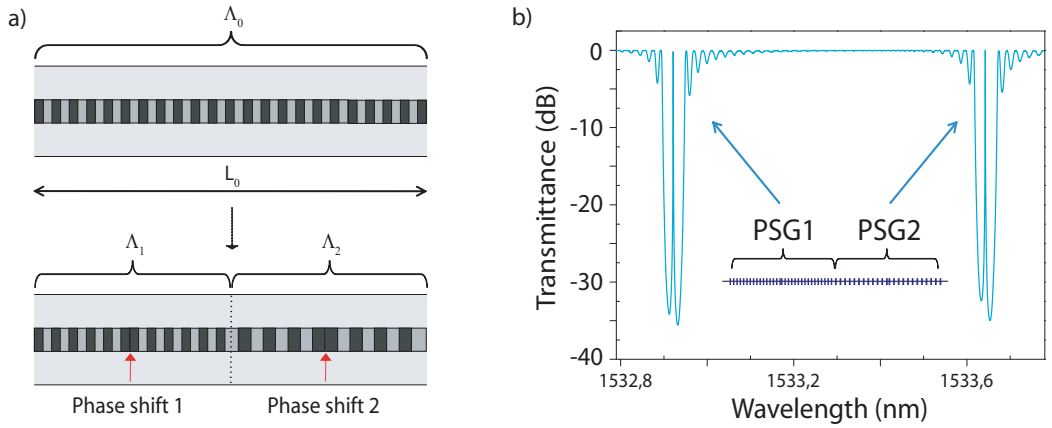

Figure 1: (a) Scheme of a uniform FBG of period Λ_0 and length L_0 (up), and the same FBG divided into two sections with periods Λ_1 and Λ_2 (down). A local phase shift is performed in the center of each section. (b) Theoretical transmittance spectrum of the FBG split in two phase shifted gratings (PSG) sections, each with an induced local π-phase shift.

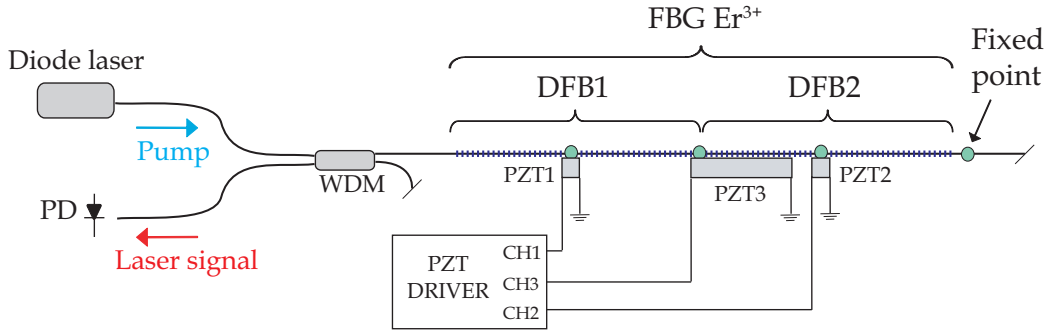

Figure 2: Configuration of the tunable dual-wavelength fiber laser.

The experimental setup is shown in Fig. 2. The pump signal, provided by a 980 nm diode laser is launched into the laser cavity through a 980/1530 WDM. The fiber laser cavity consists of a 15-cm uniform 1.53-μm centered grating written in an Er^{3+}-doped single-mode fiber. The absorption coefficient of the fiber at 979 nm and its peak absorption at 1530 nm are 13 and 20 dB/m respectively. The overall grating is glued to three piezoelectric actuators (PZT1, PZT2 and PZT3). In the case of PZT3, one of its ends is glued to the central point of the grating, and the opposite one is glued to the optical table. The right side of the fiber is also glued to the optical table (glue drops are depicted in Fig. 2 as green circles). PZT3 is 3.6 cm long and stretches one half of the grating, DFB2 section in Fig. 2, increasing in this way the original period Λ_0 only in the right half of the grating. PZT1 and PZT2 are 0.2 cm long, and they are used to induce the local phase shifts in the center of each grating section.

Each PZT is driven by its own computer controlled direct current (DC) voltage source. This permits a dynamic and independent control of two parameters, the wavelength spac-

ing between the lasing modes and the amplitudes of the lasing modes. On the one hand, the coarse wavelength spacing (determined by the variation of the period of the second section of the grating) is set by the driving voltage of PZT3. A fine wavelength spacing adjustment can be carried out by PZT1 and PZT2, as they control the induced phase shifts of the DFB sections, therefore shifting the transmission peak within each grating response. On the other hand, the amplitude of the lasing modes can be controlled by PZT1 and PZT2. The magnitude of the phase shift induced in a uniform grating not only determines the transmission peak spectral position within the grating response, but also the width of this peak; the closer is the value of the phase shift to π, the narrower is the transmission peak. In our fiber laser we have two cascaded DFB in the same active fiber, and it was observed that one of the lasing modes was predominant over the other when the first one has a narrower peak width. In this way the amplitudes can be equalized adjusting PZT1 and PZT2. Furthermore, the laser can operate in dual-wavelength or in single-wavelength emission regime, since both wavelength emissions are dynamically and independently controlled.

III. Experimental Results

We measured the optical spectrum of the laser output with a 10 pm resolution optical spectrum analyzer when pumping with 100 mW optical power. Dual-wavelength operation with equalized amplitudes of both laser modes is obtained by adjusting the DC driving voltages of the PZTs. Two single longitudinal modes with a power level of -10 dBm are emitted by the fiber laser. Fig. 3(a) shows the optical spectrum for wavelength spacings of 68 pm and 724 pm, respectively. The action of the three piezo actuators results in a continuous tuning spacing from 5 pm to 724 pm. A measurement of the laser linewidth when operating in single wavelength regime is illustrated in Fig. 3(b), showing a 0.22-pm FWHM linewidth. The measurement has been performed utilizing a recently published technique which is based on the amplification of the laser signal by means of the Brillouin backscattering peak of a tunable laser [13]. The theoretical spectral resolution of this technique is of 0.08 pm.

The dual-wavelength emission property of this type of laser has been exploited to evaluate its performance as a photonic source of mm-wave signals. A photodetector was placed in the laser output in order to generate a microwave signal via the heterodyne mixing of the two optical modes of the fiber laser. Fig. 4(a) shows the electric spectra of the photogenerated signal for different wavelength spacings. The figure corresponds with a wavelength spacing sweep of 4 GHz step, from 0.7 to 40 GHz. The upper frequency of the sweep was limited by the bandwidth of the spectrum analyzer. Nevertheless the maximum wavelength spacing observed of 724 pm would correspond with a maximum photogenerated signal frequency of 92 GHz. As an example of such extended performance, a 75 GHz frequency signal was photogenerated using an external harmonic mixer with the analyzer. This mixer downconverts the radio frequency (RF) of 75 GHz to an intermediate frequency (IF) of 0.4 GHz, using a local oscillator (LO) of 12.4 GHz provided by the analyzer. The IF signal is

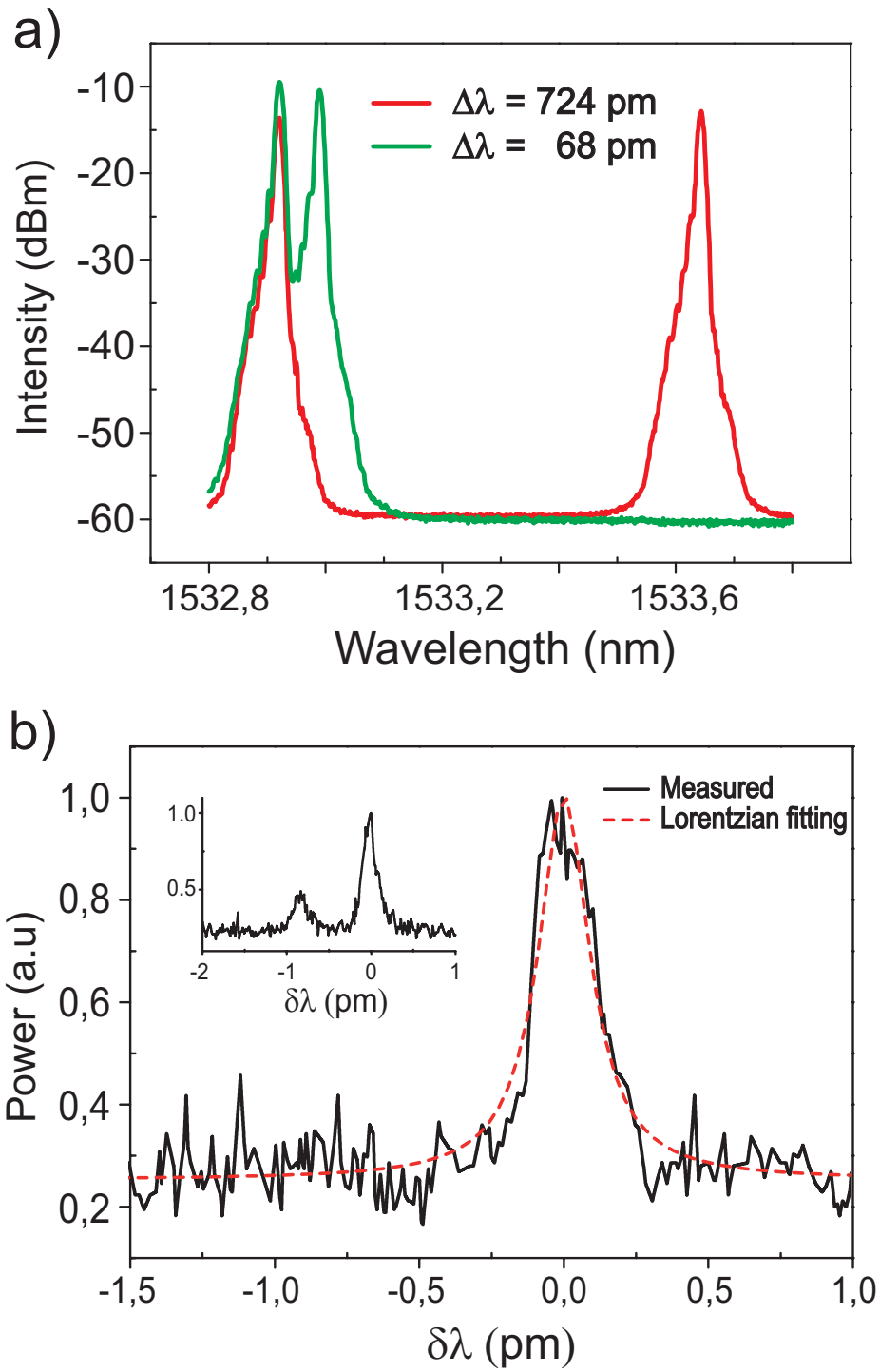

Figure 3: (a) Optical spectra of the laser output for a wavelength spacing of 724 pm and 68 pm. (b) Laser spectrum under single wavelength emission. Inset shows the two eigen polarization modes.

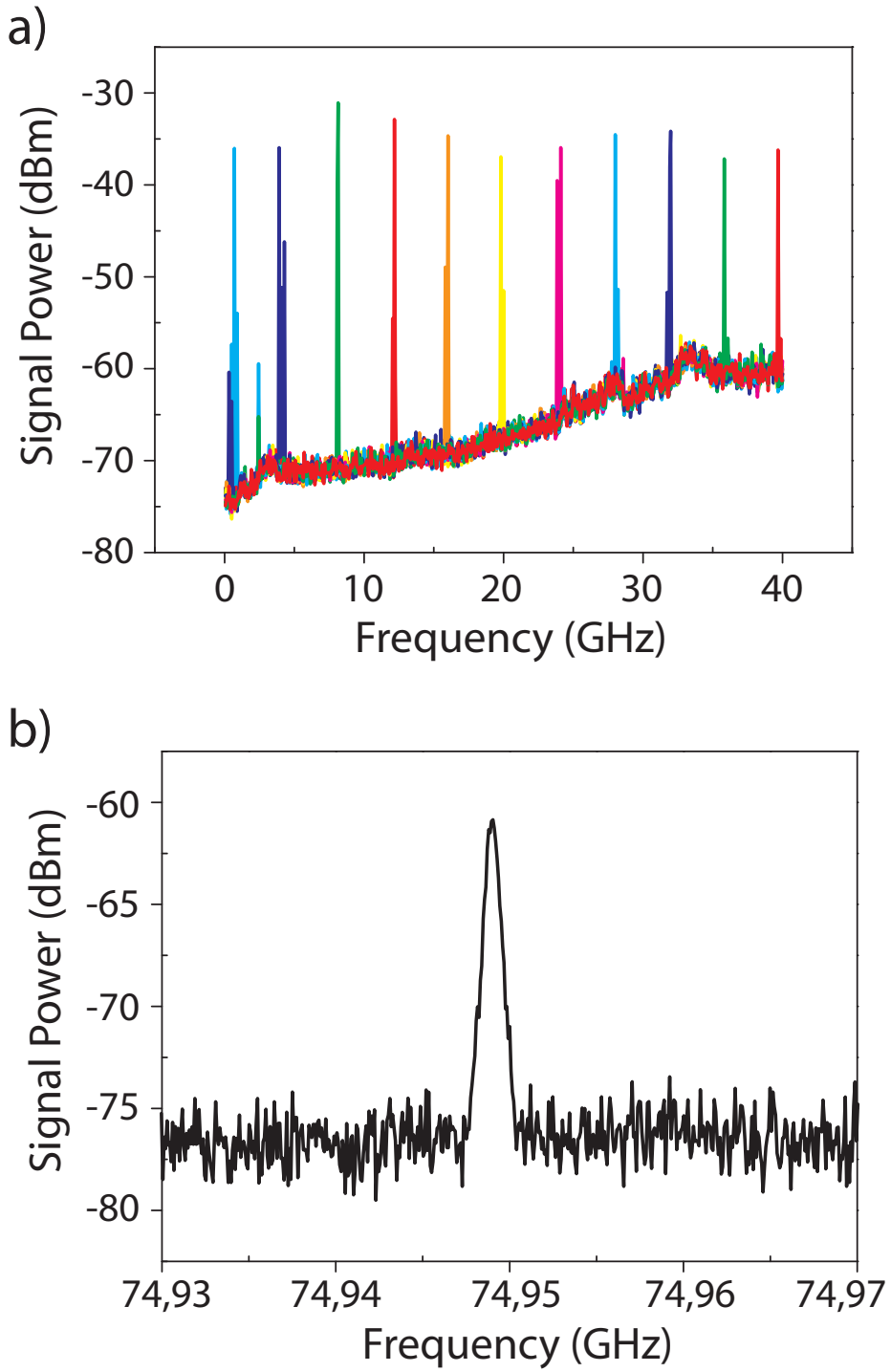

Figure 4: (a) Electric spectra of the photodetected laser output for a wavelength spacing sweep from 0.7 to 40 GHz, with a 4 GHz step. (b) Electric spectrum of a 75 GHz photogenerated signal.

obtained using the 6^{th} harmonic product following the expression $f_{IF} = f_{RF} - 6 * f_{OL}$. Its spectrum is shown in Fig. 4(b), which exhibits a 3dB bandwidth of 750 kHz and a signal-to-noise ratio of 16 dB. The external mixer introduces 28 dB of conversion loss, therefore the level of the 75 GHz photogenerated signal is expected to be of -32 dBm, in accordance with the trend observed in Fig. 4(a). The floor noise level shown in Fig. 4(a) and 4(b) is due to the spectrum analyzer and the external mixer, so a higher signal-to-noise ratio of the photogenerated signal is expected.

Due to the birefringence of the fiber, the laser emission presents two eigen polarization modes for each wavelength. These modes compete for the cavity gain, and reduce the emission stability. The typical value of birefringence of a single-mode fiber is 10^{-6}, which results in a 135 MHz separation between orthogonal polarization modes for a Bragg wavelength of 1530 nm. The inset included in Fig. 3(b) shows the optical spectrum of one of the DFB wavelengths, where two eigen polarization modes can be observed. The separation of these two modes is 0.9 pm, resulting in 115 MHz for 1530 nm. This value is in good agreement with the expected spectral separation for a typical birefringence value. In order to suppress this effect, an option could be exerting an external strain to the fiber, creating a suitable birefringence for single polarization emission. On the other hand, a polarization-dependent-loss fiber, instead of a standard fiber, could be used as active cavity of the laser. These fibers exhibit high losses in one of the orthogonal polarization, therefore only a single polarization state would be amplified appropriately for lasing.

The optical signal emitted by the fiber laser shows frequency drifts of 1MHz and considerable amplitude fluctuations due to gain competition. Since the phase shifts in the DFBs are induced by piezoelectric actuators, random electromechanical and temperature variations could also be a source of instabilities.

IV. Conclusion

A dual-wavelength DFB fiber laser source based on two cascaded phase-shifted FBGs has been proposed. By the exploitation of the electromechanical properties of piezoelectric actuators a dynamic tunability of the wavelength spacing between lasing modes is performed. The fiber laser exhibits single longitudinal mode operation of the two wavelengths, and a continuous tuning wavelength spacing range from 5 to 724 pm has been demonstrated. Furthermore, the heterodyne mixing of the two optical modes has resulted in the generation of mm-wave signals of frequencies up to 75 GHz.

References

[1] J. Chow, G. Town, B. Eggleton, M. Ibsen, K. Sugden, and I. Bennion, “Multiwavelength generation in an erbium-doped fiber laser using in-fiber comb filters,” IEEE Photon. Technol. Lett., vol. 8, pp. 60–62, 1996.

[2] H. Okamura and K. Iwatsuki, "Simultaneous oscillation of wavelength-tunable, singlemode lasers using an Er-doped fibre amplifier," Electron. Lett., vol. 28, pp. 461–463, 1992.

[3] M. Ibsen, E. Ronnekleiv, G. J. Cowle, M. N. Zervas, and R. I. Laming, "Multiple wavelength all-fibre DFB lasers," Electron. Lett., vol. 36, pp. 143–144, 2000.

[4] S. Pradhan, G. E. Town, and K. J. Grant, "Dual-Wavelength DBR Fiber Laser," IEEE Photon. Technol. Lett., vol. 18, pp. 1741–1743, 2006.

[5] J. Sun, Y. Dai, X. Chen, Y. Zhang, and S. Xie, "Stable dual-wavelength DFB fiber laser with separate resonant cavities and its application in tunable microwave generation," IEEE Photon. Technol. Lett., vol. 18, pp. 2587–2589, 2006.

[6] Y. Dai, X. Chen, J. Sun, Y. Yao, and S. Xie, "Dual-Wavelength DFB Fiber Laser Based on a Chirped Structure and the Equivalent Phase Shift Method," IEEE Photon. Technol. Lett., vol. 18, pp. 1964–1966, 2006.

[7] X. Liu, "A Novel Dual-Wavelength DFB Fiber Laser Based on Symmetrical FBG Structure," IEEE Photon. Technol. Lett., vol. 19, pp. 632–634, 2007.

[8] A. Narula-Tam, P. Lin, and E. Modiano, "Efficient routing and wavelength assignment for reconfigurable WDM networks," *IEEE J. Select. Areas Commun.*, IEEE J. Sel. Areas Commun., vol. 20, pp. 75–88, 2002.

[9] X. Yang, S. Zhong, Y. J. Chen, and D. Stone, "Precision-tuning wavelength addressable laser for reconfigurable WDM networks," IEEE Photon. Technol. Lett., vol. 12, pp. 1385–1387, 2000.

[10] L. Li, A. Schülzgen, X. Zhu, J. V. Moloney, J. Albert, and N. Peyghambarian, "1 W tunable dual-wavelength emission from cascaded distributed feedback fiber lasers," Appl. Phys. Lett., vol. 92, n. 051111, 2008.

[11] P. Pérez-Millán, J. L. Cruz, and M. V. Andrés, "Active Q-switched distributed feedback erbium-doped fiber lasers," Appl. Phys. Lett., vol. 87, n. 011104, 2005.

[12] G. E. Villanueva, P. Pérez-Millán, J. Palací, J. L. Cruz, M. V. Andrés, and J. Martí, "Dual-Wavelength DFB Erbium-Doped Fiber Laser With Tunable Wavelength Spacing," IEEE Photon. Technol. Lett., vol. 22, pp. 254–256, 2010.

[13] J. M. S. Domingo, J. Pelayo, F. Villuendas, C. D. Heras, and E. Pellejer, "Very high resolution optical spectrometry by stimulated Brillouin scattering," IEEE Photon. Technol. Lett., vol. 17, pp. 855–857, 2005.

Chapter 3

Mode-locked fiber lasers

3.1 Introduction

Ultrafast optical sources have attracted great research interest for decades, and nowadays short pulsed laser systems find numerous applications in areas of fundamental research as well as for telecommunication, medical and industrial applications. Ultrafast laser systems are used for time resolved studies in chemistry [1], optical frequency metrology [2], OTDM communication systems [3], terahertz generation [4], two photon and CARS spectroscopy and microscopy [5], and optical coherence tomography [6]. Other medical related applications are eye laser surgery and dentist drills [7]. In the industry, ultrafast lasers are used for micro-machining and marking [8,9]. The corner stone of ultrafast optics is the mode-locked laser, and development of mode-locked lasers has been a huge research field in itself. Mode-locked fiber lasers have become indispensable tools in many fields as their use is no longer relegated to the optics community. These devices have become commercially available in the last decade, and put an emphasis on long-term performance and reliability as these devices are beginning to be integrated into complex systems for very different areas.

In this chapter we study different mode-locked erbium-doped fiber laser architectures. Active and passive mode-locking are explored to obtain a complete set of mode-locked fiber lasers able to fulfil target specifications of photonic-assisted analog to digital applications [10]. Mach-Zehnder modulators represent the best option to build actively mode-locked lasers with a fiber ring cavity, allowing control of the pulse repetition frequency provided by external microwave signal synthesizers. To passively mode-lock our erbium-doped fiber lasers, we will employ semiconductor saturable absorbers. The use of intracavity polarizing fiber is also explored: control of the passive mode-locking operation regime is demonstrated via polarization state adjustment. Numerical calculations obtained from nonlinear Schrödinger equation model accompany the experimental results.

Lastly, carbon nanotubes have proven to be ultrafast optical nonlinear materials, finding recent application as saturable absorbers in passive mode-locking [11]. One challenge of dealing with carbon nanotubes is their integration in optical fiber cavities. We study an innovative structure where interaction of light with nanotubes deposited on fiber cladding is assisted through a tilted fiber Bragg grating.

3.2 Active and passive mode-locked fiber lasers

Mode-locked fiber lasers base their optical pulsed operation on longitudinal cavity mode phase locking. Other optical pulsed sources, like Q-switched lasers, are based on more intuitive pulsing mechanisms like temporal variation of the cavity Q factor. Pulse formation in mode-locked lasers requires oscillating longitudinal modes to keep a common phase reference, thus the temporal summation of continuous wave oscillating modes results in a coherent pulsed pattern. This phenomenon was previously illustrated in figure 1.7. Depending on how the phase reference is imposed to the cavity longitudinal modes, mode-locking can be classified as active or passive mode-locking. In this thesis, we study the design of mode-locked fiber lasers for microwave photonics applications. In particular, we focus on how high repetition rate optical sources are of special interest in photonic-assisted analog to digital converters (PADC).

An analog to digital converter (ADC) is a device that converts an analog input signal to a digital number sequence proportional to the magnitude of the signal. The main limitations of traditional electronic analog to digital conversion are:

- Noise contributions (thermal, shot, flicker,...), mostly affecting ADC resolution at lower frequencies.
- Jitter: The uncertainty due to the clock phase noise limits the accuracy when sampling the input signal, hence limiting the maximum input frequency in the ADC.
- Ambiguity: Circuits in charge of comparisons between the input signal and certain references need some time to generate the digital signal and recover from the comparison. Ambiguity is the main limitation at high frequencies.

PADCs take advantage of low jitter pulsed optical sources to overcome the electronic oscillator limitations. Depending on which ADC process (sampling and/or quantization) is carried out in the optical domain, PADCs are divided into: 1) Photonic assisted ADC in which a photonic device is added to an electronic ADC to improve performance, 2) photonic sampling and electronic quantization ADC, 3) electronic sampling and photonic quantization ADC, and 4) photonic sampling and quantization ADC. The photonic technology is still very immature for quantizing the

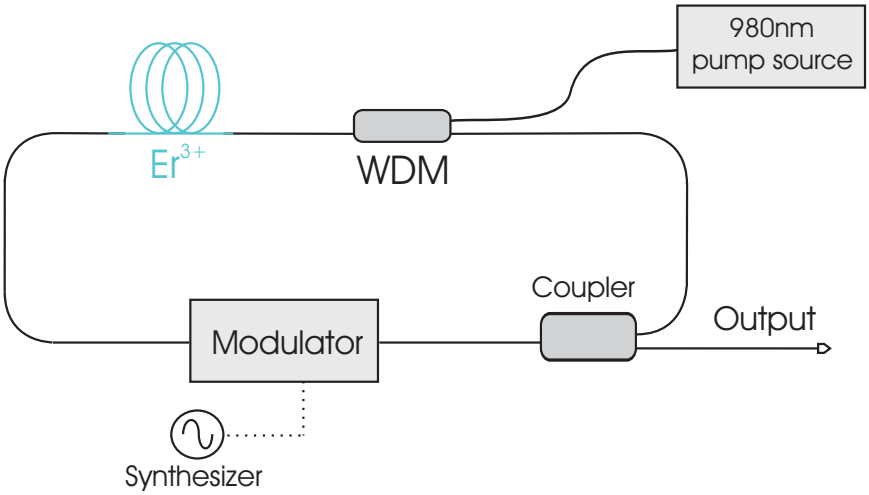

Figure 3.1: Experimental setup of an active mode-locked erbium-doped fiber laser

sampled signal, being then more convenient using architectures based on photonic sampling and electronic quantization than full photonic ADCs [12, 13].

One interesting PADC scheme in terms of reduced complexity and improved performance in terms of jitter noise is the implementation of a photonic sampling and track-and-hold placed as a front-end of a standard electronic ADC [14]. It consists of a pulsed optical source that feeds an optical intensity modulator, and then the optical signal is transferred to the electrical domain by photodetection. The analog radio frequency (RF) signal to be digitalized modulates the optical pulse train. The combination of optical source, modulator and photodetector provides a photonic sampling stage for the subsequent electronic quantization stage. The use of very stable optical pulsed laser, with a jitter of few femtoseconds, low amplitude noise and ultra-short temporal duration (femtosecond range) contributes to an outstanding performance improvement beyond the fundamental electronic limitations. Mode-locked fiber lasers are excellent candidates as compact low-noise PADC pulsed optical sources.

Intensity modulators are usually employed in active mode-locking fiber ring lasers [15]. In active mode-locked lasers, the cavity loss is periodically modulated, and optical signal levels at minimums of cavity loss are promoted to build up. The modulation frequency has to match exactly the fundamental frequency of the cavity or a multiple of it. In this sense, the loss modulation induces the longitudinal oscillating modes to arrange their optical phase to a common reference, and eventually a pulsed pattern is obtained. Pulse shortening is limited by the finite gain bandwidth of the optical laser medium, and steady-state pulses show a width much smaller than the modulation window. A ring cavity active mode-locked erbium-doped fiber laser scheme is shown in figure 3.1. The main advantage of active mode-locking is the external control of the pulse repetition frequency through electronic local oscillators or synthesizers. The commercial availability of high bandwidth modulators easily allows repetition frequencies over 40 GHz [16]. For the fabrication of actively mode-locked fiber lasers,

electro-optic Mach-Zehnder modulators (MZM) were used in this thesis.

An optical Mach-Zehnder modulator is an intensity modulator based on the electro-optic effect of a crystal and a Mach-Zehnder interferometer. Figure 3.2 broadly depicts the structure of a MZM. One of the electro-optic crystals most used in modulators for telecommunication applications is lithium niobate ($LiNbO_3$). Other electro-optic materials used in Mach-Zehnder modulators are indium phosphide (InP) and gallium arsenide (GaAs). Materials showing electro-optical effect (or Pockels effect) are able to modify their refractive index under an applied electrical field. Light that propagates in such crystals are influenced by the variable medium refractive index. This effect is exploited in electro-optical modulators to convert temporal signal variations into optical phase variations. If an interferometric structure is build in the crystal, then optical phase variations turn to intensity variations. In figure 3.2, a Mach Zehnder interferometer is integrated in the electro-optic crystal by means of optical waveguides, being diffused titanium the most common waveguide structure for $LiNbO_3$ crystals. When one arm of the interferometer suffers a refractive index change, the interferometer output experiences an intensity change. The application of electric fields in the interferometer arms is realized by means of metallic RF electrodes. The structure of figure 3.2 shows an unbalanced single drive configuration, as only one arm is modulated by the electric signal. Even though this is the simplest Mach-Zehnder configuration, unbalanced single drive modulators are not used in practice due to the chirp that this kind of modulators adds to the optical signal. Instead, balanced single drive and balanced differential drive configurations include a control of the inserted chirp as both interferometric arms are modulated. Fundamental modulation bandwidth limits are imposed by electrode design. Accurate travelling wave electrode designs provide bandwidths over 50 GHz. Another property of MZMs is their dependence with optical input polarization, so they generally need a polarization controller to optimize the modulation depth.

On the other hand, passive mode-locked lasers achieve the phase locking process

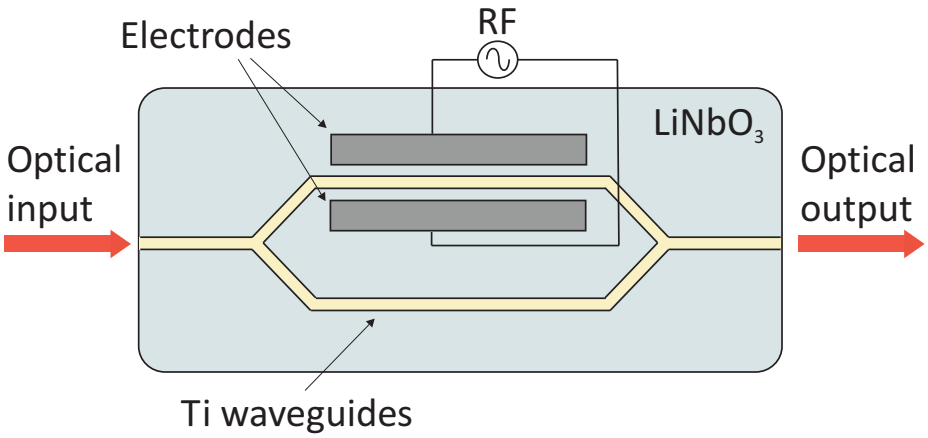

Figure 3.2: Mach-Zehnder modulator estructure. A Mach-Zehnder interferometer with one arm modulated by the RF signal provides an optical intensity modulation of the input light.

without external assistance in contrast to active mode-locking. Passive mode-locking is accomplished through an intensity-dependent mechanism implemented in the cavity. If this mechanism induces lower losses when high intensity level signals propagate, then pulsed signals are promoted against continuous wave and noisy signals, which suffer higher insertion losses. This effect is repeated each roundtrip until a steady-state pulsed regime is obtained, i. e., the oscillating longitudinal modes have acquired a common phase reference. There are several ways to achieve intensity-dependent losses or saturable absorption. For fiber lasers, the most common passive mode-locking techniques are non-linear polarization rotation (NLPR) [17–19] and saturable absorbers (SA) [20, 21]. We will focus on the latter.

Saturable absorbers exhibit insertion losses that saturate with the optical input intensity (see equation (1.7) on page 14). For the fiber lasers developed, we will use semiconductor saturable absorbers (SESA). These devices can work in transmission or reflection operation, the latter being known as semiconductor saturable absorber mirror (SESAM), and they are commercially available for mode-locking lasers [22]. SESAs and SESAMs are based on saturable absorber layers made of semiconductor material with a direct band gap slightly lower than the photon energy, and they are generally made up of InGaAs quantum wells. SESAMs include a Bragg mirror to perform the reflectivity, usually made of GaAs/AlAs structures. When light is launched to the saturable absorber, electron-hole pairs are created in the semiconducting layer. As the number of photons increases, more electrons are excited, however only a certain number of electron-hole pairs can be created, hence the absorption is saturated. The electron-hole pairs recombine non-radiatively and, after a certain period of time, the saturable absorber is ready to absorb photons again. The key parameters for a saturable absorber are its dynamic response, recovery time, wavelength range, saturation intensity, modulation depth and the non-saturable losses. Equation (1.7) (page 14) assumes an instantaneous SA. If we take into account the recovery time, then the insertion loss derivative follows the expression

$$\frac{\partial \alpha(t)}{\partial t} = -\frac{\alpha - \alpha_0}{\tau_{SA}} - \alpha \frac{|A(t)|}{E_{SA}}, \tag{3.1}$$

with α_0 being the saturation absorption, $A(t)$ is the instantaneous amplitude of the incoming pulse, τ_{SA} is the SA recovery time and E_{SA} the saturation energy. A comparison between an instantaneous SA and a SA with 10 ps of recovery time is shown together with the optical pulse profile in figure 3.3. In our passive mode-locking fiber lasers with ring cavity structure, a fiber pigtailed transmission SESA is introduced in the cavity, while for linear cavities, a SESAM butt-coupled to an optical fiber is used.

The experimental results obtained with the different mode-locked fiber laser setups are accompanied by numerical calculations. In order to simulate pulsed mode-locked fiber lasers, the nonlinear Schrödinger equation (NLSE) is used [23]. NLSE describes pulse propagation in nonlinear and dispersive mediums. A general form of the NLSE is

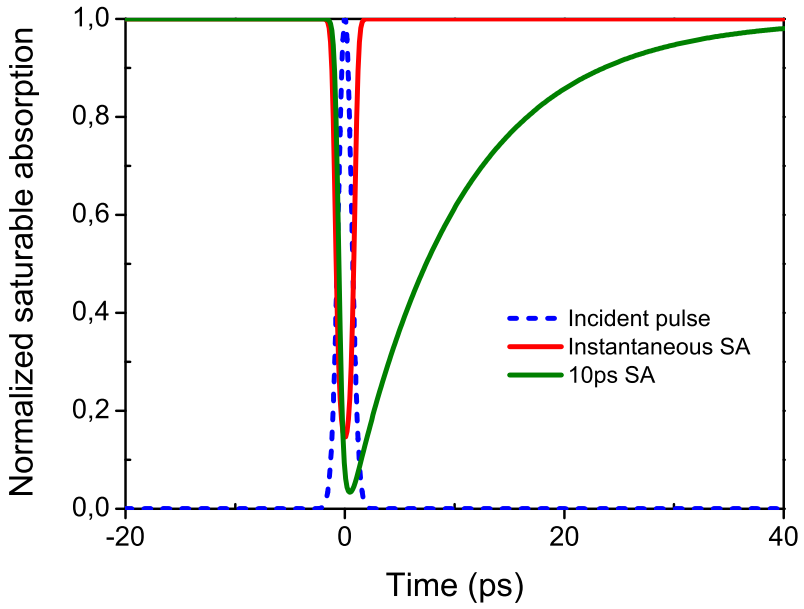

Figure 3.3: Normalized saturable absorbance for both instantaneous and 10ps recovery time saturable absorber. The optical incoming pulse shape is also shown.

$$\frac{\partial A}{\partial z} + j\frac{\beta_2}{2}\frac{\partial^2 A}{\partial T^2} + \frac{\alpha}{2}A - \left(\frac{g}{2} + \frac{D_g}{2}\frac{\partial^2}{\partial T^2}\right)A = j\gamma|A|^2 A. \tag{3.2}$$

NLSE works with the slow-varying envelope A of an optical pulse and not with the instantaneous optical filed of angular frequency ω_0. Equation (3.2) models the optical fiber effects of dispersion and nonlinearity (Kerr effect) through the parameters β_2 and γ respectively. β_2 is defined as the second derivative of the propagation constant, and represents chromatic dispersion. Chromatic dispersion in an optical fiber comes from the dependence of the effective index on frequency, due to the presence of medium dispersion and waveguide dispersion. The dependence of refractive index on optical intensity results in nonlinear effects. In equation (3.2), more complex nonlinear effects such as stimulated Raman scattering and self-steepening are neglected. The temporal variable T represents a group velocity moving-frame through the relation $T = t - \beta_1 z$. Optical loss and gain are given by the parameters α and g respectively, and the gain is assumed to have a parabolic spectral response. Gain bandwidth Ω_g determines the parameter $D_g = g/\Omega_g^2$.

Optical pulses propagating through optical fibers experience nonlinear effects, dispersion, and losses/gain. Nonlinearity produces self phase modulation (SPM), since the own pulse modifies the medium in which it propagates. The principal consequence of SPM is a modification of the pulse spectrum, usually resulting in spectral broadening. Chromatic dispersion causes a wavelength-dependent propagation velocity. Since pulse spectra have finite bandwidth, different spectral components travel at different speeds, and the pulse suffers a temporal broadening and becomes chirped. Optical fiber losses are in practice considered constant with frequency. However, optical gain,

generally coming from pumped rare earth doped fibers, has a spectral response with a finite bandwidth. In mode-locked fiber lasers the gain bandwidth determines intrinsically the maximum emission bandwidth, therefore limiting the minimum achievable pulse temporal width.

Mode-locking operation was introduced in section 1.3 as a regime where multiple lasing longitudinal modes of an optical cavity keep a common phase reference among them. Therefore, the temporal summation of all the oscillating modes yields a pulsed and periodic signal (refer to figure 1.7 on page 11). In the frequency domain, the spectrum of an optical pulsed signal is equal to discrete components separated by the repetition frequency of the pulse train. These spectral components follow the envelope of the Fourier transform of the slow-varying pulse amplitude, and this spectrum is centered at the optical carrier wavelength. When working with the NLSE, we compute the propagation of the slow-varying amplitude of a single pulse. Since mode-locking implies a shared phase reference among spectral components, then the phase of the slow-varying envelope Fourier transform has to be linear in mode-locking operation. Figure 3.4 illustrates the calculated output pulse of a passively mode-locked fiber laser operating in solitonic regime (one of the lasers developed in this thesis), in temporal and spectral domain. A linear phase of the spectrum is clearly seen in figure 3.4 (b). The temporal and spectral shapes correspond to the theoretical pulse solution of the mode-locked equation under saturable absorber effects, which has the expression [24]:

$$A = A_0 \operatorname{sech}\left(\frac{T}{\tau}\right)^{1+j\beta}. \tag{3.3}$$

The hyperbolic secant pulse of equation (3.3) has a pulse duration τ, a pulse amplitude A_0 and a chirp parameter β.

The NLSE is solved using the split-step Fourier transform method [25]. Linear effects in NLSE such as dispersion are easily treated in the frequency domain, whereas nonlinear interactions are often (but not always) more conveniently handled in the

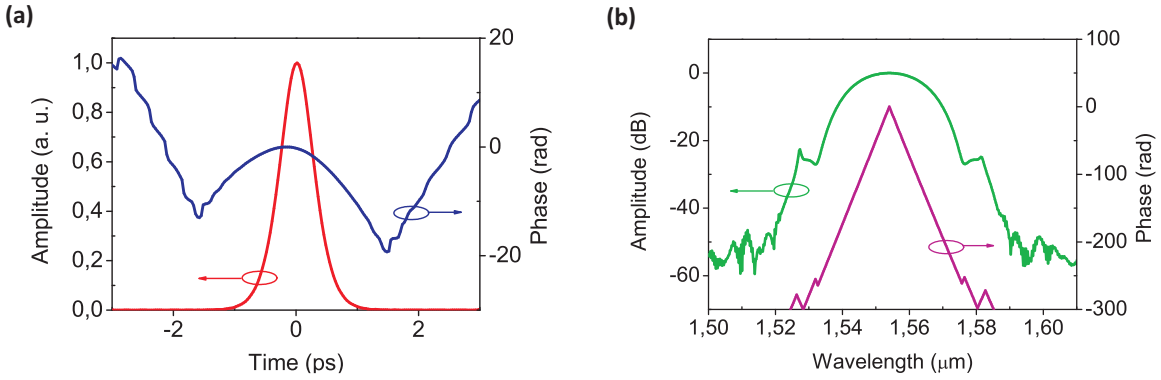

Figure 3.4: Calculated pulse for a passively mode-locked fiber laser. (a) Temporal amplitude and phase. (b) Magnitude and phase of the pulse spectrum.

time domain. Whenever required, switching between both domains can be done with a fast Fourier transform algorithm. The (weak) dispersive and nonlinear effects corresponding to short pieces of fiber are alternately applied. The numerical errors associated with the finite longitudinal step size are minimized with a special symmetrization technique, which allows for higher accuracies without excessively increased computation times.

Numerical calculations in mode-locked fiber ring lasers have been carried out propagating an optical pulse through the different fiber sections. When the optical pulse reach the end on the last fiber section (i. e., it completes a roundtrip), then it is injected to the first section again, to start with the next roundtrip. This process is repeated until a steady-state solution is obtained. NLSE computes the propagation of optical pulses through optical fibers. The rest of components of the fiber laser, such as intensity modulators, saturable absorbers and so on, have been modelled locally. For instance, the effects of a Mach-Zehnder modulator are applied to the propagating pulse through the following insertion losses expression:

$$IL_{MZM}(\omega_{RF}) = IL_{MZM\,0} + M\left(1 - \cos\left(\omega_{RF}T\right)\right), \tag{3.4}$$

where $IL_{MZM\,0}$ are the insertion losses in decibels of the MZM, M is the modulation depth, and ω_{RF} is the modulation angular frequency.

3.3 Fiber laser with intracavity polarizing fibers

In the previous section, active and passive mode-locking employing intensity modulators and saturable absorbers have been described. For the passive mode-locked fiber laser scheme, the use of intracavity sections of polarizing fiber has been studied. The initial purpose of using polarizing fiber in a ring cavity was the mode-locking through nonlinear polarization rotation mechanism. NLPR fiber lasers usually use bulk polarizers, necessitating the coupling between fiber and bulk segments and also inducing insertion loss. The use of polarizing fibers avoids this coupling stage [26, 27].

A polarizing (PZ) fiber, also known as single-polarization fiber, is an optical fiber which presents different propagation losses depending on the light polarization state. 45º tilted fiber Bragg gratings have demonstrated to constitute high-bandwidth all-fiber polarizers [27]. Another way to implement single-polarization comprises a fiber optical design that only supports guidance in one polarization state for a given bandwidth or, in other words, the cut-off frequencies for both orthogonal polarizations have to be highly distanced. Bow-tie high-birefringence and high-elliptical cladding fibers can exhibit this kind of single-polarization guidance [28, 29]. In this thesis we have used the latter one, being commercially available and ready to splice with standard single mode fibers.

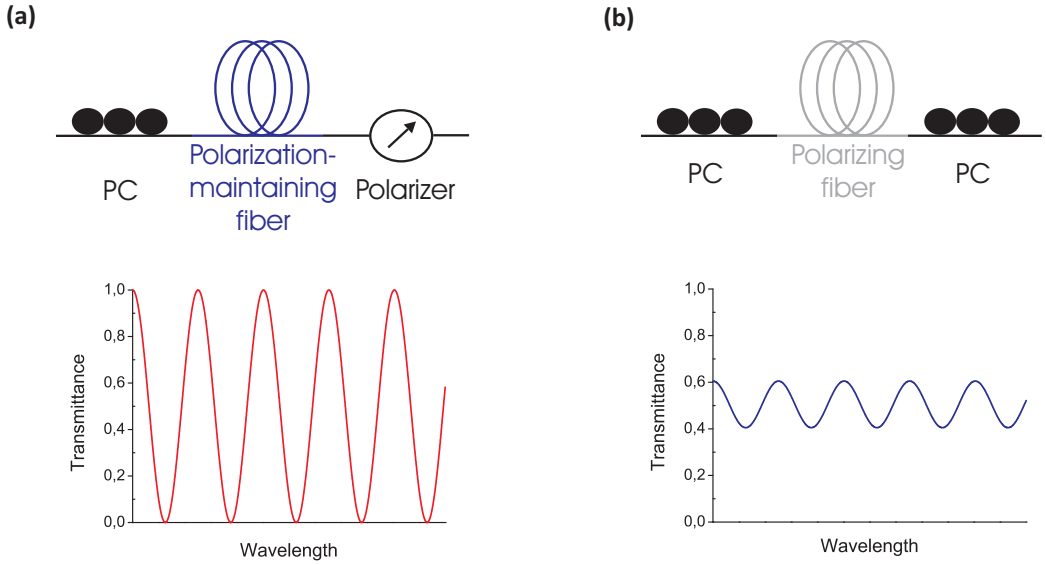

Figure 3.5: (a) Lyot filter scheme (up) and spectral response for a $\pi/4$ orientation between PM fiber birefringence axis and polarizer axis (down). (b) Polarizing fiber scheme (up) and spectral response (down). Spectral filtering is dependent on the polarizing ratio.

The insertion of a section of polarizing fiber in a ring cavity yields a polarization dependent loss, promoting single-polarization laser emission. In addition, the high-elliptical cladding polarizing fiber is highly birefringent, so orthogonal polarization components are not only unequally attenuated, but also are propagated with different velocities. The combination of high birefringence fibers and polarizers can result in a periodic spectral filter, known as fiber Lyot filter [30]. Traditional fiber Lyot filters are built from a polarization controller, a polarization-maintaining (PM) fiber and a polarizer (see figure 3.5 (a)). The filter depth depends on the angle formed by the polarizer angle and the PM birefringent angle, being maximum for a $\pi/4$ orientation. The periodicity of the filter is defined by the length and the birefringence of the PM fiber. In our laser proposal, the action of the PZ fiber also induces spectral filtering, but the polarizing fiber principle is not exactly the same as the Lyot filter.

The key difference between the polarizing fiber and a Lyot fiber is the polarizing ratio. A Lyot filter works with an ideal polarizer, i. e., with an infinite extinction ratio. The polarization-dependent loss of the PZ fiber is proportional to the PZ fiber length, and the extinction ratio is intentionally finite and much lower than conventional polarizers. In our cavity, two polarization controllers are allocated asides the polarizing fiber, as figure 3.5 (b) shows. It is possible to analyze the equivalent system of a high birefringence fiber, a polarizer with a finite extinction ratio (and the polarizing axis aligned with the birefringence axis of the fiber), and a polarization controller using the Jones matrix formalism. Taking their Jones matrix expressions as follows:

High birefringence fiber: $PM = \begin{pmatrix} 1 & 0 \\ 0 & e^{-j\Delta\varphi} \end{pmatrix}$, (3.5)

polarizer with finite extinction ratio: $PZ = \begin{pmatrix} 1 & 0 \\ 0 & \tau \end{pmatrix}$, (3.6)

polarization controller: $PC = \begin{pmatrix} \cos(\theta)e^{j\frac{\Delta\phi}{2}} & \sin(\theta)e^{j\frac{\Delta\phi}{2}} \\ -\sin(\theta)e^{-j\frac{\Delta\phi}{2}} & \cos(\theta)e^{-j\frac{\Delta\phi}{2}} \end{pmatrix}$, (3.7)

where $\Delta\varphi$ denotes the linear phase shift between two polarization components induced by the fiber, θ and $\Delta\phi$ are the rotation angle and the phase shift between components introduced by the polarization controller respectively, and τ represents the polarizing losses. The power transmission for the x component is:

$$|T_x|^2 = \cos^2(\theta) + \tau^2 \sin^2(\theta) + \tau \sin(2\theta)\cos(\Delta\varphi). \tag{3.8}$$

The last term represents the filtering effect, weighted by the polarizing losses τ. In comparison with the Lyot filter response, the filtering depth of the PZ fiber is determined by the polarizing extinction ratio, fixed by the length of the PZ fiber, and by the polarization controller angle θ. The maximum filtering depth is τ. This weak effect will be responsible for, under certain angles of both polarization controllers, a multiwavelength spectral emission with separation between modes dependent on the birefringence and the length of the polarizing fiber. For the fiber length used in experiments, the spectral separation is in the range of 100 GHz.

Besides, the elliptical cladding polarizing fiber also exhibits dispersion birefringence, i. e., different chromatic dispersion for each orthogonal polarization. Thus adjusting the input polarization state will also provide a control in the dispersion introduced by the polarizing fiber. This effect will be useful for our mode-locked laser, as pulse propagation under soliton regime is sensible to the cavity net dispersion. In conjunction with the weak spectral filtering effect, the PZ fiber will allow operating regimes of high and low dispersion solitonic regimes, and a 100 GHz multiwavelength regime. This last one is equivalent to a harmonic multiplication of the pulse repetition frequency thanks to the spectral filtering.

The numerical calculations carried out for this scheme cannot use the scalar NLSE (3.2) any longer. Instead, two orthogonal polarizations have to be taken into account; therefore the coupled nonlinear Schrödinger equations (CNLSE) must be solved. These equations take the form

$$\left(\frac{\partial}{\partial z}+\beta_{1x}\frac{\partial}{\partial t}+j\frac{\beta_{2x}}{2}\frac{\partial^2}{\partial t^2}+\frac{\alpha_x}{2}-\frac{g}{2}-\frac{D_g}{2}\frac{\partial^2}{\partial t^2}\right)A_x = j\gamma\left(|A_x|^2+\frac{2}{3}|A_y|^2\right)A_x+j\frac{\gamma}{3}A_x^*A_y^2e^{-j2\Delta\beta_0 z}, \tag{3.9a}$$

$$\left(\frac{\partial}{\partial z}+\beta_{1y}\frac{\partial}{\partial t}+j\frac{\beta_{2y}}{2}\frac{\partial^2}{\partial t^2}+\frac{\alpha_y}{2}-\frac{g}{2}-\frac{D_g}{2}\frac{\partial^2}{\partial t^2}\right)A_y = j\gamma\left(|A_y|^2+\frac{2}{3}|A_x|^2\right)A_y+j\frac{\gamma}{3}A_y^*A_x^2e^{j2\Delta\beta_0 z}, \tag{3.9b}$$

Now, both slow-varying envelopes A_x and A_y are propagated, representing the two linear orthogonal polarizations. In comparison to the scalar NLSE shown in equation (3.2), the temporal variable is not normalized to the group velocity since in birefringent mediums the group velocities differ from ortoghonal polarizations. Medium birefringence is denoted by the modal birefringence $\Delta\beta_0 = \beta_{0x} - \beta_{0y}$, group birefringence β_{1i} and dispersion birefringence β_{2i}, for $i = x, y$. Note the explicit polarization dependence of optical losses α_i and chromatic dispersion β_{2i}, aimed to properly model the PZ fiber of the cavity. Polarization controllers will be locally modelled by three waveplates ($\lambda/4$ - $\lambda/2$ - $\lambda/4$) through their Jones matrix. The rest of considerations of the scalar case are applicable for the CNLSE resolution.

3.4 Carbon nanotube-based saturable absorbers

Intensity-dependent cavity loss is the fundamental mechanism to passively mode-locking fiber lasers. Several options can produce intensity-dependent losses, like nonlinear polarization rotation or the use of saturable absorbers. The most common saturable absorbers used in mode-locked fiber lasers are semiconductor SAs. Recently, effective saturable absorption is being reported in new materials, such as carbon nanotubes (CNTs). CNTs have proven to be a highly nonlinear optical material, with ultrafast response, and wide bandwidth, suitable for passive mode-locking [11]. Several passive mode-locked fiber lasers using carbon nanotubes have been published in the last years [31–36], showing a great potential as nonlinear material in the near infrared (NIR).

Carbon nanotubes are allotropes of carbon with a cylindrical nanostructure. A common view of the CNT structure is imagining a one-atom-thick sheet of carbon atomes, known as graphene, which is rolled to form a cylinder (see figure 3.6 left). The cylinder diameter ranges few nanometers, and its length is usually about hundreds of micrometers. These dimensions provide very large aspect ratios, so carbon nanotubes perform as one dimensional material. CNTs exhibit remarkable electrical conductivities (1,000 times greater than copper) [37], mechanical (tensile strength

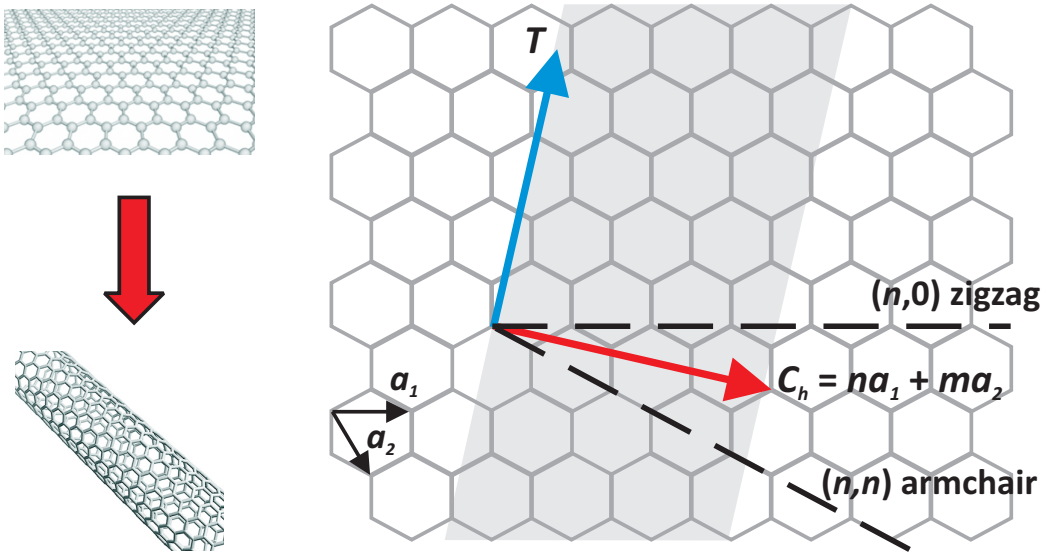

Figure 3.6: Carbon nanotube chirality. The rolling angle of the graphene sheet defines the nanotube chirality, and indexes (n, m) determine it through the grid basis $\boldsymbol{a_1}$ and $\boldsymbol{a_2}$.

100 times greater than stainless steel) [38] and thermal properties (thermal conductivity 10 times greater than copper) [39]. The one dimensional nanotube structure also provides interesting optical properties. CNTs can be categorized as single-walled nanotubes (SWNT) and multi-walled nanotubes (MWNT). The former consist of only one graphene layer, while the latter have several concentric graphene layers. In our optical nonlinear application, we will focus on single walled nanotubes.

There are infinite possible combinations of rolling a graphene sheet to form a carbon nanotube. The rolling angle defines the chirality of the nanotube. Figure 3.6 right illustrates this concept. A hexagonal grid represents the graphene sheet, where each vertex represents a carbon atom. The chirality vector $\boldsymbol{C_h}$ is equivalent to the circumference of the nanotube, establishing how the sheet is rolled up. The longitudinal nanotube axis is represented by the vector $\boldsymbol{T}$. If we set a grid basis through the unitary vectors $\boldsymbol{a_1}$ and $\boldsymbol{a_2}$, it is possible to express the chirality through two indexes (n, m) as

$$\boldsymbol{C_h} = n\boldsymbol{a_1} + m\boldsymbol{a_2}. \tag{3.10}$$

Tubes having $n = m$ (chiral angle = 30°) are called "armchair" and those with $m = 0$ (chiral angle = 0°) "zigzag". Given a pair of indexes, it is easy to calculate the nanotube diameter through the expression

$$d = \frac{|\boldsymbol{C_h}|}{\pi} = \frac{a}{\pi}\sqrt{n^2 + nm + m^2}, \tag{3.11}$$

where a denotes the modulus of vectors $\boldsymbol{a_1}$ and $\boldsymbol{a_2}$, and is equal to 0.246 nm. De-

pending on the index pair, a carbon nanotube behaves as a metal or a semiconductor. Metallic nanotube chiralities fulfill the relation $n-m = 3k$ (k integer), while semiconducting nanotube chiralities obey $n-m \neq 3k$. Due to their one dimensional structure, carbon nanotubes present discontinuities in their density of states (DOS), called Van Hove singularities. Optical transitions occur between Van Hove singularities appearing at the conduction (c_1, c_2, ...) and valence (v_1, v_2, ...) bands, generally for v_1-c_1, v_2-c_2, ... states, as cross-over transitions ($v_p - c_q$, $p \neq q$) are dipole-forbidden and thus are extremely weak. Bandgap energies are directly related to the structure of the carbon nanotube, consequently, it is relatively easy to selectively excite nanotubes having certain (n, m) indexes, as well as to detect optical signals from individual nanotubes. A useful tool to identify carbon nanotubes is the Kataura plot [40], which relates the nanotube diameter and its bandgap energies for all nanotubes in a diameter range.

Corresponding to optical bangaps, semiconducting SWNTs show optical absorption spectral peaks. The wavelength of the absorption peaks depends on the nanotube diameters. Typical nanotube diameters in a sample range 0.7-1.5 nm and exhibit bandgap energies within 1.2-0.6 eV, corresponding to the optical wavelength of 1-2 μm. This wavelength range is suitable for most photonic applications, and can be tuned by choosing a proper diameter. Nevertheless, selective growth of one particular chirality of semiconducting nanotubes is not yet possible with the current fabrication processes. Therefore, the sample is always a mixture of several or many kinds of semiconducting and metallic CNTs. Chirality distribution is determined by the fabrication method, and mean tube diameter is controllable by fabrication conditions in some extent. A random distribution of tube diameters provides a wide bandwidth of saturable absorbance, being beneficial for passive mode-locking applications.

3.4.1 Nonlinear optical properties

Similar to semiconductor saturable absorbers, the optical absorption of SWNT can saturate with high-intensity light since the possible states at conduction band become full and those at valence band empty. However, the temporal response of CNTs is inherently faster than semiconductor materials, with recovery times of hundreds of femtoseconds [41]. In addition, third-order nonlinearities $\chi^{(3)}$ responsible for saturable absorption and Kerr effect are reported to be very high due to the resonant nature of nanotubes. Theoretically predicted $\Re(\chi^{(3)})$ under the resonance condition is as high as $\sim 10^{-6}$ esu, which corresponds to the nonlinear refractive index $n_2 \sim 2 \cdot 10^{-8}$ cm^2/W [42], although it is highly wavelength dependent. This is an extremely high third-order nonlinearity, compared with other optical materials, such as silica glass ($n_2 \sim 3 \cdot 10^{-16}$ cm^2/W) and silicon ($n_2 \sim 4 \cdot 10^{-14}$ cm^2/W), and with highly nonlinear polymer composites like PTS ($n_2 \sim 3 \cdot 10^{-12}$ cm^2/W) and polydiacetylene 9-BCMU ($n_2 \sim 1.9 \cdot 10^{-10}$ cm^2/W).

In nonlinear optics field, the nonlinear coefficient γ is used to express the accumulated nonlinear phase suffered by a propagating optical signal per optical power and

distance, and it is expressed as

$$\gamma = \frac{2\pi n_2}{\lambda_0 A_{eff}}, \tag{3.12}$$

where λ_0 and A_{eff} are the wavelength of light and effective area respectively. The nonlinear refractive index coefficient $2{\cdot}10^{-8}$ cm^2/W of CNTs results in a γ coefficient of $1.0134{\cdot}10^8$ W^{-1}km^{-1}. Here, it is assumed $A_{eff} = 80\ \mu$m^2, which is a typical value for single mode optical fibers. This nonlinear coefficient is substantially high compared to commercially available highly nonlinear fibers and nonlinear photonic crystal fibers, with coefficients around 10 W^{-1}km^{-1} [43, 44]. High nonlinear coefficients and fast response times are usually in trade-off relation. Typically, optical fiber nonlinearities, like Kerr effect, have fast responses with low nonlinear coefficient. On the other hand, semiconductor based devices have high nonlinear coefficients with slower response times. CNTs posses a much higher nonlinear coefficient with ultrafast response due to their nanostructures and bundled conditions.

The high third-order nonlinearity of SWNTs at optical frequencies has made this nanocomposite an ideal candidate for passive mode-locking and ultrafast all-optical switching. Several mode-locked fiber lasers using nanotubes have been proposed in the last years. Compared to semiconductor absorbers, not only the nonlinear temporal response of SWNTs is faster, but the optical bandwidth is exceedingly wider, due to the random nanotube diameter distribution explained previously. Passive mode-locking of three different fiber lasers (Yb-, Er- and Tm:Ho-doped emitting at 1.05, 1.56 and 1.99 μm respectively) using a single SWCNT sample has been demonstrated [45]. CNT-based absorbers can be fabricated to operate both in transmission or reflection, which allows the use of either ring or linear cavity configuration [31]. Integration of nanotubes in optical cavities has been approached with different techniques, such as free-space [31, 46], fiber-end [47], waveguide [48], and fiber structures [49–51].

Another advantage of SWNTs for photonics applications is their possible combination with integrated devices. Light propagating through waveguides covered with an external layer of CNTs experiences high third-order nonlinearity in short lengths, resulting in compact nonlinear optical devices. Planar waveguides loaded with carbon nanotubes have proven all-optical ultrafast switching effects [52]. Also, Four-Wave Mixing (FWM) has been demonstrated in a similar structure, showing potential application in high-bit-rate wavelength conversion applications [53]. Integration of CNTs in photonic circuits opens a promising technology in which carbon nanotubes cannot only be exploited as nonlinear materials, but also as light emitters [54] and photodetectors [55].

3.4.2 Fabrication and characterization of CNT-based fiber devices

The ultrafast saturable absorption characteristics of SWNTs have led to their use in passive mode-locked lasers. In fiber lasers, integration of nanotubes in the fiber cavity is the most challenging part. Some techniques used for incorporating nanotubes in fiber cavities are:

- CNT composite polymers [56].
- CNT deposition on D-shaped fibers [57].
- Fiber microchannels filled with CNTs [58].
- CNT selective deposition on fiber ends [59].
- Hollow fibers filled with CNTs [60].
- CNT deposition in tapered fibes [61].

D-shaped, hollow and tapered optical fibers have been proposed to take advantage of the evanescent field interaction with SWNTs, distributing that interaction along the fiber length. The distributed interaction overcomes some inherent drawbacks of intracavity transversal CNT films configurations, such as need for alignment and focusing stages, low CNT burn thresholds, and low nonlinear interaction length. Nevertheless, these techniques require special optical fiber, which are quite fragile and complex to handle. In this thesis we present an innovative technique to allow a distributed interaction of light with CNTs in standard optical fibers. The proposed technique makes use of tilted fiber Bragg gratings (TFBG) to allow propagating light to couple to the outer fiber medium.

A TFBG is a fiber Bragg grating in which the index modulation planes are not orthogonal to the fiber axis but form a particular tilt angle. Figure 3.7 (a) depicts the structure of a TFBG. The plane inclination enhances the coupling of light from core mode to counter-propagating cladding mode resonances. Consequently, the grating transmission response is a multinotch response consisting of numerous cladding mode resonances in addition to the core mode resonance, as figure 3.7 (b) illustrates. In conventional FBGs, the core mode resonance wavelength (Bragg wavelength) is directly related to the grating period Λ (see equation (2.2) on page 24). In the case of a TFBG, the core mode resonance frequency is

$$\lambda_{Bragg} = 2n_{eff}\frac{\Lambda}{\cos(\theta)}, \tag{3.13}$$

where the actual grating period Λ is projected along the fiber axis due to the tilt angle θ. Cladding mode resonance frequencies can be obtained through the following expression [62]:

$$\lambda_{Cladding}(i) = (n_{eff}(i) + n_C(i)) \frac{\Lambda}{\cos(\theta)}, \tag{3.14}$$

being $n_{eff}(i)$ the effective index of the core mode at the wavelength of the ith cladding-mode resonance, and $n_C(i)$ is the cladding-mode effective index at the same wavelength. Then, when light is injected to a TFBG with a wavelength equal to $\lambda_{Cladding}(i)$, then it will couple to the counter-propagating cladding mode i, with a coupling strength determined by diverse factors as grating length, modulation depth, etc. The counter-propagating energy travels with a cladding mode profile, so its mode profile is not further confined to the fiber core, but extents to the cladding, and can interact with the external medium. This interaction has been exploited in multiple sensing applications [63]. We make use of cladding mode resonances in this chapter to allow interaction of light propagating through the fiber core with carbon nanotubes. For this purpose, an external layer of CNTs will be deposited on an optical fiber with a TFBG written in it. Two techniques of CNT deposition have been studied. The first one consisted of dip-coating of the optical fiber in a SWNT suspension, and the sec-

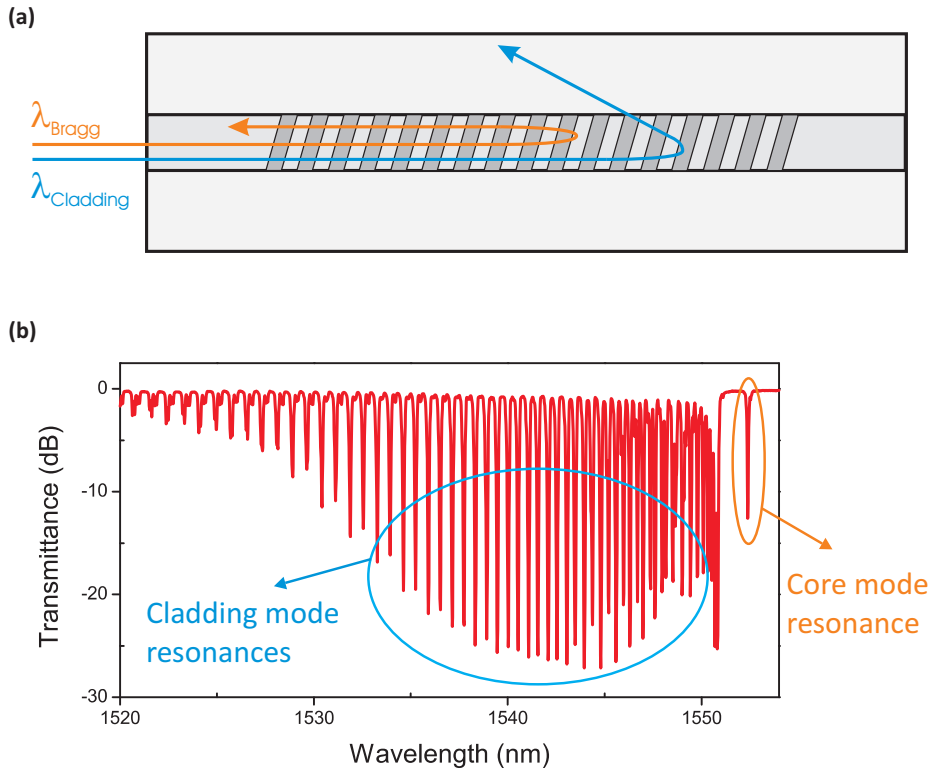

Figure 3.7: (a) Tilted fiber Bragg grating structure. (b) Linear transmission response of a 4 deg tilted fiber Bragg grating.

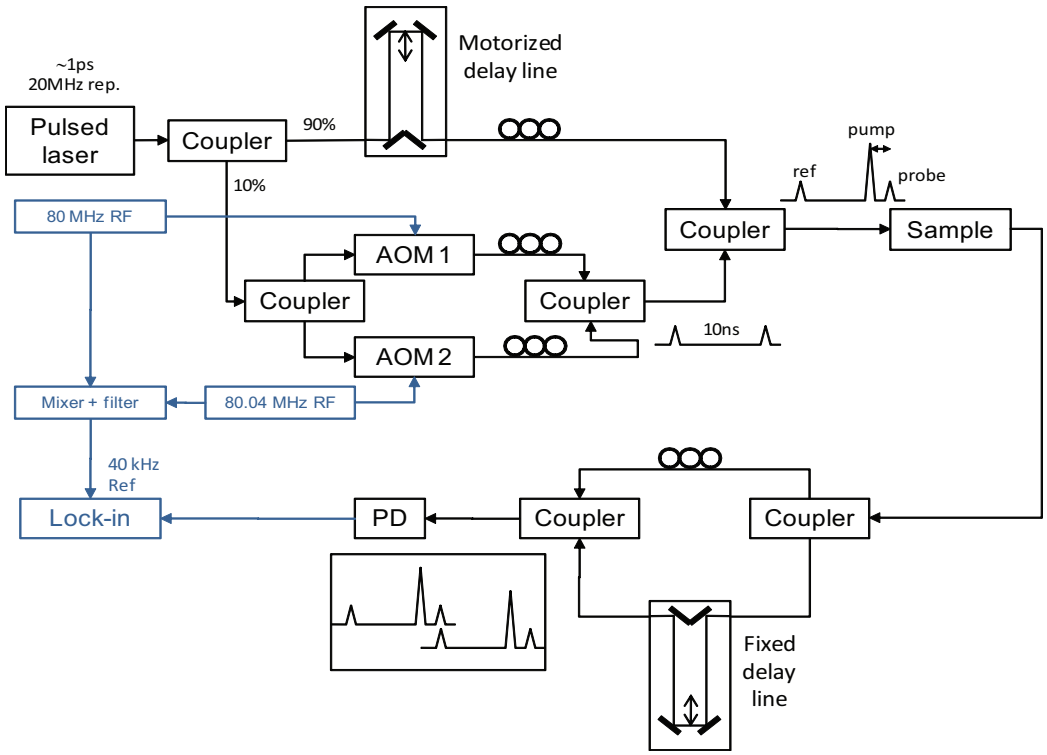

Figure 3.8: Pump-probe phase sensitive set-up. Before the sample the input train consists of a probe, a pump and a reference pulse. After transmitting through the sample, the reference and probe pulses are beaten in time and the beating reference signal is detected by a lock-in amplifier.

ond one was based on wrapping of a SWNT film around the optical fiber. Dip-coating provided a thinner and more homogeneous layer of SWNTs on the fiber. In contrast, the wrapping technique produced a much thicker coating, but with less control of the uniformity of the wrapping.

Effective nonlinear interaction of injected light with SWNTs is demonstrated by a pump-probe phase-sensitive experiment [64]. This nonlinear effect cannot be characterized through continuous wave set-ups like common FWM characterization setups, as intense CW signals produce an overheating of the whole structure, and the cladding mode spectral shifts observed are due to thermal effects, hiding actual CNT nonlinear effects. Even more, CW intense signals can damage the CNT outer layer. For this reason, it is necessary an optical pulsed set-up, able to provide an optical signal with low average powers and high peak powers, of levels ranging kW, suitable for nonlinear excitation.

The set-up employed is shown in figure 3.8. An initial optical pulse is processed to obtain a three-pulse train; a pump, a probe and a reference pulse. The reference and the probe pulses are modulated by means of acusto-optic modulators with slightly different frequencies, in our case, with 80 and 80.04 MHz. This pulse train is launched to the sample, the CNT-coated TFBG, after optimization of the pump, probe and reference polarization states. After the sample, the optical train enters an interferometer

in order to beat the reference and the probe pulses. The difference frequency component of 40 kHz is detected through a lock-in amplifier. With this setup, the reference pulse passes through the sample without exciting nonlinear effects. Then, the pump probe with a high intensity interacts with the optical fiber external layer through cladding mode resonance coupling, exciting the nonlinearities of the CNT layer. Finally, a probe pulse propagates through the sample under the excited nonlinearities, experiencing a different propagation compared to the reference pulse. Changes of amplitude and phase of the probe pulse results in measured changes of phase and amplitude of the 40 kHz beat note. A delay line in the pump pulse path allows the nonlinear temporal response capture. All the setup is based on optical fiber, without any free-space stage requirement, and the effective temporal resolution is set by the laser pulse width of 1 ps.

Bibliography

[1] C. L. Thomsen, D. Madsen, S. R. Keiding, J. T. Gersen, and O. Christiansen, "Two-photon dissociation and ionization of liquid water studied by femtosecond transient absorption spectroscopy," *The Journal of Chemical Physics*, vol. 110, no. 7, pp. 3453–3462, 1999.

[2] T. Udem, R. Holzwarth, and T. W. Hänsch, "Optical frequency metrology," *Nature*, vol. 416, pp. 233–237, 2002.

[3] L. A. Jiang, E. P. Ippen, and H. Yokoyama, "Semiconductor mode-locked lasers as pulse sources for high bit rate data transmission," *Journal of Optical and Fiber Communications Research*, vol. 2, pp. 1–31, 2005, 10.1007/s10297-004-0022-0.

[4] P. U. Jepsen, R. H. Jacobsen, and S. R. Keiding, "Generation and detection of terahertz pulses from biased semiconductor antennas," *Journal of the Optical Society of America B*, vol. 13, no. 11, pp. 2424–2436, Nov. 1996.

[5] H. N. Paulsen, K. M. Hilligse, J. Thøgersen, S. R. Keiding, and J. J. Larsen, "Coherent anti-Stokes Raman scattering microscopy with a photonic crystal fiber based light source," *Optics Letters*, vol. 28, no. 13, pp. 1123–1125, Jul. 2003.

[6] I. Hartl, X. D. Li, C. Chudoba, R. K. Ghanta, T. H. Ko, J. G. Fujimoto, J. K. Ranka, and R. S. Windeler, "Ultrahigh-resolution optical coherence tomography using continuum generation in an air–silica microstructure optical fiber," *Optics Letters*, vol. 26, no. 9, pp. 608–610, May 2001.

[7] P. Weigl, A. Kasenbacher, and K. Werelius, "Dental applications," in *Femtosecond Technology for Technical and Medical Applications*, ser. Topics in Applied Physics, F. Dausinger, H. Lubatschowski, and F. Lichtner, Eds. Springer Berlin / Heidelberg, 2004, vol. 96, pp. 167–187.

[8] A. Tünnermann, J. Limpert, and S. Nolte, "Ultrashort pulse fiber lasers and amplifiers," in *Femtosecond Technology for Technical and Medical Applications*, ser. Topics in Applied Physics, F. Dausinger, H. Lubatschowski, and F. Lichtner, Eds. Springer Berlin / Heidelberg, 2004, vol. 96, pp. 35–54.

[9] D. Breitling, C. Föhl, F. Dausinger, T. Kononenko, and V. Konov, "Drilling of metals," in *Femtosecond Technology for Technical and Medical Applications*, ser.

Topics in Applied Physics, F. Dausinger, H. Lubatschowski, and F. Lichtner, Eds. Springer Berlin / Heidelberg, 2004, vol. 96, pp. 131–156.

[10] G. C. Valley, "Photonic analog-to-digital converters," *Optics Express*, vol. 15, no. 5, pp. 1955–1982, Mar. 2007.

[11] S. Yamashita, "A tutorial on nonlinear photonic applications of carbon nanotube and graphene," *Lightwave Technology, Journal of*, vol. 30, no. 4, pp. 427 –447, Feb. 2012.

[12] E. Jacobs, J. Sobti, V. Vella, R. Nguyen, D. Albares, R. Olsen, C. Chang, S. Sun, M. Choe, S. Beccue, R. Yu, and J. van der Wagt, "Optically clocked track-and-hold for high-speed high-resolution analog-to-digital conversion," in *Microwave Photonics, 2004. MWP'04. 2004 IEEE International Topical Meeting on*, Oct. 2004, pp. 190 – 192.

[13] R. Williamson, R. Younger, P. Juodawlkis, J. Hargreaves, and J. Twichell, "Precision calibration of an optically sampled analog-to-digital converter," in *Holey Fibers and Photonic Crystals/Polarization Mode Dispersion/Photonics Time/Frequency Measurement and Control, 2003 Digest of the LEOS Summer Topical Meetings*, Jul. 2003, pp. MC4.2/22 – MC4.2/23.

[14] M. Piqueras, P. Villalba, J. Puche, and J. Martí, "High performance photonic ADC for space and defence applications," in *Microwaves, Communications, Antennas and Electronics Systems (COMCAS), 2011 IEEE International Conference on*, Nov. 2011, pp. 1 – 6.

[15] J. D. Kafka, T. Baer, and D. W. Hall, "Mode-locked erbium-doped fiber laser with soliton pulse shaping," *Optics Letters*, vol. 14, no. 22, pp. 1269–1271, Nov. 1989.

[16] L. Schares, R. Paschotta, L. Occhi, and G. Guekos, "40-GHz mode-locked fiber-ring laser using a Mach-Zehnder interferometer with integrated SOAs," *Lightwave Technology, Journal of*, vol. 22, no. 3, p. 859, Mar. 2004.

[17] F. O. Ilday and F. W. Wise, "Nonlinearity management: A route to high-energy soliton fiber lasers," *Journal of the Optical Society of America B*, vol. 19, no. 3, pp. 470–476, Mar. 2002.

[18] H. Haus, "Mode-locking of lasers," *Selected Topics in Quantum Electronics, IEEE Journal of*, vol. 6, no. 6, pp. 1173 –1185, Nov./Dec. 2000.

[19] F. Ilday, J. Buckley, L. Kuznetsova, and F. Wise, "Generation of 36-femtosecond pulses from a ytterbium fiber laser," *Optics Express*, vol. 11, no. 26, pp. 3550–3554, Dec. 2003.

[20] I. Jung, F. Kärtner, N. Matuschek, D. Sutter, F. Morier-Genoud, Z. Shi, V. Scheuer, M. Tilsch, T. Tschudi, and U. Keller, "Semiconductor saturable

absorber mirrors supporting sub-10-fs pulses," *Applied Physics B: Lasers and Optics*, vol. 65, pp. 137–150, 1997.

[21] U. Keller, "Recent developments in compact ultrafast lasers," *Nature*, vol. 424, pp. 831–838, 2003.

[22] http://www.batop.de.

[23] G. P. Agrawal, *Nonlinear Fiber Optics, third ed.* San Diego, CA: Academic Press, 2001.

[24] H. A. Haus, J. G. Fujimoto, and E. P. Ippen, "Structures for additive pulse mode locking," *J. Opt. Soc. Am. B*, vol. 8, no. 10, pp. 2068–2076, Oct. 1991.

[25] R. H. Hardin and F. D. Tappert, "Applications of the split-step Fourier method to the numerical solution of nonlinear and variable coefficient wave equation," *SIAM Review Chronicles*, vol. 15, p. 423, 1973.

[26] D. Panasenko, P. Polynkin, A. Polynkin, J. Moloney, M. Mansuripur, and N. Peyghambarian, "Er-Yb femtosecond ring fiber oscillator with 1.1-W average power and GHz repetition rates," *Photonics Technology Letters, IEEE*, vol. 18, no. 7, pp. 853 –855, 2006.

[27] C. Mou, H. Wang, B. G. Bale, K. Zhou, L. Zhang, and I. Bennion, "All-fiber passively mode-locked femtosecond laser using a 45°-tilted fiber grating polarization element," *Optics Express*, vol. 18, no. 18, pp. 18 906–18 911, Aug. 2010.

[28] http://www.fibercore.com.

[29] http://www.verrillon.com.

[30] W. S. Man, H. Y. Tam, M. S. Demokan, P. K. A. Wai, and D. Y. Tang, "Mechanism of intrinsic wavelength tuning and sideband asymmetry in a passively mode-locked soliton fiber ring laser," *Journal of the Optical Society of America B*, vol. 17, no. 1, pp. 28–33, Jan. 2000.

[31] S. Set, H. Yaguchi, Y. Tanaka, and M. Jablonski, "Ultrafast fiber pulsed lasers incorporating carbon nanotubes," *IEEE Journal of Selected Topics in Quantum Electronics*, vol. 10, no. 1, pp. 137–146, Feb. 2004.

[32] J. Nicholson and D. DiGiovanni, "High-repetition-frequency low-noise fiber ring lasers mode-locked with carbon nanotubes," *Photonics Technology Letters, IEEE*, vol. 20, no. 24, pp. 2123 –2125, Dec. 2008.

[33] A. G. Rozhin, Y. Sakakibara, S. Namiki, M. Tokumoto, H. Kataura, and Y. Achiba, "Sub-200-fs pulsed erbium-doped fiber laser using a carbon nanotube-polyvinylalcohol mode locker," *Applied Physics Letters*, vol. 88, no. 5, p. 051118, 2006.

[34] A. V. Tausenev, E. D. Obraztsova, A. S. Lobach, A. I. Chernov, V. I. Konov, P. G. Kryukov, A. V. Konyashchenko, and E. M. Dianov, "177 fs erbium-doped fiber laser mode locked with a cellulose polymer film containing single-wall carbon nanotubes," *Applied Physics Letters*, vol. 92, no. 17, p. 171113, 2008.

[35] F. Shohda, T. Shirato, M. Nakazawa, J. Mata, and J. Tsukamoto, "147 fs, 51 MHz soliton fiber laser at 1.56 μm with a fiber-connector-type SWNT/P3HT saturable absorber," *Optics Express*, vol. 16, no. 25, pp. 20 943–20 948, Dec. 2008.

[36] Y.-W. Song, S. Yamashita, and S. Maruyama, "Single-walled carbon nanotubes for high-energy optical pulse formation," *Applied Physics Letters*, vol. 92, no. 2, p. 021115, 2008.

[37] S. Hong and S. Myung, "Nanotube Electronics: A flexible approach to mobility," *Nature Nanotechnology*, vol. 2, pp. 207–208, 2007.

[38] M. Meo and M. Rossi, "Prediction of Young's modulus of single wall carbon nanotubes by molecular-mechanics based finite element modelling," *Composites Science and Technology*, vol. 66, pp. 1597 – 1605, 2006.

[39] E. Pop, D. Mann, Q. Wang, K. Goodson, and H. Dai, "Thermal conductance of an individual single-wall carbon nanotube above room temperature," *Nano Letters*, vol. 6, no. 1, pp. 96–100, 2006.

[40] H. Kataura, Y. Kumazawa, Y. Maniwa, I. Umezu, S. Suzuki, Y. Ohtsuka, and Y. Achiba, "Optical properties of single-wall carbon nanotubes," *Synthetic Metals*, vol. 103, pp. 2555 – 2558, 1999.

[41] J.-S. Lauret, C. Voisin, G. Cassabois, C. Delalande, P. Roussignol, O. Jost, and L. Capes, "Ultrafast carrier dynamics in single-wall carbon nanotubes," *Phys. Rev. Lett.*, vol. 90, p. 057404, Feb. 2003.

[42] V. Margulis and T. Sizikova, "Theoretical study of third-order nonlinear optical response of semiconductor carbon nanotubes," *Physica B: Condensed Matter*, vol. 245, no. 2, pp. 173 – 189, 1998.

[43] http://www.ofsoptics.com.

[44] http://www.nktphotonics.com.

[45] S. Kivistö, T. Hakulinen, A. Kaskela, B. Aitchison, D. P. Brown, A. G. Nasibulin, E. I. Kauppinen, A. Härkönen, and O. G. Okhotnikov, "Carbon nanotube films for ultrafast broadband technology," *Opt. Express*, vol. 17, no. 4, pp. 2358–2363, Feb. 2009.

[46] Y. Sakakibara, A. Rozhin, H. Kataura, Y. Achiba, and M. Tokumoto, "Carbon nanotube-poly(vinylalcohol) nanocomposite film devices: applications for femtosecond fiber laser mode lockers and optical amplifier noise suppressors," *Japanese Journal of Applied Physics*, vol. 44, pp. 1621–1625, 2005.

[47] T. Schibli, K. Minoshima, H. Kataura, E. Itoga, N. Minami, S. Kazaoui, K. Miyashita, M. Tokumoto, and Y. Sakakibara, "Ultrashort pulse-generation by saturable absorber mirrors based on polymer-embedded carbon nanotubes," *Opt. Express*, vol. 13, no. 20, pp. 8025–8031, Oct. 2005.

[48] K. Kashiwagi, S. Yamashita, Y. Nasu, H. Yaguchi, C. S. Goh, and S. Y. Set, "Planar waveguide-type saturable absorber based on carbon nanotubes," *Applied Physics Letters*, vol. 89, no. 8, pp. 081 125 –081 125–3, Aug. 2006.

[49] Y.-W. Song, S. Yamashita, C. S. Goh, and S. Y. Set, "Carbon nanotube mode lockers with enhanced nonlinearity via evanescent field interaction in d-shaped fibers," *Opt. Lett.*, vol. 32, no. 2, pp. 148–150, Jan. 2007.

[50] Y.-W. Song, K. Morimune, S. Y. Set, and S. Yamashita, "Polarization insensitive all-fiber mode-lockers functioned by carbon nanotubes deposited onto tapered fibers," *Applied Physics Letters*, vol. 90, no. 2, p. 021101, 2007.

[51] K. Kieu and M. Mansuripur, "Femtosecond laser pulse generation with a fiber taper embedded in carbon nanotube/polymer composite," *Opt. Lett.*, vol. 32, no. 15, pp. 2242–2244, Aug. 2007.

[52] K. Kashiwagi, S. Yamashita, H. Yaguichi, C. S. Goh, and S. Y. Set, "All optical switching using carbon nanotubes loaded planar waveguide," in *Conference on Lasers and Electro-Optics/Quantum Electronics and Laser Science Conference and Photonic Applications Systems Technologies*. Optical Society of America, 2006, p. CMA5.

[53] K. K. Chow, S. Yamashita, and S. Y. Set, "Four-wave-mixing-based wavelength conversion using a single-walled carbon-nanotube-deposited planar lightwave circuit waveguide," *Opt. Lett.*, vol. 35, no. 12, pp. 2070–2072, Jun. 2010.

[54] E. Adam, C. M. Aguirre, L. Marty, B. C. St-Antoine, F. Meunier, P. Desjardins, D. Ménard, and R. Martel, "Electroluminescence from single-wall carbon nanotube network transistors," *Nano Letters*, vol. 8, no. 8, pp. 2351–2355, 2008.

[55] I. A. Levitsky and W. B. Euler, "Photoconductivity of single-wall carbon nanotubes under continuous-wave near-infrared illumination," *Applied Physics Letters*, vol. 83, no. 9, pp. 1857–1859, 2003.

[56] A. Martinez, S. Uchida, Y.-W. Song, T. Ishigure, and S. Yamashita, "Fabrication of Carbon nanotube poly-methyl-methacrylate composites for nonlinear photonic devices," *Optics Express*, vol. 16, no. 15, pp. 11 337–11 343, Jul. 2008.

[57] K. K. Chow and S. Yamashita, "Four-wave mixing in a single-walled carbon-nanotube-deposited D-shaped fiber and its application in tunable wavelength conversion," *Optics Express*, vol. 17, no. 18, pp. 15 608–15 613, Aug. 2009.

[58] A. Martinez, K. Zhou, I. Bennion, and S. Yamashita, "In-fiber microchannel device filled with a carbon nanotube dispersion for passive mode-lock lasing," *Optics Express*, vol. 16, no. 20, pp. 15 425–15 430, Sep. 2008.

[59] J. W. Nicholson, R. S. Windeler, and D. J. DiGiovanni, "Optically driven deposition of single-walled carbon-nanotube saturable absorbers on optical fiber end-faces," *Optics Express*, vol. 15, no. 15, pp. 9176–9183, Jul. 2007.

[60] S. Y. Choi, F. Rotermund, H. Jung, K. Oh, and D.-I. Yeom, "Femtosecond mode-locked fiber laser employing a hollow optical fiber filled with carbon nanotube dispersion as saturable absorber," *Optics Express*, vol. 17, no. 24, pp. 21 788–21 793, Nov. 2009.

[61] K. K. Chow, M. Tsuji, and S. Yamashita, "Single-walled carbon-nanotube-deposited tapered fiber for four-wave mixing based wavelength conversion," *Applied Physics Letters*, vol. 96, no. 6, p. 061104, 2010.

[62] G. Laffont and P. Ferdinand, "Tilted short-period fibre-Bragg-grating-induced coupling to cladding modes for accurate refractometry," *Measurement Science and Technology*, vol. 12, no. 7, p. 765, 2001.

[63] J. Albert, "Tilted fiber Bragg gratings as multi-sensors," *Optics and Photonics News*, vol. 22, no. 10, pp. 28–33, Oct. 2011.

[64] T. Vallaitis, C. Koos, R. Bonk, W. Freude, M. Laemmlin, C. Meuer, D. Bimberg, and J. Leuthold, "Slow and fast dynamics of gain and phase in a quantum dot semiconductor optical amplifier," *Optics Express*, vol. 16, no. 1, pp. 170–178, Jan. 2008.

Articles chapter 3

1. G. E. Villanueva, María Ferri, and P. Pérez-Millán, "Active and passive mode-locked fiber lasers for high-speed high-resolution photonic analog to digital conversion," *Quantum Electronics, IEEE Journal of*, vol. 48, no. 11, pp. 1443–1452, Nov. 2012.

2. G. E. Villanueva, and P. Pérez-Millán, "Dynamic control of the operation regimes of a mode-locked fiber laser based on intracavity polarizing fibers: experimental and theoretical validation," *Optics Letters*, vol. 37, no. 11, pp. 1971–1973, Jun. 2012.

3. G. E. Villanueva, M. B. Jakubinek, B. Simard, C. J. Oton, J. Matres, L.-Y. Shao, P. Pérez-Millán, and J. Albert, "Linear and nonlinear optical properties of carbon nanotube-coated single-mode optical fiber gratings," *Optics Letters*, vol. 36, no. 11, pp. 2104–2106, Jun. 2011.

Active and passive mode-locked fiber lasers for high-speed high-resolution photonic analog to digital conversion

Guillermo E. Villanueva,[1] María Ferri,[1] and Pere Pérez-Millán[2]

[1]Nanophotonics Technology Center, Universidad Politécnica de Valencia,
Camino de Vera s/n, 46022 Valencia, Spain
[2]Departamento de Física Aplicada-ICMUV, Universidad de Valencia,
Dr. Moliner 50, 46100 Burjassot, Spain

ABSTRACT

We present a complete set of mode-locked fiber lasers designed for photonic analog to digital conversion. Design, simulation, fabrication and characterization of Er-doped fiber lasers have been carried out optimizing their performance to suit the requirements of high speed and high resolution photonic-assisted analog to digital converters. The required properties have been approached by active mode-locking based on amplitude modulation of the cavity losses through a Mach-Zehnder modulator, and passive mode-locking based on fast semiconductor saturable absorbers and intracavity polarizing fibers. The use of an intracavity polarizing fiber in combination with a fast saturable absorber allows dynamic control of the operation regimes through polarization control. In addition to these oscillators designed with ring cavity structure, a short linear cavity with fundamental repetition frequency of the order of 1 GHz is studied, and an effective continuous tunability of the repetition frequency is obtained via an electromechanical transducer. Pulsed repetition rates up to 20 GHz, pulsewidths down to 500 fs and time jitters below 180 fs have been obtained. Fiber lasers based on standard and commercially available telecom devices have been demonstrated to be a low-cost, compact and versatile optical source for photonic-assisted analog to digital conversion.

I. Introduction

Interest in ultra-short optical pulse sources is rapidly growing due to the wide range of emerging areas where subpicosecond pulses are providing new advances, from ultra-high-bit-rate optical communications (such as OFDM systems [1]) to ultrafast spectroscopy [2] and biomedical applications [3]. Mode-locked fiber lasers are reliable, compact and cost-effective sources of stable sub-picosecond pulses [4]. Fiber lasers offer a set of properties suitable for the generation of ultrashort pulses through mode-locking techniques, either active or passive. The bandwidth of the gain provided by fibers doped with rare earths is of the order of tens of nanometers, allowing the generation of pulses with timewidths of hundreds of femtoseconds. Also, the fabrication of erbium-doped fiber lasers is of lower cost

than other mode-locked laser technologies, since they are based mostly on telecom standard components and free space optics is avoided. In this work we present a study of different laser cavities and mode-locking techniques intended to obtain a pulsed optical source with the optimum properties required to be implemented in a photonics-assisted analog to digital converter (PADC), where the source will act as optical clock of the sampling process [5]. High-speed high-resolution PADCs require pulsed signals of repetition rates of tens of GHz, pulse durations of hundreds of fs and time jitters of tens of fs [6], which have been the aimed properties of the lasers developed in this work.

This objective has been approached by designing, simulating, fabricating and characterizing active and passive mode-locking fiber sources with different cavity structures. When implementing active mode-locking through cavity loss modulation, repetition frequencies of tens of GHz and dynamic frequency tunability through external clock synthesizers are possible. Alternatively, passive mode-locking employing a fast saturable absorber (SA) avoids the use of external electronic devices, providing ultra-short optical pulses through saturable absorption shaping and solitonic pulse propagation [7]. Nevertheless the repetition frequency of passive mode-locked lasers is usually fixed by the natural cavity optical length. In the passive SA mode-locked scheme of this work, several techniques of harmonic mode-locking to achieve higher repetition rates are investigated. An innovative passive mode-locked structure based on an intracavity polarizing fiber has been studied [8], and a dynamic control of its operation regimes has been shown. By controlling the state of polarization of the oscillating signal, this laser was able to emit in high and low dispersion solitonic mode-locked regime, and 100 GHz multiwavelength regime. Finally, a short linear cavity fiber laser mode-locked by a semiconductor saturable absorber mirror (SESAM) is proposed. The fundamental repetition frequency of the cavity is 1.4 GHz, and can be dynamically tuned through fiber stretching via a transducer actuator, achieving a tuning range of $\sim$0.5 MHz. Pulsed repetion rates up to 20 GHz, pulsewidths down to 500 fs, amplitude noise lower than 0.56% and time jitters below 180 fs have been obtained by the different mode-locked fiber laser schemes.

II. Photonic-assisted analog to digital conversion

Analog to digital conversion is a field where photonics have found direct and intensive application in overcoming the limitations of traditional electronic converters. Bandwidth and equivalent number of bits (ENOB) are ADC key performance parameters, and the main limits imposed to ADC electronics are the following: a) Noise contributions, b) jitter and c) ambiguity. The traditional solution to increase the maximum frequency that can be digitalized by ADCs is implemented employing electronic Track-and-Holds (T&H), which enable the fast sampling of the RF signals and are placed as an analog front-end of the ADC, allowing the direct digitalization at frequencies of dozens of GHz. Nevertheless, due to intrinsic limitations of the sampling electronics, T&H presents the characteristics of having a limited dynamic range at high frequencies. On the other hand, advanced telecom-

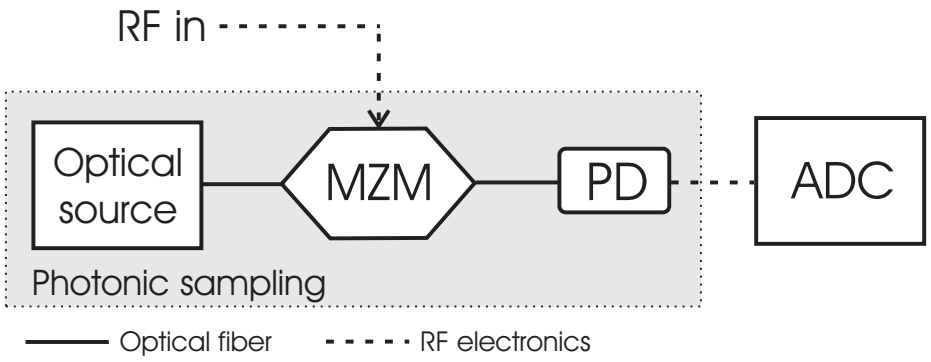

Figure 1: Photonic sampling ADC scheme. MZM: Mach-Zehnder modulator. PD: Photodiode.

munications systems, such as high-bit-rate satellite links, need for compact and reduced subsystems. Photonic-assisted ADCs overcome fundamental limitations of traditional electronics thanks to the use of highly stable optical pulsed sources and high bandwidth optical devices.

PADC implementations can be generally divided into four main classes, depending on which part of the conversion (sampling and quantization) is performed by photonics: 1) Photonic assisted ADC in which a photonic device is added to an electronic ADC to improve performance, 2) photonic sampling and electronic quantizing ADC, 3) electronic sampling and photonic quantizing ADC, and 4) photonic sampling and quantizing ADC [5]. It can be deduced from the results obtained through many years of research in the photonic digitalization area that the tendency has been a wide increase of the sampling frequency without bringing, unluckily, a wide increase in the number of bits. The use of photonic components like mode-locked lasers or Mach-Zehnder modulators increases considerably the performance of analog-to-digital converters since these devices allow to raise the sampling rates and the maximum input frequencies up to values not achievable by current electronic devices with high performance. Nevertheless, the photonic technology is still very immature for quantizing the sampled signal, being then more convenient using architectures based on photonic sampling and electronic quantization than full photonic ADCs.

Fig. 1 shows the architecture of the photonic sampling ADC. This configuration enables an optimum sampling of the radio frequency (RF) signal thanks to the use of a very stable optical pulsed laser, with a jitter of few femtoseconds, low amplitude noise and ultra-short temporal duration (fs range)[9]. The RF signal is sampled using an electro-optical modulator, which exhibits ultra low second-order distortion, a very low third order distortion and an infinite decoupling between the sampling and the quantification parts of the system. These characteristics enable to have a frequency independent dynamic range, optimizing the digitalization system performance and eventually overcoming the electrical ADCs and T&Hs limitations.

Applying a sub-sampling configuration enables the direct down-conversion of high frequency channels eliminating the necessity of RF down-conversion and filtering chains before the digitalization. This RF electronics saving is considerable when a high number of channels are considered. Therefore, transparent digitalization of Ka band (26.5-40 GHz) channels is possible using sampling rates of few GHz, since this sample rate must be double the channel bandwidth, usually in the order of hundreds of MHz. Sampling frequency f_S of the PADC is set by the pulse repetition frequency of the optical source. The maximum input frequency to the photonic sampling ADC is generally limited by the modulator bandwidth, easily over 50 GHz for off-the-shelf Mach-Zehnder modulators. In terms of optical source requirements, temporal (jitter) and amplitude stability are important to improve the ENOB of traditional electronic converters. The optical pulses width has to be short enough to perform a clear and non-ambiguous sample of the RF input signal, and pulsewidths of hundreds of fs are highly desired. Furthermore, when sub-sampling down-conversion is applied, the sampled signal must not cross an integer multiple of $f_S/2$ to prevent overlapping of the aliased components. Sources with tunable repetition frequency capacity are desirable to prevent from this situation, and tuning ranges of hundreds of kHz are sufficient for the bandwidths and carrier frequencies considered. Besides, strict payload weight and volume specification in space applications requires very compact and light optical sources implementations.

Fiber lasers are excellent candidates as compact PADC pulsed optical sources. Mode-locked fiber lasers provide pulse trains with high amplitude stability and time jitters of tens of fs. Repetition frequency of GHz in fiber lasers can be tailored with different approaches. In the next section, several mode-locked fiber laser architectures have been implemented and validated as theoretically as experimentally.

III. Mode-locking fiber laser implementations

In this section the four types of fiber lasers developed are presented, focusing on the description of the working principle and cavity structure of the sources. Numerical simulations of the cavities' operation are carried out, and experimental characterization of the pulsed emission in the optical, electrical and time domains is presented. In order to numerically model the fiber laser emission features, pulse propagation is computed through the nonlinear Schrödinger equation (NLSE), which takes the following form [10]:

$$\frac{\partial A}{\partial z} + j\frac{\beta_2}{2}\frac{\partial^2 A}{\partial T^2} + \frac{\alpha}{2}A - \left(\frac{g}{2} + \frac{D_g}{2}\frac{\partial^2}{\partial T^2}\right)A = j\gamma|A|^2 A. \tag{1}$$

NLSE describes the propagation of the slow-varying envelope $A(z,T)$ of an optical pulse. Parameters β_2, α and g denote the group-velocity dispersion, attenuation and gain of the optical fiber respectively. The bandwidth of the gain medium is modeled by the gain dispersion D_g through the relation $D_g = g/\Omega_g^2$, where Ω_g is the half-width at half-maximum

(HWHM) gain bandwidth, assuming a parabolic approximation. The right-handed term of the equation expresses the self-phase modulation (SPM) nonlinearity through the γ coefficient. The SPM coefficient is given by the nonlinear refractive n_2 of the optical fiber and the effective area A_{eff} of the laser mode in the fiber core according to $\gamma = 2\pi n_2/(\lambda_0 A_{eff})$. More complex nonlinear effects such as stimulated Raman scattering and self-steepening are neglected in (1). A frame of reference moving with the pulse at the group velocity vg is used in the NLSE by the transformation $T = t - \beta_1 z$. Regarding the active medium gain, we assume a saturation over the propagation of many optical pulses, i.e., with the average power. Thus we always consider that the gain is saturated to its stationary value corresponding to the average power P_{avg}.

The NLSE is solved using the split-step Fourier transform method. For the particular laser design with a polarizing fiber in the cavity (see section III.C), both linear polarizations will be taken into account solving the coupled nonlinear Schrödinger equations (CNLSE). In order to simulate the ring laser cavities, the optical pulse is propagated through the different fiber sections that make up each cavity, injecting the resulting pulse into the first section as a roundtrip is completed, and the output is extracted after convergence. This convergence is checked by stabilization of parameters like pulse peak power or pulsewidth, usually reached in few thousands of roundtrips, depending on the particular cavity configuration. The fiber laser simulation strategy was the propagation of the optical pulse through the different fiber sections that each particular cavity contains, and the discrete application of lumped optical elements such as modulators, polarization controllers and saturable absorbers. Computed pulse temporal wavefuctions and optical spectrums are extracted from calculations.

Phase and amplitude noise of the studied mode-locked fiber lasers are evaluated by measuring the sidebands power spectra of the photodetected harmonics spectra. In mode-locked optical sources, amplitude and phase noise on the optical power envelope cause a broadening of the individual harmonics [11]. The relative power level for amplitude noise sidebands remains constant for increasing harmonic number, whereas for phase noise sidebands the relative level increases as the square of the harmonic number. The power integral of noise sidebands relates to phase and amplitude noise with the expresion

$$\sigma_n^2 = \sigma_A^2 + 2\pi n f_0 \sigma_{AT}^2 + (2\pi n f_0)^2 \sigma_T^2, \tag{2}$$

where σ_n^2 is the noise power of the n^{th} harmonic integrated over both the positive and negative sidebands, σ_A^2 is the root mean square (RMS) amplitude noise, f_0 is the pulse repetition frequency, σ_{AT}^2 is the RMS amplitude to time jitter noise and σ_T^2 is the RMS time jitter. Analyzing the integrated noise power of several harmonics in a given frequency range, it is possible to estimate the RMS amplitude and jitter noise of the optical source.

A. Actively mode-locked laser based on electrooptic modulators

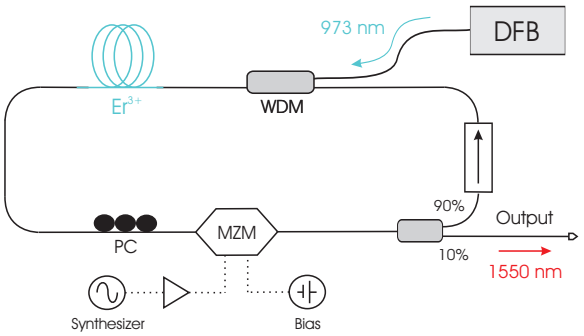

Figure 2: Actively mode-locked erbium-doped fiber laser with a ring structure cavity. DFB: distributed feedback diode laser PC: Polarization controller MZM: Lithium niobate ($LiNbO_3$) Mach-Zehnder modulator. WDM: 980 / 1550 wavelength division multiplexer.

The pulsed regime of this type of laser is based on the active modulation of the cavity losses using a Mach-Zehnder electro-optical modulator (MZM) [12]. With active mode-locking it is possible to control the mode-locked repetition frequency from an external modulation signal. The periodic loss modulation promotes the phase of longitudinal cavity modes to arrange in a locked reference to produce an optical pulse in the minimum of cavity losses.

The cavity structure is depicted in Fig. 2. It consisted of a ring cavity with 3 m of erbium doped fiber Fibercore DHB1500 (peak absorption of 15 dB/m at 1530 nm), pumped by a 976 nm diode laser through a 980/1550 nm wavelength division multiplexer (WDM). The amplitude modulation was performed by a JDS Uniphase OC-192 Mach-Zehnder modulator. A polarization controller provides the optimum state of polarization for the MZM input. An optical isolator is inserted in the ring to prevent bidirectional lasing operation. Finally, a 90:10 output coupler extracts the optical output of the fiber laser.

For the numerical simulation, the effect of the MZM was discretely modeled as a loss modulation:

$$IL_{MZM}(\omega_{RF}) = IL_{MZM0} + M\left(1 - \cos(\omega_{RF}T)\right), \tag{3}$$

where IL_{MZM0} are the insertion losses in decibels of the MZM biased at quadrature bias (QB) point, M is the modulation depth (in decibels), ω_{RF} is the modulation angular frequency and T is the delayed frame time.

Experimental stable emission of very low amplitude and phase noise is observed when the frequency of the synthesizer is adjusted to a multiple of the fundamental resonant frequency of the ring cavity, with output powers over 5 dBm. Tunable repetition rate of the pulsed emission is obtained in the whole synthesizer band: 0 - 20 GHz. Optical spectra of the laser working at repetition frequencies of 1.3 and 9.8 GHz are depicted in Fig. 3,

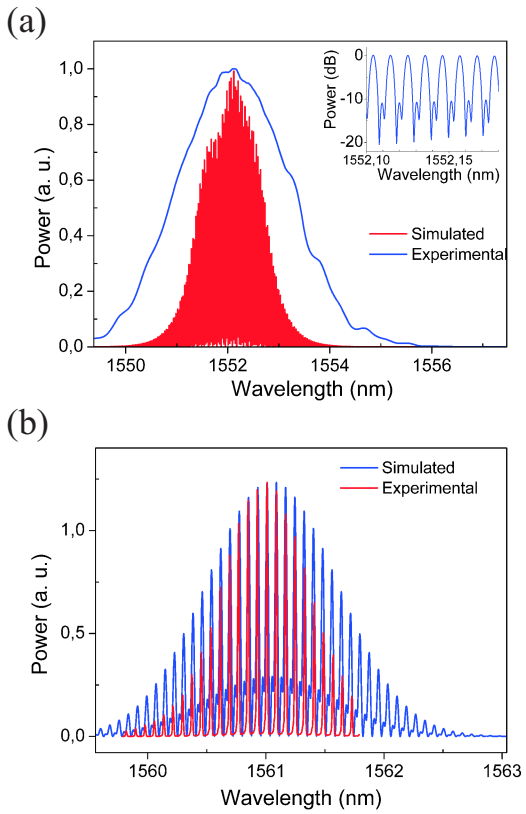

Figure 3: (a) Calculated and experimental optical spectra of the actively modelocked emission at a pulsed repetition rate of 1.3 GHz, a pump current of 460 mA and a MZM modulation RF power of 20 dBm. Inset zooms in on the simulated optical components showing an optical separation of 10 pm. (b) Calculated and experimental optical spectra at a repetition rate of 9.8 GHz, pump current of 460 mA and modulation RF power of 15 dBm (linear scale).

compared with the simulated spectra. Experimental spectrum shows a wider bandwidth than the simulated one in Fig 3a. The optical pulse propagation in the cavity can be influenced by chromatic dispersion and nonlinearity to perform a solitonic pulse shaping, and this effect has not been reflected in numerical calculations as intensely as in experimental results. In this way, temporal width can be reduced and optical spectrum become wider. The signals have been detected also with a 50 GHz photodetector and their corresponding electric spectra have been analyzed, yielding spurious-free harmonics with SNR over 80 dB and linewidths below the resolution of the electrical spectrum analyzer, 1Hz. The relative power density of the noise sidebands of the first eight harmonics have been measured to calculate the amplitude noise and time jitter. The equipment used is limited to 2.5 GHz, so a modulation frequency of 216.74 MHz was applied in order to capture enough harmonics. Integration of noise spectra from 10 Hz to 1 MHz allows us to estimate the amplitude and time jitter from (2). Fig. 4 shows the noise sidebands and the integrated power with the fitted parabolic function. From this curve, a time jitter of 4.6 ps and an amplitude noise of 2.27% are obtained.

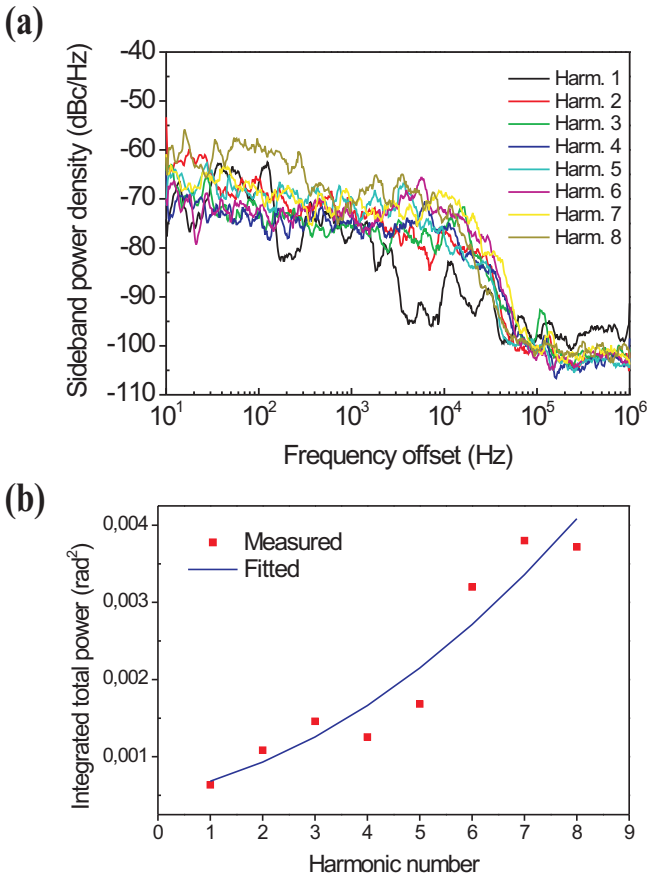

Figure 4: (a) Sideband power spectra of the first up to the eighth harmonic for the actively mode-locked fiber laser (b) Integrated sideband power against harmonic number.

B. Passively mode-locked laser based on semiconductor saturable absorbers

One technique to passively mode-lock the fiber laser is the use of a saturable absorber within the optical cavity. In comparison with active mode-locking described in the previous section, saturable absorbers modulate passively the losses of the cavity experienced by the propagated pulse, as the insertion losses of the absorber are dependent of the signal intensity. This type of fiber laser results simple and robust. Very few components are needed for its manufacture and, consequently, it is of an appreciably lower cost of fabrication than the other mode-locking methods under study.

However, the pulsed emission is generated at the fundamental resonant frequency of the cavity, typically of the order of tens of MHz. Hence, frequency conversion methods are needed to obtain pulses at the repetition frequencies of several GHz required by fast photonic ADCs. We have tested frequency conversion methods based on 1) Vernier effect and 2) Intracavity filtering with ring resonators with high coupling constant [13], [14].

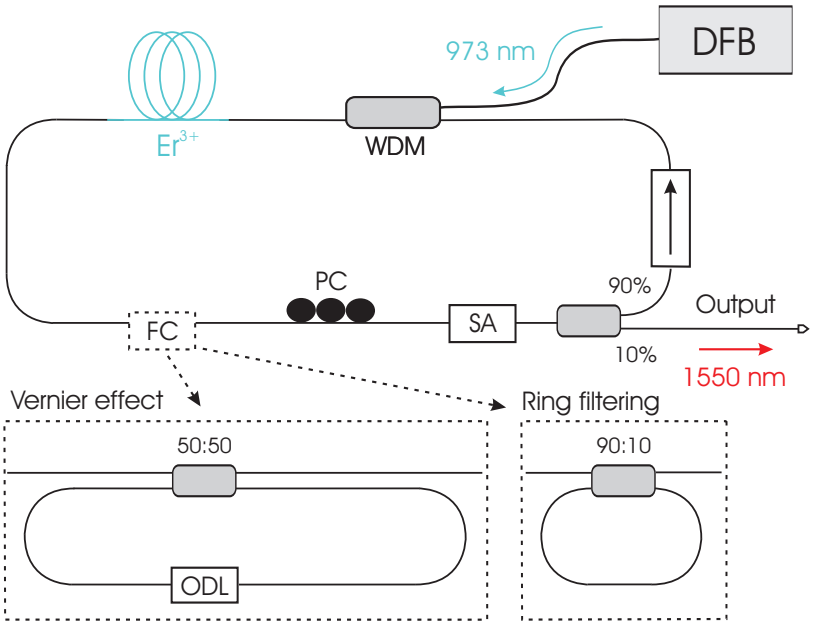

Figure 5: Passively mode-locked erbium-doped fiber laser with a ring structure cavity. DFB: distributed feedback diode laser PC: Polarization controller. SA: Semiconductor saturable absorber working in transmission. WDM: 980 / 1550 wavelength division multiplexer. FC: Frequency conversion module. ODL: Optical delay line. Two different frequency conversion approaches have been studied; Vernier effect and intracavity ring filtering.

The laser structure is shown in Fig. 5, which consists of 3 m of erbium doped fiber Fibercore DHB1500, pumped by a 976 nm diode laser through a 980/1550 WDM. The passive mode-locking is achieved through a Batop GmbH fiber pigtailed fast semiconductor saturable absorber, with a relaxation time of 2 ps, saturation energy of 235 pJ and 15% of modulation depth. A polarization controller is included to adjust the state of polarization within the cavity. An isolator guarantees unidirectional lasing operation, and the laser output is extracted via a 90:10 output coupler. Two frequency conversion techniques have been put into practice: a second coupled cavity to exploit the Vernier effect and an intracavity ring filter. Fig. 5 shows the two schemes introduced in the cavity as a frequency conversion module. The first technique is based in the insertion of a fiber ring through an optical coupler. This ring has a length comparable with the main cavity length. The overall repetition frequency will be the lowest common multiple of both the main cavity and the secondary ring [13]. With precise control in the length of the secondary ring, the original repetition frequency has been multiplied from tens of MHz to 1.3 GHz. The second solution implemented consisted of the insertion of fiber ring filters in the cavity. In this way, the longitudinal modes of the cavity are filtered by the high free spectral range (FSR) ring. Several rings with different finesses have been explored. The finesse of a fiber ring filter is directly related to the coupling ratio of the optical coupler, and coupling ratios from 0.1 to 10^{-4} were performed. On the other hand, FSRs of GHz require rings of tens of cm long. Both methods have provided effective repetition frequency multiplication. Neverthe-

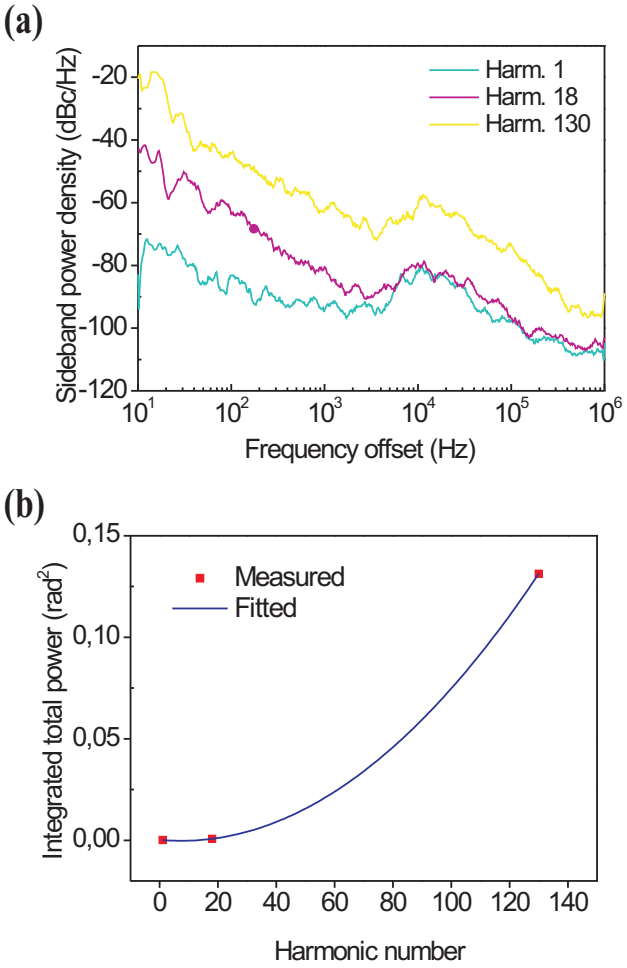

Figure 6: (a) Sideband power spectra of 1st, 18th and 130th harmonic for the fast SA ML passively mode-locked fiber laser (b) Integrated sideband power against harmonic number.

less, they showed insufficient suppression of spurious harmonics, with a resulting 1.3 GHz pulsed signal with SNR below 15 dB.

The SA effect in the numerical calculation was evaluated as an insertion loss dependent on the pulse intensity:

$$A(\text{after SA}, T) = A(\text{before SA}, T) \exp\left(-\frac{q\left(A(z,T)\right) + q_{non}}{2}\right). \tag{4}$$

To take into account the temporal response of the absorber, the SA losses obey the expression

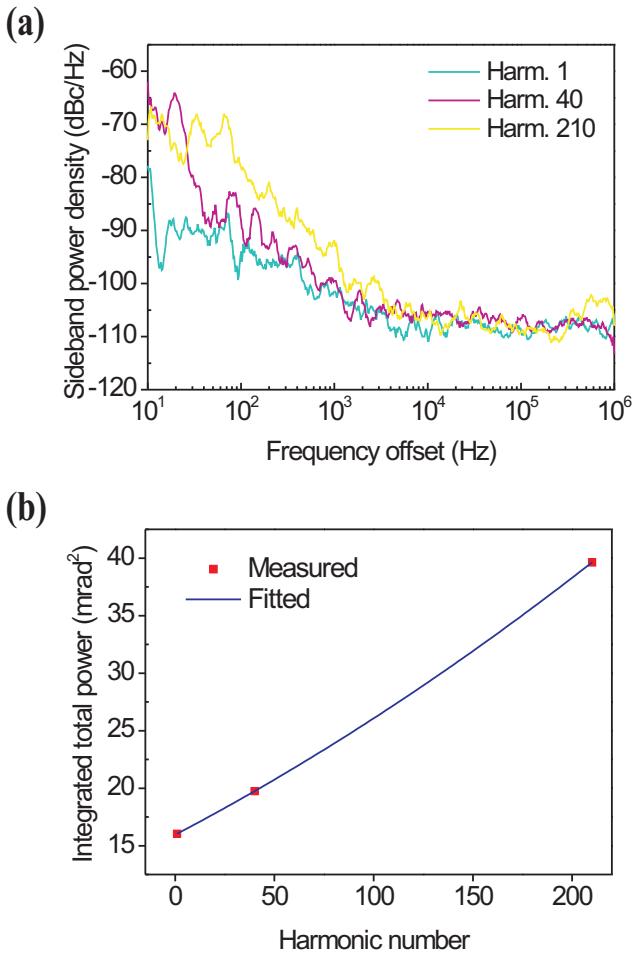

Figure 7: (a) Sideband power spectra of 1st, 40th and 210th harmonic for the solitonic passively mode-locked fiber laser (b) Integrated sideband power against harmonic number.

$$\frac{\partial q\left(A(z,T)\right)}{\partial T} = -\frac{q-q_0}{\tau_{SA}} - q\frac{|A(z,T)|}{E_{SA}}. \tag{5}$$

In (5), τ_{SA}, q_0 and E_{SA} are the temporal response, the saturable loss and the saturation energy of the saturable absorber respectively. Saturable absorption also includes an amplitude-independent term q_{non} to account the non-saturable losses, which is directly added to the saturable term as (4) shows. Optical pulses are propagated through fiber sections solving the NLSE, whereas the SA effect is applied discretely.

Several combinations between nonlinear coefficient and dispersion of the fibers integrating the cavities have been studied to generate "self-starting" ultrafast mode-locked (fast SA ML) regime and soliton regime [15], [16]. Solitonic shaping has produced pulses of 500 fs timewidth with a stability of several hours in a laboratory environment. Temporal

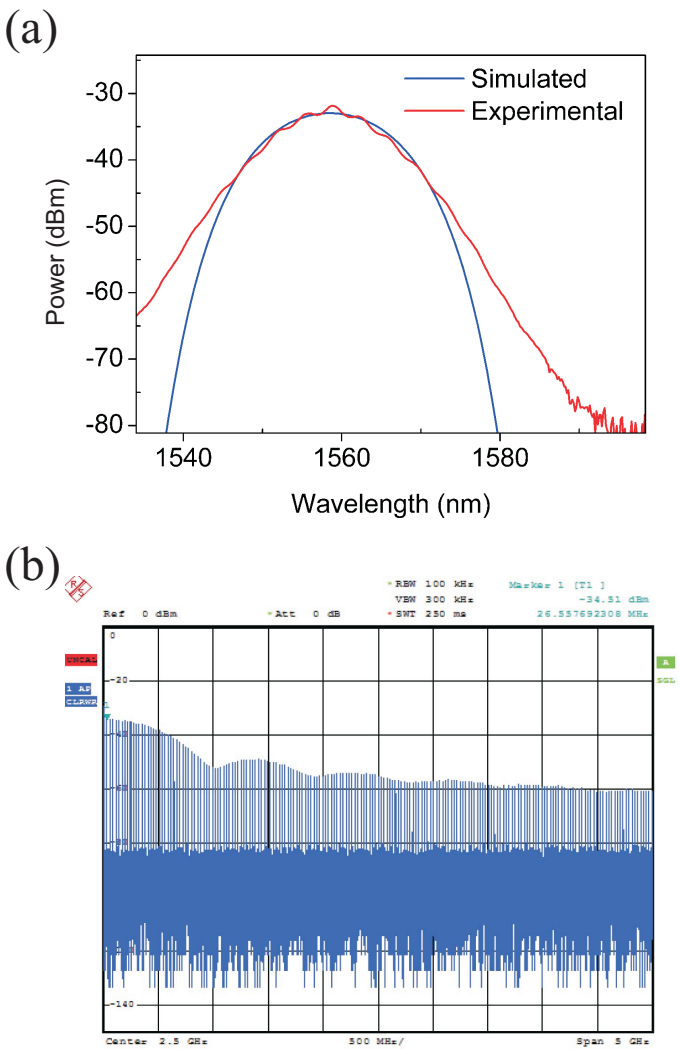

Figure 8: (a) Simulated and measured optical spectrum of the laser emission at a pulsed repetition rate of 27 MHz, with a Gaussian-shaped bandwidth $\Delta\lambda_{FWHM}$=10 nm. (b) Electrical spectrum of the photodetected signal. Span of 5 GHz and resolution of 100 kHz.

measurements with a high-speed oscilloscope gave pulse duration jitter values below 30 fs. Noise sidebands of harmonics 1, 18 and 130 are shown in Fig. 6a. Higher order harmonics are chosen due to the relative low fundamental repetition frequency (27 MHz). The RMS amplitude noise and time jitter derived from integrated noise power (see Fig. 6b) are 52.3 ps and 2.33% respectively for the fast SA ML regime. When the laser operates in solitonic regime, phase and amplitude noise improve substantially. Fig. 7 illustrates the spectral sidebands for the 1st, 40th and 210th harmonics and the integrated noise fitted curve. RMS amplitude noise of 0.56% and RMS time jitter of 180 fs are obtained from the application of (2). It should be noted that relative sideband power densities shown in Fig. 7a are limited to values greater than 110 dBc/Hz, due to equipment noise limitations.

For this reason, better amplitude noise and time jitter of several tens of femtoseconds are expected from the fiber laser. Fig. 8a shows the emission spectrum for the simulated and the experimental case, showing a full width at half maximum of 10 nm. The dispersion of SMF and Er doped-fiber were – 20 and 15 ps^2/km respectively, and a nonlinear coefficient of 1.5 mrad/(W·m) is assumed. The electrical photodetected spectrum is shown in Fig. 8b, where a repetition frequency of 27 MHz is measured.

C. Passively mode-locked laser based on intracavity polarizing fibers

As explained in the previous section, passive modelocking with fast saturable absorbers, not limited by the speed of electronic signal generators, allows the generation of ultra-short pulses in the regimes of fast SA ML and soliton modelocking. On the other hand, Lyot filters based on the combination of in-line polarizers and birefringent fibers have been exploited for the generation of a multiwavelength emission regime [17]. Recently, polarizing (PZ) fibers with very low losses and ready to be spliced to standard fibers are commercially available. In this section we demonstrate that introducing a PZ fiber in the cavity of a SA mode-locked laser, pulsed soliton mode-locking with controllable cavity dispersion and multiwavelength emission regimes can be obtained by controlling the state of polarization at the input and output of the PZ fiber. In comparison with other laser structures incorporating high-birefringent fibers to implement intracavity Lyot filters [17], our proposal performs the polarizing effect in a fiber, and does not require a polarizer.

The cavity of the fiber laser is shown in Fig. 9. The saturable absorber performs the mode-locking stabilization mechanism. The fiber laser, without the PZ fiber, operates in a soliton regime. When inserting the PZ fiber in combination with two polarization con-

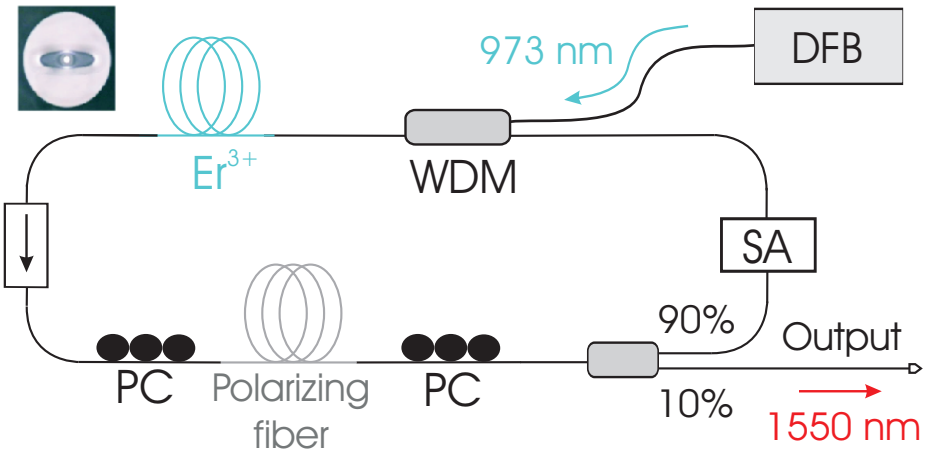

Figure 9: Scheme of the PZ fiber based passively mode-locked fiber laser setup. DFB: Distributed feedback pump diode laser; WDM: 980/1550 Wavelength Division Multiplexer; Er^{3+}: erbium-doped fiber, PC: Polarization controller; SA: Semiconductor saturable absorber. Up left) Cross section of the PZ fiber.

trollers, it is possible to control the polarization-dependent losses applied to the optical pulse each roundtrip. Together with its inherent high birefringence, the PZ fiber can partially implement an intracavity multiwavelength Lyot filter [18], with configurability via the polarization controllers. The filtering effect of the PZ fiber results in a multiwavelength emission, therefore the fiber laser can be dynamically adjusted to operate in a pulsed or in a multiwavelength regime. Furthermore, this kind of single-polarization fibers exhibits different chromatic dispersion in each principal axis known as birefringence dispersion [19]. The PZ fiber birefringence dispersion provides a tool to control the roundtrip accumulated dispersion of the oscillating optical signal. Adjusting the cavity dispersion budget can allow the control of the solitonic mode-locking operation.

The fiber ring cavity is composed of the following components: 3 m of erbium doped fiber Fibercore DHB1500, pumped by a 400 mW diode laser at 976 nm through a 980/1550 nm wavelength division multiplexer (WDM); 3 m of Verrillon highly birefringent polarizing fiber (birefringence Δn=10^{-3}, 0.6 dB/m extinction ratio); A Batop fiber pigtailed fast semiconductor saturable absorber (the same used in the previous section); An optical isolator to prevent bidirectional lasing operation; Two polarization controllers (PC) asides the polarizing fiber; A 90:10 output coupler; And finally $\sim$8 m of single-mode fiber (from all component pigtails). The cross section of the PZ fiber is shown in the upper left side of Fig. 9, where a highly elliptical cladding can be observed. The estimated x and y polarization dispersions of the PZ fiber were 20 and 53 ps^2/km respectively.

In order to numerically model the fiber laser taking into account the amplitude polarization, the scalar NLSE (1) has to be extended to the two orthogonal polarizations. Two equations are derived, so-called the coupled nonlinear Schrödinger equation (CNLSE). The SA insertion loss model is described in the previous section. Each PC is modelled in the simulations by three waveplates ($\lambda/4$ - $\lambda/2$ - $\lambda/4$) through their Jones matrix.

The PZ fiber is considered as a Lyot filter in which the polarizing axes is identical to the birefringence axis, ideally leading to no spectral filtering. In contrast to a conventional Lyot filter where an ideal polarizer is required, the PZ fiber shows an intended finite polarization extinction rate. The PZ fiber introduces a spectral filtering proportional to the polarizing lossess [8]. The operating regimes of the laser depend on the relative orientation of the state of polarization of the light with regard to the polarization axis of the PZ fiber. The polarization state is adjusted by the two polarization controllers. An orientation resulting in a low extinction ratio wavelength filtering results in a non-effective suppression of stimulation of the filtered wavelengths, hence the laser operates in a low dispersion solitonic regime with a repetition rate corresponding to the original FSR of the ring cavity (15 MHz) and with a pulsewidth of 25 ps estimated from oscilloscope trace. Due to the unexpected high time-bandwidth product, multipulse bunching is likely to occur, but the 7ps oscilloscope resolution was not sufficient to identify multipulse emission. Simulations provide pulsewidths of 580 and 630 fs for the high and low dispersion soliton regime respectively, and pulses energies of 100 pJ. Fig. 10 shows the calculated and measured optical output

spectrum, showing a bandwidth of 8.2 nm FWHM. Depending on the effective amount of polarization dispersion induced in the PZ fiber by the orientation of the PCs, a larger net anomalous dispersion can be obtained and the laser works under a high dispersion soliton regime. The calculated average cavity dispersion for the low and high dispersion regimes were - 3.71 and - 0.073 ps^2/km respectively, and the temporal pulsewidth in this regime is 600 fs, obtained from autocorrelation measurement. The differences in the Kelly sidebands observed in the calculated and simulated spectra in Fig. 10 are attributed to deviations in estimated cavity length and dispersion. When switching from high to low dispersion soliton regime, Kelly sidebands are no longer visible, as their spectral positions shift away from central wavelength due to the lower dispersion [20]. In terms of amplitude and phase noise, this laser behaves equally than the passively mode-locked fiber laser studied in section III.B. Noise sidebands of photodetected harmonics are similar to sidebands shown in Fig. 7, and, as in the latter case, RMS amplitude noise and time jitter below 0.56% and 180 fs are expected respectively.

The third operation regime is achieved when an orientation results in a high extinction ratio wavelength filtering, yielding a multiwavelength emission with a FSR of 106 GHz. The 106 GHz wavelength spacing is in accordance with the length and birefringence of the PZ fiber from the expression

$$\Delta\lambda = \frac{\lambda^2}{\Delta n L_{PZ}}, \tag{6}$$

where Δn and L_{PZ} denote the modal birefringence and length of the polarizing fiber respectively. Fig. 10b shows the experimental optical output spectra for the three operation regimes. Each regime is achieved by fine adjustment of the polarization through the two PCs. For the two modelocked regimes, a stable pulsed output signal is obtained. In contrast to CW multiwavelength lasers, in which NLPR can be exploited as gain equalization [18], the multiwavelength regime constitutes a harmonic mode-locking of 106 GHz pulse repetition frequency. Unfortunately, no stable pulse emission was achieved from this regime. We believe spectral filter finesse and pumping power are not high enough to reach stable harmonic mode-locking. Fig. 10a includes the three operation regimes simulated spectra. Amplitude and wavelength levels are adjusted for comparison with experimental plots.

D. Short cavity passively mode-locked laser

In addition to the ring structures analyzed in previous sections, another approach to achieve pulse repetition frequencies in the range of GHz has been studied by implementing short optical cavities. With a cavity length of few centimeters, the fundamental repetition frequency is established in the GHz range. A fiber ring cavity structure with such cavity lengths is not easy to implement since standard couplers and isolators required for this structure are themselves of several centimeter length already. Instead, linear Fabry-Pérot

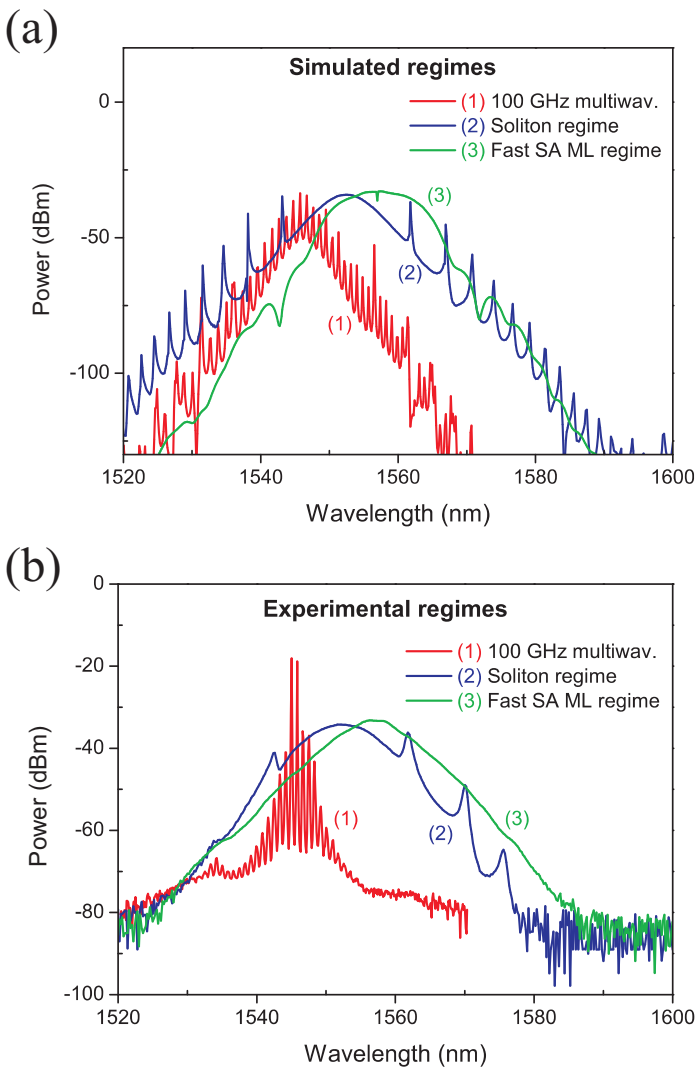

Figure 10: Optical output spectra of the three operation regimes of the laser: 100 GHz multiwavelength emission, high dispersion and low dispersion soliton operation. (a) Calculated spectra. (b) Measured spectra.

fiber cavities have shown to be excellent solutions for very-short cavity mode-locked fiber lasers [21]. In this section, we have studied a 7 cm-long Fabry-Pérot cavity fiber laser mode-locked through a semiconductor saturable absorber mirror (SESAM). Moreover, the repetition frequency of the cavity is continuously tuned by stretching the cavity length through an actuator.

The scheme of the fiber laser is shown in Fig. 11. A 7 cm section of Nufern Er/Yb-doped double-clad fiber (70 dB/m of peak core absorption at 1530 nm) composes the cavity. The pump signal, coming from a 980/1550 WDM, is coupled to the cavity through a dichroic mirror deposited in the end facet of the active fiber. The dichroic mirror has a reflectance of 98.5% at 1550 nm, and a transmittance of 96% at 980 nm. The other end facet of the

cavity is coupled to a Batop SESAM with a modulation depth, saturation fluence and time response of 22%, 30 μJ/cm^2 and 2 ps respectively. A plumbum (lead) zirconate titanate (PZT) piezoelectric actuator is stuck to the active fiber in order to mechanically stretch the cavity length. The dimensions of the actuator are 5x5x36 mm, and it is controlled by a 0-100V DC source. The lasing signal at 1550 nm is extracted from the cavity through the partially reflective dichroic mirror, and is forwarded to the 1550 nm WDM port. The whole structure results in a high compact fiber-based system.

The short cavity fiber laser emits a pulsed signal with an average power of -12 dBm when pumped at 160 mW, with a fundamental repetition frequency of 1.398 GHz. Fig. 12a shows the optical spectrum obtained from simulation and experimental characterization. The full width half maximum is $\Delta\lambda_{FWHM}$=1.6 nm. In contrast to the ring structures analyzed previously, the whole cavity consists of active fiber with normal dispersion, therefore pulse formation is carried out exclusively by saturable absorption, without solitonic pulse shaping. Due to the effects of the SA temporal response and the chromatic dispersion of the fiber, optical pulses develop a longer leading wing (see inset of Fig. 12a), and asymmetric spectra are observed both experimentally and theoretically in Fig. 12a. Temporal pulse durations are approximately 3 ps. The low output power of the laser prevented us from performing noise measurements.

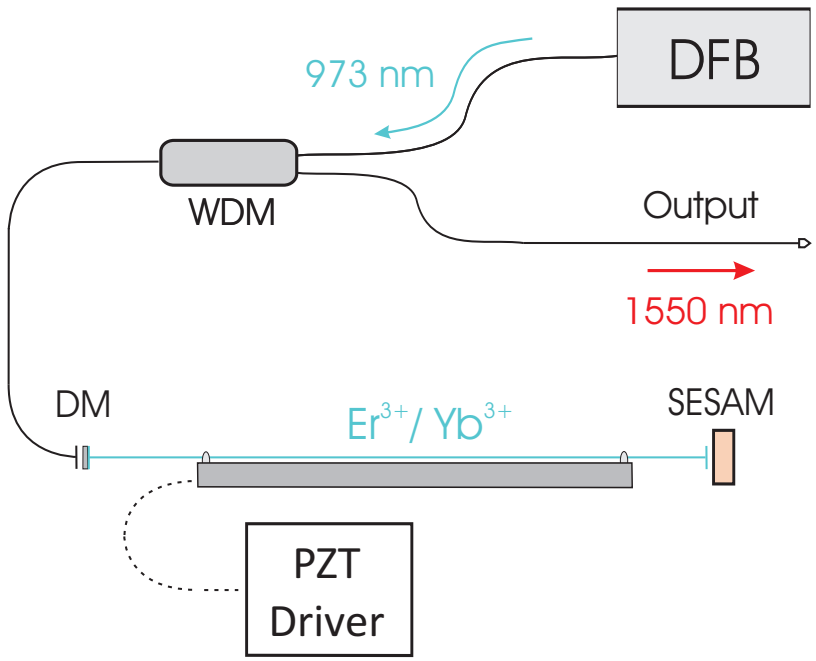

Figure 11: Scheme of the short cavity passively mode-locked fiber laser setup. DFB: Distributed feedback pump diode laser; WDM: 980/1550 Wavelength division multiplexer; Er^{3+}/Yb^{3+}: Erbium/ytterbium-doped fiber; DM: Dichroic mirror; SESAM: Semiconductor saturable absorber mirror.

Table I: Performance of fiber lasers summary.

Fiber laser	**Pulse duration**	**Pulse repetition frequency**	**Emitted power**	**RMS temporal jitter [10Hz,1MHz]**	**RMS amplitude noise [10Hz,1MHz]**	**Compactness**
A. Active MLL	4 ps	[0,20] GHz Highly tunable	0 - 5 dBm	4.6 ps	2.27%	Low
B. Passive MLL	500 fs	27 MHz (fundamental) 1.3 GHz (with conversion techniques)	0 - 5 dBm	52.3 ps <180 fs (solitonic)	2.33% <0.56% (solitonic)	Moderate
C. Polarizing fiber based MLL	600 fs	15 MHz (fundamental) 106 GHz (unstable)	0 - 5 dBm	<180 fs	<0.56%	Moderate
D. Short cavity MLL	3 ps (simulated)	1.39 GHz (fundamental) 500 kHz of fine tunability	< -10 dBm	-	-	High

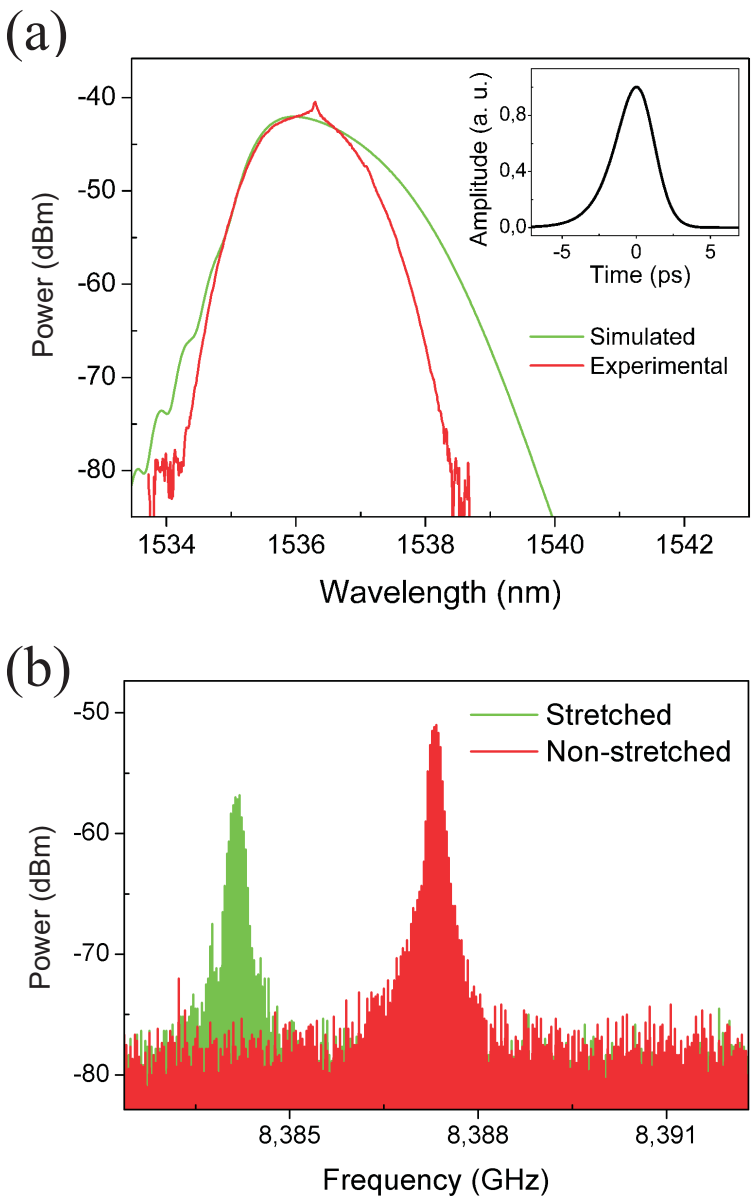

Figure 12: (a) Simulated and measured optical spectrum of the short cavity laser emission, showing a bandwidth of $\Delta\lambda_{FWHM}$=1.6 nm. Inset shows the temporal pulse. (b) Spectrum of the photodetected laser output under cavity stretching. The spectral component plot corresponds to the sixth harmonic, showing a tuning range of 3.2 MHz.

The PZT actuator stuck to the cavity allows the tunability of the laser fundamental repetition rate. The actuator piezoelectric longitudinal displacement is 1100ppm, corresponding to 39.6 μm. To experimentally validate the repetition frequency tunability, the optical output was photodetected and the electrical spectrum was analyzed. Fig. 12b shows the sixth harmonic component of the photodetected signal, corresponding to 8.387 GHz, when the PZT actuator is not stretched and fully stretched. Due to the stretch effect of the actuator,

the cavity length is increased and the fundamental repetition frequency is proportionally decreased. A maximum frequency shift of 3.2 MHz for the sixth harmonic component is obtained; therefore a continuous fundamental frequency tuning range of 533 kHz is achieved by mechanical stretching.

IV. Conclusion

Mode-locked fiber lasers are excellent candidates as pulsed optical sources in PADC. Ultrashort optical pulses of hundreds of femtoseconds with repetition frequencies easily scalable over the GHz range, presenting very low levels of amplitude and jitter noise, are the key for exceedingly improve the ENOB in photonic sampling ADC in comparison with state of the art electronic ADC. Moreover, fiber lasers offer a very compact and cost-effective solution in contrast to free-space solid state counterparts.

Table I compiles key parameters from the presented mode-locked fiber lasers. Depending on the particular requirements, one option offers better performance than the others: High tunability is accomplished by active mode-locking, exceptional amplitude and time jitter is provided by solitonic passive mode-locked fiber lasers, and simple and compact lasers can be obtained with the short cavity structure. These fiber laser approaches are only a sample of the versatility that fiber lasers offer. An actively mode-locked implementation allows the total control of repetition frequency and its stability through external reference synthesizers. Ultrashort optical pulses are easily achieved with compact and low-cost passively mode-locked cavities. Even though the fundamental repetition frequencies of such passive mode-locked solution are low, manifold frequency conversion techniques are available to further increase the free spectral range of the cavity. On the other hand, the use of commercially available polarizing fiber as intracavity polarizing section has proven to provide dynamic control of the polarization extinction ratio as well as dispersion budget, and different operation regimes for a single cavity structure have been demonstrated through polarization state control. Lastly, short cavity fiber lasers, of several centimeters long, deliver optical pulses with a fundamental repetition frequency of GHz and fine tunability of hundreds of kHz, representing a potentially very high compact source for space telecommunication applications.

References

[1] M. Ogusu, K. Inagaki, T. Ohira, I. Ogura, and H. Yokoyama, “Wavelength-division multiplexing of two-mode injection-locked Fabry-Perot lasers using optically harmonic modelocked master laser,” Electron. Lett., vol. 37, pp. 889–890, 2001.

[2] T. Gherman, and D. Romanini, “Modelocked cavity-enhanced absorption spectroscopy,” Opt. Express, vol. 10, pp. 1033–1042, 2002.

[3] Y. M. Lee, R. Y. Tu, A. C. Chiang, and Y. C. Huang, "Average-power mediated ultrafast laser osteotomy using a mode-locked Nd:YVO4 laser oscillator," J. Biomed. Opt., vol. 12, pp. 060505, 2007.

[4] M. E. Fermann, and I. Hartl, "Ultrafast fiber laser technology," IEEE J. Sel. Top. Quantum Electron., vol. 15, pp. 191–206, 2009.

[5] G. Valley, "Photonic analog-to-digital converters," Opt. Express, vol. 15, pp. 1955–1982, 2007.

[6] E. W. Jacobs, J. B. Sobti, V. F. Vella, R. Nguyen, D. J. Albares, R. B. Olsen, C. T. Chang, S. K. Sun, M. J. Choe, S. Beccue, R. Yu, and J. P. A. van der Wagt, "Optically clocked track-and-hold for high-speed high-resolution analog-to-digital conversion," Microwave Photonics, 2004. MWP'04. 2004 IEEE International Topical Meeting on, pp. 190–192, 2004.

[7] L.E. Nelson, D.J. Jones, K. Tamura, H.A. Haus, and E.P. Ippen, "Ultrashort-pulse fiber ring lasers," Appl. Phys. B, vol. 65, pp. 277–294, 1997.

[8] G. E. Villanueva, and P Pérez-Millán, "Dynamic control of the operation regimes of a mode-locked fiber laser based on intracavity polarizing fibers. Experimental and theoretical validation," Opt. Lett., vol. 37, pp. 1971–1973, 2012.

[9] M. A. Piqueras, P. Villalba, J. Puche, and J. Marti, "High performance photonic ADC for space and defence applications," Microwaves, Communications, Antennas and Electronics Systems (COMCAS), 2011 IEEE International Conference on, pp. 1–6, 2011.

[10] G. P. Agrawal, Nonlinear Fiber Optics, 3rd edn., Academic Press, New York, 2001, ch 4.

[11] D. von der Linde, "Characterization of the noise in continuously operating mode-locked lasers," Appl. Phys. B, vol. 39, pp. 201–217, 1986.

[12] J. Kafka, T. Baer, and D. Hall, "Mode-locked erbium-doped fiber laser with soliton pulse shaping," Opt. Lett., vol. 14, pp. 1269–1271, 1989.

[13] C. Chaichuay, P. P. Yupapin, and P. Saeung, "The serially coupled multiple ring resonator filters and Vernier effect," Appl. Opt., vol. 39, pp. 175–194, 2009.

[14] J. S. Wey, J. Goldhar, and G. L. Burdge, "Active harmonic modelocking of an erbium fiber laser with intracavity Fabry-Perot filters," J. Lightwave Technol., vol. 15, pp. 1171–1180, 1997.

[15] D. J. Richardson, R. I. Laming, D. N. Payne, V. J. Matsas, and M. W. Phillips, "Pulse repetition rates in passive, selfstarting, femtosecond soliton fibre laser," Electron. Lett., vol. 27, pp. 1451–1453, 1991.

[16] F. X. Kärtner, J. Aus der Au, and U. Keller, "Mode-Locking with slow and fast saturable absorbers-what's the difference?," IEEE J. Sel. Top. Quantum Electron., vol. 4, pp. 159–168, 1998.

[17] Z. Zhang, L. Zhan, K. Xu, J. Wu, Y. Xia, and J. Lin, "Multiwavelength fiber laser with fine adjustment, based on nonlinear polarization rotation and birefringence fiber filter," Opt. Lett., vol. 33, pp. 324–326, 2008.

[18] P. S. Liang, Z. X. Zhang, Q.Q. Kuang, and M. H. Sang, "All-fiber birefringent filter with fine tunability and changeable spacing," Laser Phys., vol. 19, pp. 2124–2128, 2009.

[19] D. Marcuse, "Simplified analysis of a polarizing optical fiber," IEEE J. Quantum Electron., vol. 26, pp. 550–557, 1990.

[20] N. J. Smith, K. J. Blow, and I. Andonovic, "Sideband generation through perturbations to the average soliton model," J. Lightwave Technol., vol. 10, pp. 1329–1333, 1992.

[21] S. Yamashita, T. Yoshida, S. Y. Set, P. Polynkin, and N. Peyghambarian, "Passively mode-locked short-cavity 10GHz Er:Yb-codoped phosphate-fiber laser using carbon nanotubes," Proceedings of SPIE 6453, pp. 64531Y-64531Y-9, 2007.

Dynamic control of the operation regimes of a mode-locked fiber laser based on intracavity polarizing fibers: experimental and theoretical validation

Guillermo E. Villanueva,[1] and Pere Pérez-Millán[2]

[1]Nanophotonics Technology Center, Universidad Politécnica de Valencia,
Camino de Vera s/n, 46022 Valencia, Spain
[2]Departamento de Física Aplicada-ICMUV, Universidad de Valencia,
Dr. Moliner 50, 46100 Burjassot, Spain

ABSTRACT

An intracavity polarizing fiber is proposed to control the emission regime of a passively mode-locked fiber laser. Stable operation in self-starting high and low dispersion soliton mode-locking and 100 GHz multiwavelength regimes is demonstrated through numerical simulations and experimental validation. Mode-locking stability is ensured by a saturable absorber in the ring cavity. Effective selection of operation regime is dynamically carried out controlling the intracavity polarization state.

Mode-locked fiber lasers have proven to be suitable sources of ultra-short optical pulses for applications like ultra-high-bit-rate communications, ultrafast spectroscopy and biomedicine. Fiber lasers fully exploit the advantages of optical fibers, such as compact waveguiding, large gain, effective heat dissipation and low-cost components [1]. When implementing passive mode-locking, pulse shaping is not further limited by the speed of external electronic signal generators in comparison to active mode-locking, allowing stable sub-picosecond pulses [2]. A well established technique for passively mode-locking is the use of fast saturable absorbers (SA), allowing single-polarization self-started soliton mode-locking [3,4]. On the other hand, Lyot filters based on the combination of in-line polarizers and birefringent fibers have been exploited for the generation of a multiwavelength emission regime [5]. Recently, polarizing (PZ) fibers with very low losses and ready to be spliced to standard fibers are commercially available, and they have been employed for non-linear polarization rotation (NLPR) mode-locking in fiber lasers [6]. In this work we demonstrate that introducing a PZ fiber in the cavity of a SA mode-locked laser, pulsed soliton mode-locking with controllable cavity dispersion and multiwavelength emission regimes can be obtained by controlling the state of polarization at the input and output of

the PZ fiber. Simulation and experimental validation of the proposed structure demonstrates the dynamic control of the three operating regimes. In comparison with other laser structures incorporating high-birefringent fibers and polarizers to implement intracavity Lyot filters [5], our proposal performs the polarizing effect in a fiber, and does not require a polarizer.

The cavity of the fiber laser is shown in Fig. 1. A saturable absorber performs the mode-locking stabilization mechanism. The fiber laser, without the PZ fiber, operates in a solitonic mode-locked regime. When inserting the PZ fiber in combination with two polarization controllers, it is possible to control the polarization-dependent losses applied to the optical pulse each roundtrip. Together with its inherent high birefringence, the PZ fiber can partially implement an intracavity multiwavelength Lyot filter [7], with configurability via the polarization controllers. The filtering effect of the PZ fiber results in a multiwavelength emission, therefore the fiber laser can be dynamically adjusted to operate in a pulsed or in a multiwavelength regime. Furthermore, this kind of single-polarization fibers exhibits different chromatic dispersion in each principal axis known as birefringence dispersion [8]. The PZ fiber birefringence dispersion provides a tool to control the roundtrip accumulated dispersion of the oscillating optical signal. Adjusting the cavity dispersion budget allows the control of the solitonic mode-locking operation.

In order to numerically model the fiber laser emission performance, pulse propagation is computed through the non-linear Schrödinger equation (NLSE). As polarization of the optical pulse has to be taken into account, then the coupled NLS equations (CNLSE) will be considered [9]. These are given by

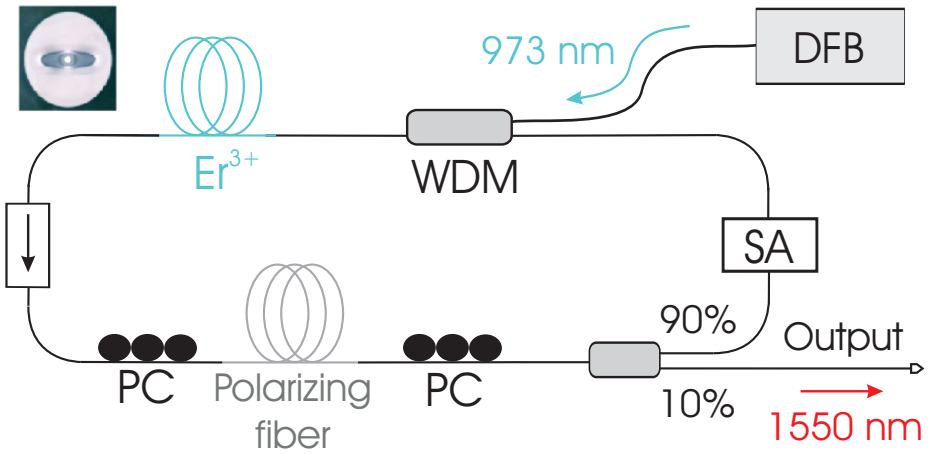

Figure 1: Scheme of the passively mode-locked fiber laser setup. DFB: Distributed feedback pump diode laser; WDM: 980/1550 Wavelength Division Multiplexer; Er^{3+}: erbium-doped fiber, PC: Polarization controller; SA: Semiconductor saturable absorber.

$$\left(\frac{\partial}{\partial z}+\beta_{1x}\frac{\partial}{\partial t}+j\frac{\beta_{2x}}{2}\frac{\partial^2}{\partial t^2}+\frac{\alpha_x}{2}-\frac{g}{2}-\frac{D_g}{2}\frac{\partial^2}{\partial t^2}\right)A_x = j\gamma\left(|A_x|^2+\frac{2}{3}|A_y|^2\right)A_x+j\frac{\gamma}{3}A_x^*A_y^2e^{-j2\Delta\beta_0 z}, \tag{1}$$

$$\left(\frac{\partial}{\partial z}+\beta_{1y}\frac{\partial}{\partial t}+j\frac{\beta_{2y}}{2}\frac{\partial^2}{\partial t^2}+\frac{\alpha_y}{2}-\frac{g}{2}-\frac{D_g}{2}\frac{\partial^2}{\partial t^2}\right)A_y = j\gamma\left(|A_y|^2+\frac{2}{3}|A_x|^2\right)A_y+j\frac{\gamma}{3}A_y^*A_x^2e^{j2\Delta\beta_0 z}, \tag{2}$$

Equations (1) and (2) describe the propagation of the slow-varying envelopes A_x and A_y for both linear polarizations. Birefringence of the optical fiber is denoted by the modal birefringence $\Delta\beta_0 = \beta_{0x} - \beta_{0y}$, group birefringence β_{1i} and dispersion birefringence β_{2i}, for $i = x, y$. Parameters α_i and g denote the attenuation and gain of the optical fiber respectively. The bandwidth of the gain medium is modeled by the gain dispersion D_g through the relation $D_g = d/\Omega_g^2$, where Ω_g is the half-width at half-maximum (HWHM) gain bandwidth, assuming a parabolic approximation. Note the explicit polarization dependence of optical losses α_i and chromatic dispersion β_{2i}, aimed to properly model the PZ fiber of the cavity. Nonlinear terms are governed by the fiber nonlinear coefficient γ. In Eq. (1) and (2), more complex nonlinear effects such as stimulated Raman scattering and self-steepening are neglected. The CNLSE are solved using the split-step Fourier transform method.

The fiber ring cavity is composed of the following components: 3 m of erbium doped fiber Fibercore DHB1500 (peak absorption of 15 dB/m at 1530 nm), pumped by a 400 mW diode laser at 976 nm through a 980/1550 nm wavelength division multiplexer (WDM); 3 m of Verrillon highly birefringent polarizing fiber (birefringence Δn = 10^{-3}, 0.6 dB/m extinction ratio); A Batop fiber pigtailed fast semiconductor saturable absorber (relaxation time 2 ps, saturation energy 235 pJ, modulation depth 15%); An optical isolator to prevent bidirectional lasing operation; Two polarization controllers (PC) asides the polarizing fiber; A 90:10 output coupler; And finally $\sim$8 m of single-mode fiber (SMF), from all component pigtails. The dispersion of SMF and Er doped-fiber were –20 and 15 ps^2/km respectively, and the estimated x and y polarization dispersions of the PZ fiber were 20 and 53 ps^2/km. A nonlinear coefficient of 1.5 mrad/(W·m) is assumed. The cross section of the PZ fiber is shown in the inset of Fig. 1, where a highly elliptical cladding can be observed.

Optical pulses are propagated through fiber sections solving the CNLSE, and the PCs and SA effects are applied discretely. Each PC is modeled by three waveplates ($\lambda/4$ - $\lambda/2$ - $\lambda/4$) through their Jones matrix. In each simulation, an initial 1ps Gaussian pulse is injected, and the output is extracted after convergence (usually reached in $\sim$1000 roundtrips).

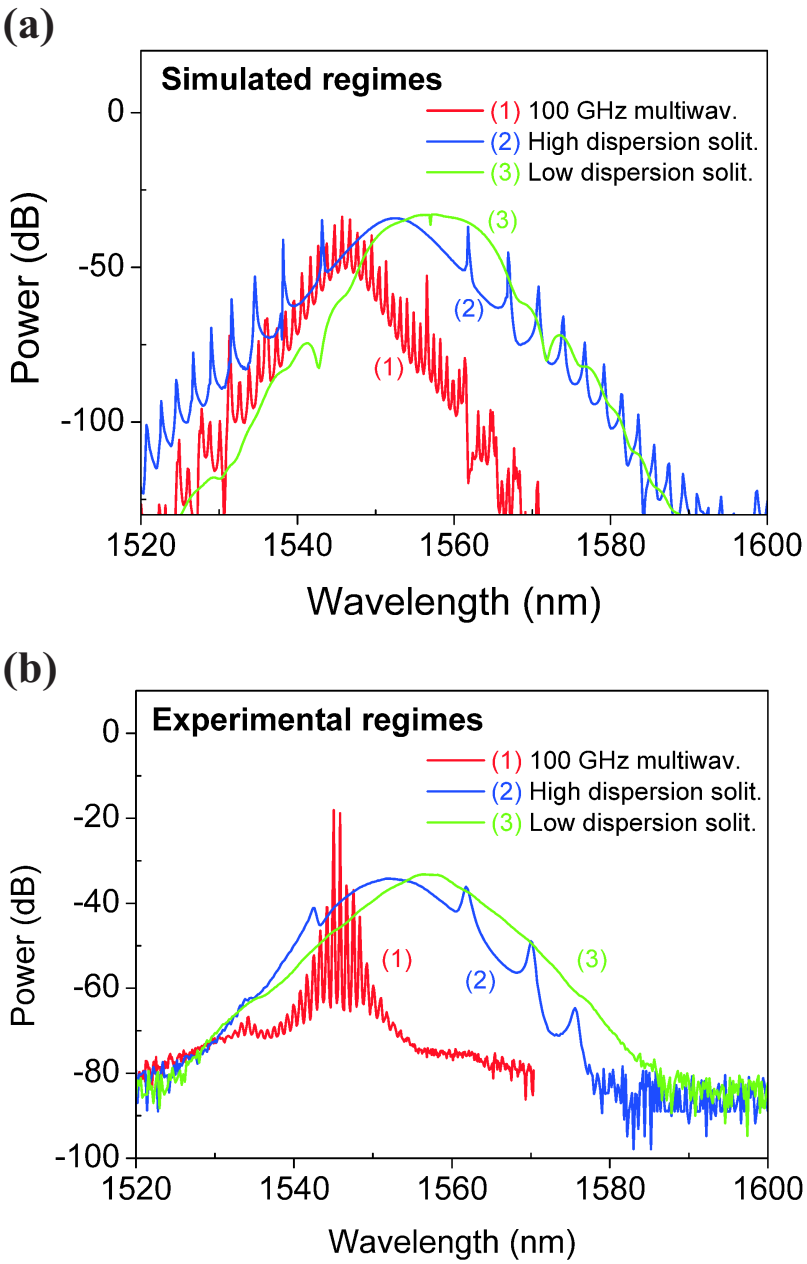

Figure 2: Optical output spectra of the three operation regimes of the laser. a) Calculated. b) Measured.

The PZ fiber is considered as a Lyot filter in which the polarizing axes is identical to the birefringence axis, ideally leading to no spectral filtering. In contrast to a conventional Lyot filter where an ideal polarizer is required, the PZ fiber shows an intended finite polarization extinction rate. Then a PZ fiber section can be analyzed as a high-birefringence fiber and a finite extinction ratio polarizer. If we include a polarization controller next to the PZ fiber, a spectral filtering can be deduced from the x polarization components power transmission, given by

$$|T_x|^2 = \cos^2(\theta) + \tau^2 \sin^2(\theta) + \tau \sin(2\theta)\cos(\Delta\varphi), \tag{3}$$

where $\Delta\varphi$ denotes the linear phase shift between two polarization components induced by the fiber, θ is the rotation angle between components introduced by the polarization controller and τ are the polarizing losses. The operating regimes of the laser depend on the relative orientation of the state of polarization of the light with regard to the polarization axis of the PZ fiber. The polarization state is adjusted by the polarization controllers. An orientation resulting in a low wavelength filtering results in a non-effective suppression of stimulation of the filtered wavelengths, hence the laser operates in a low dispersion solitonic regime with a repetition rate corresponding to the original FSR of the ring cavity ($\sim$15 MHz) and with a pulsewidth of 25 ps estimated from oscilloscope trace (see Fig. 4). Due to the unexpected high time-bandwidth product, multipulse bunching is likely to occur, but the 7ps oscilloscope resolution was not sufficient to identify multipulse emission. Simulations provide pulsewidths of 580 and 630 fs for the high and low dispersion soliton regime respectively, and pulses energies of 100 pJ. Figure 2(a) and 2(b) shows the calculated and measured optical output spectrum respectively, showing a bandwidth of 8.2 nm FWHM. Depending on the effective amount of polarization dispersion induced in the PZ fiber by the orientation of the PCs, a larger net anomalous dispersion can be obtained and the laser works under a high dispersion soliton regime. The calculated average cavity dispersion for the low and high dispersion regimes were - 3.71 and - 0.073 ps^2/km respectively, and the measured temporal pulsewidth in this regime is 0.6 ps (obtained from autocorrelation trace of Fig. 4-down). The differences in the Kelly sidebands observed in the calculated and simulated spectra in Fig. 2 are attributed to deviations in estimated cavity length and dispersion. When switching from high to low dispersion soliton regime, Kelly sidebands are no longer visible, as their spectral positions shift away from central wavelength due to the low net dispersion [10]. Due to the polarizing effect of the PZ fiber, pulse shaping through NLPR can be expected, presenting a hybrid mode-locking mechanism [11] with adjustable NLPR mechanism through polarization control. We could not mode-lock the laser without the SA for the same pumping and polarizing conditions. From the literature, NLPR is generally more unstable than SA mode-locking, and our laser shows good pulse stability, so we believe SA is the predominant mode-locking mechanism. Figure 3 shows simulated high dispersion solitonic pulse shaping for an initial 1 ps-width Gaussian pulse, reaching a 580 fs-width steady-state in 200 roundtrips.

The third operation regime is achieved when an orientation results in a high extinction ratio wavelength filtering, yielding a multiwavelength emission with a FSR of 106 GHz. The 106 GHz wavelength spacing is in accordance with the length and birefringence of the PZ fiber following the relation

$$\Delta\lambda = \frac{\lambda^2}{\Delta n L_{PZ}}, \tag{4}$$

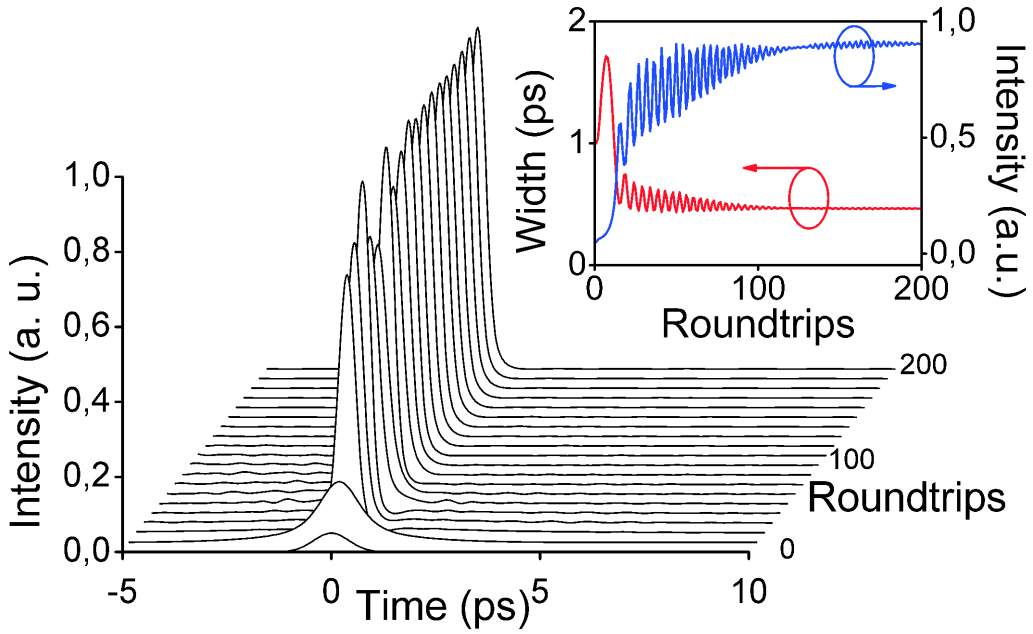

Figure 3: Calculated stable mode-locked pulse formation in the high dispersion solitonic regime. A Gaussian pulse of 1 ps width is employed as initial wavefunction. Inset: pulse width and peak intensity evolution.

where Δn and L_{PZ} denote the modal birefringence and length of the PZ fiber respectively. Figure 2(b) shows the experimental optical output spectra for the three operation regimes. Each regime is achieved by fine adjustment of the polarization through the two PCs. For the two mode-locked regimes, a stable pulsed output signal is obtained. In contrast to CW multiwavelength lasers, in which NLPR can be exploited as gain equalization [5], the multiwavelength regime constitutes a harmonic mode-locking of 106 GHz pulse repetition frequency. Unfortunately, no stable pulse emission was achieved from this regime. We believe spectral filter finesse and pumping power are not high enough to reach stable harmonic mode-locking. Figure 2(a) includes the three operation regimes simulated spectra. Figure 4 shows the temporal wavefunctions for both pulsed regimes.

In conclusion, a fiber laser with dynamic control of its operation regime has been proposed. High and low dispersion soliton mode-locking, in addition to 106 GHz multiwavelength regimes are demostrated by a single cavity, and the dynamic selection of a particular working regimes is performed via polarization control of the oscillating signal within the cavity. The operation control is based on a section of polarizing fiber inserted in the ring cavity, providing polarizing properties, in addition to a high modal, group and dispersion birefringence. Effective regime control is demonstrated and evaluated experimentally and computionally. Pulsewidths of 600 fs and wavelengths spacing of 106 GHz for multiwavelength and solitonic operation respectively are obtained, finding potential application in high-bit-rate communications.

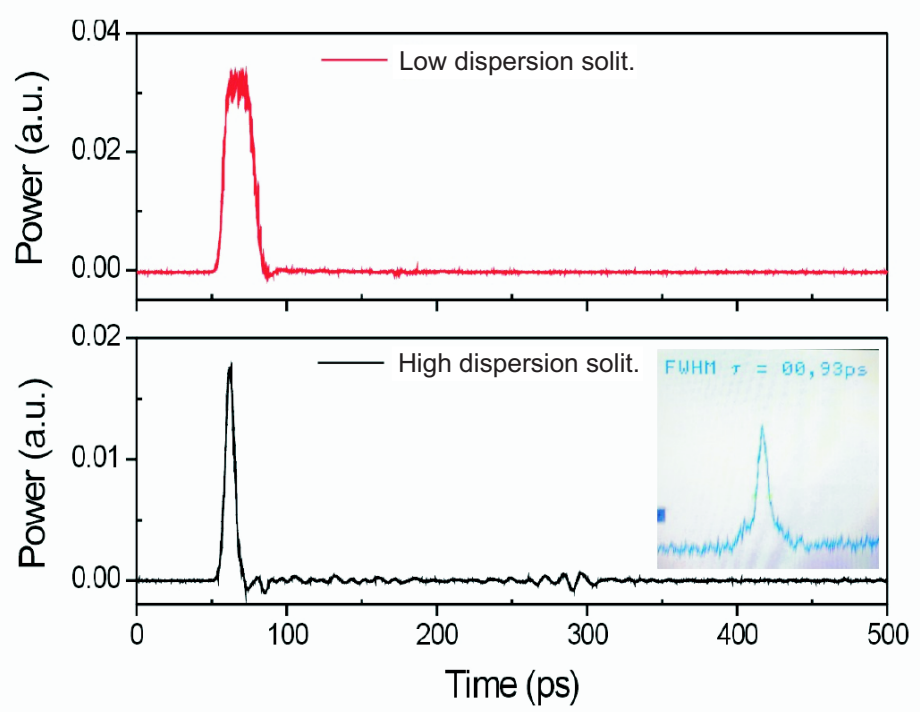

Figure 4: Pulsed temporal wavefunction of the laser output in low dispersion soliton regime and in high dispersion soliton regime with an oscilloscope resolution of 7 ps. Inset: Autocorrelation trace of the high dispersion soliton regime pulses with a resolution of 10 fs.

References

[1] M. E. Fermann, and I. Hartl, "Ultrafast fiber laser technology," IEEE J. Sel. Topics Quantum Electron., vol. 15, pp. 191–206, 2009.

[2] E. P. Ippen, "Principles of passive mode locking," Appl. Phys. B, vol. 58, pp. 159, 1994.

[3] H. Haus, "Theory of mode locking with a slow saturable absorber," IEEE J. Quantum Electron., vol. 11, pp. 736–746, 1975.

[4] F. X. Kärtner, J. Aus der Au, and U, Keller, "Mode-locking with slow and fast saturable absorbers-What's the difference?," IEEE J. Sel. Topics Quantum Electron., vol. 4, pp. 159–168, 1998.

[5] Z. Zhang, L. Zhan, K. Xu, J. Wu, Y. Xia, and J. Lin, "Multiwavelength fiber laser with fine adjustment, based on nonlinear polarization rotation and birefringence fiber filter," Opt. Lett., vol. 33, pp. 324–326, 2008.

[6] S. Li, X. Chen, D. Kuksenkov, J. Koh, M. Li, L. Zenteno, and D. Nolan, "Wavelength tunable stretched-pulse mode-locked all-fiber erbium ring laser with single polarization fiber," Opt. Express, vol. 14, pp. 6098–6102, 2006.

[7] P. S. Liang, Z. X. Zhang, Q. Q. Kuang, and M. H. Sang, "All-fiber birefringent filter with fine tunability and changeable spacing," Laser Phys., vol. 19, pp. 2124–2128, 2009.

[8] D. Marcuse, "Simplified analysis of a polarizing optical fiber," IEEE J. Quantum Electron., vol. 26, pp. 550–557, 1990.

[9] C. R. Menyuk, "Pulse propagation in an elliptically birefringent Kerr medium," IEEE J. Quantum Electron., vol. 25, pp. 2674–2682, 1989.

[10] N. J. Smith, K. J. Blow, and I. Andonovic, "Sideband generation through perturbations to the average soliton model," J. Lightw. Technol., vol. 10, pp. 1329–1333, 1992.

[11] A. Ruehl, D. Wandt, U. Morgner, and D. Kracht, "On wave-breaking free fiber lasers mode-locked with two saturable absorber mechanisms," Opt. Express, vol. 16, pp. 8181–8189, 2008.

Linear and nonlinear optical properties of carbon nanotube coated single mode optical fiber gratings

Guillermo E. Villanueva,[1] Michael B. Jakubinek,[2] Benoit Simard,[2] Claudio J. Oton,[1] Joaquín Matres,[1] Li-Yang Shao,[3] Pere Pérez-Millán,[1] and Jacques Albert[3]

[1]Nanophotonics Technology Center, Universidad Politécnica de Valencia, Camino de Vera s/n, 46022 Valencia, Spain
[2]Steacie Institute for Molecular Sciences, National Research Council Canada, 100 Sussex Dr., Ottawa ON K1A 0R6, Canada
[3]Advanced Photonic Components Group, Carleton University, 1125 Colonel By Drive, Ottawa ON K1S 5B6, Canada

ABSTRACT

Single-wall carbon nanotube deposition on the cladding of optical fibers has been carried out to fabricate an all-fiber nonlinear device. Two different nanotube deposition techniques were studied. The first consisted of repeatedly immersing the optical fiber into a nanotube supension, increasing the thickness of the coating in each step. The second deposition involved wrapping a thin film of nanotubes around the optical fiber. For both cases, interaction of transmitted light through the fiber core with the external coating was assisted by the cladding mode resonances of a tilted fiber Bragg grating. Ultrafast nonlinear effects of the nanotube-coated fiber were measured by means of a pump-probe pulses experiment.

Single-wall carbon nanotubes (SWNTs) have found innovative applications in the optical field due to their nonlinear properties in the near IR. Depending on the chirality of SWNTs, they can be either metallic or semiconducting, the latter being the desired behavior for nonlinear optical performance. Many optical applications could benefit from using SWNTs as nonlinear materials, such as noise suppression, wavelength conversion and passive mode-locking [1-3]. A challenge when designing SWNT-based devices is incorporating the nanotubes in such a way as to enhance their interaction with light. One common method involves dispersing SWNTs in a solvent and spraying onto substrates in order to produce a nanotube film in the middle of a light beam [3]. Some inherent drawbacks in these configurations are the need for alignment and focusing stages, low SWNT burn thresholds and low nonlinear interaction length. Solutions that overcome these challenges are based on SWNT

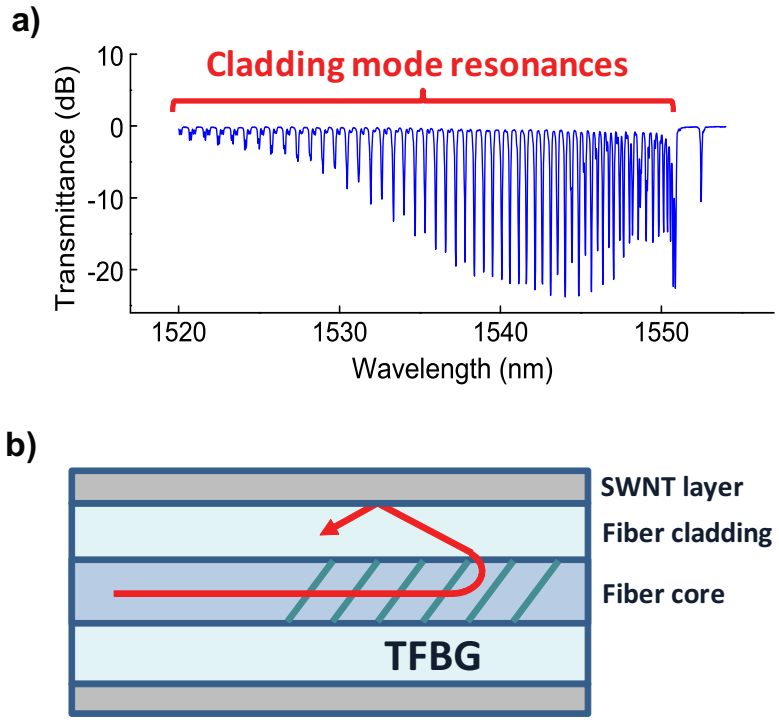

Figure 1: (a) Measured linear transmission response of a 4 degree tilted fiber Bragg grating. (b) Nanotube-coated TFBG structure. Light for which the wavelength matches a cladding mode resonance couples to a cladding mode, interacting with the outer SWNT layer.

deposition onto optical fibers. Tapered, D-shaped and hollow optical fibers have been proposed to take advantage of the evanescent field interaction with SWNTs, distributing that interaction along the fiber length [4-6]. Nevertheless, manufacturing and handling these kinds of fibers is quite complex and delicate. In this work we propose for the first time SWNT deposition on standard optical fiber cladding for nonlinear applications. Interaction of light propagating through the fiber core with the outer SWNT coating is achieved via cladding mode resonances in a tilted fiber Bragg grating (TFBG). Two nanotube deposition methods have been carried out: dip-coating of the optical fiber in a SWNT suspension and wrapping of a SWNT film around the optical fiber.

A TFBG is a kind of grating in which the index modulation planes are not orthogonal to the fiber axis, but form a particular tilt angle. This inclination enhances the coupling of light from core mode to counter-propagating cladding mode resonances. Consequently, the grating transmission response is a multi-notch response consisting of numerous cladding mode resonances in addition to the core mode resonance (see Fig. 1(a)). The transverse mode profile of cladding modes spreads to the cladding of the fiber and interacts with the outer medium interface. Therefore cladding mode resonance frequencies depend on the refractive index of the outer medium in addition to other parameters. This feature can be exploited for refractive sensing applications [7]. In our device, the external coating is a

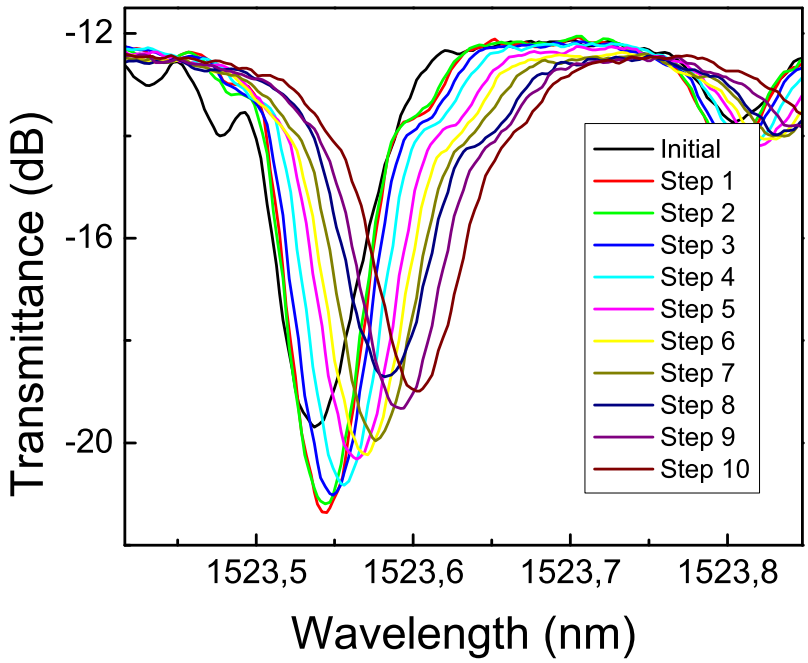

Figure 2: Cladding mode resonance monitored for one to ten dip-coating cycles. All responses are wavelength and amplitude equalized with regard to the Bragg resonance.

layer of SWNTs, and interaction with light is allowed through cladding mode resonances. As SWNTs are a nonlinear material for optical wavelengths, the outer refractive index depends on the light intensity and an intensity-dependent TFBG transmission response is obtained. Fig. 1(b) depicts the SWNT-coated optical fiber structure.

Deposition of the SWNT coating was done either by dip-coating in a suspension of SWNTs in N,N-dimethylformamide (DMF) (dip-coated), or by collecting sections of a freely floating SWNT film around the optical fiber cladding (film-wrapped). Both approaches used high purity SWNTs ($\sim$ 1.3 nm in diameter and $>$ 1 μm in length) produced by a laser-oven method [8], and deposited onto single mode fibers with a TFBG written in them. Both gratings had a length of 20 mm, a tilt angle of 4 degrees and a center wavelength of 1552 nm. They were fabricated using a phase mask and a 248 nm pulsed irradiation from a KrF excimer laser. An example of TFBG transmittance in this study, measured when injecting light from a 1550 nm centered broadband source into an uncoated fiber, is shown in Fig. 1(a).

For dip-coating, $\sim$10 mg SWNTs were first functionalized by bath sonication (2 hr) in 70% nitric acid. These SWNTs were recovered by filtration, rinsed with nanopure water ($>$ 18 MΩ cm) and by sonication (2 hr) in nanopure water, and then re-dispersed by sonication in 10 mL DMF. After the acid-treatment the SWNTs disperse readily in DMF producing a black suspension. The optical fibers were then coated by dipping the section containing the TFBG, sequentially, in a 0.1 wt% aqueous solution of 3-aminopropyltriethoxysilane

(APTES), followed by the SWNT/DMF suspension, and finally in pure water. APTES has been used in the preparation of CNT networks on glass, silicon, and PET. In that approach submerging the substrate in an ATPES solution results in formation of an amino-terminated, silanized surface. This surface is positively charged and the COOH-functionalized SWNTs adsorb readily. The last step of water immersion was intended to homogenize the SWNT distribution and provide a well-known external medium when measuring TFBG transmission spectra. Repeated dipping cycles were used to increase the amount of SWNT coating and the deposition was monitored by measuring the transmission spectrum of the grating after each of ten dipping cycles. Cladding mode resonances are related to the outer medium properties, therefore the amount of deposited SWNTs will be reflected in these resonances. Fig. 2 shows, in detail, one high order cladding mode centered at 1523.6 nm for each dipping step. To quantitatively compare resonance wavelength shifts and depth changes, all spectra have been normalized in amplitude and wavelength to the Bragg mode resonance (which is inherently immune to coating and external media changes). A clear shift ($\sim$ 67 pm) of the cladding mode resonance towards higher wavelength is observed. Monitoring this relative shift of cladding mode resonance wavelength provides a direct indicator of SWNT coating thickness for consecutive dip-coating cycles. The amplitude of the resonance depends on many factors but mostly on the overlap between the core mode, cladding mode and index modulation. When the first carbon nanotubes are deposited, the cladding mode field amplitude is more strongly perturbed because of the new boundary condition. This justifies the amplitude increase observed between the initial state and step 1 in Fig. 2, whereas subsequent dipping steps decrease the depth.

For the film-wrapped TFBG, a floating SWNT film was first prepared as previously described [9]. In this case SWNTs (4 mg/L) were dispersed in a 2 wt% aqueous sodium cholate solution, followed by production of a thin film by vacuum filtration of $\sim$ 10 mL through a cellulose acetate filter membrane (47 mm diameter, 0.22 μm pore size), and then detachment of the film by submersion in water. Part of the floating film was collected by slowly lifting and rotating the optical fiber as it was pulled through the film in order to obtain a SWNT coating over the TFBG. The film tears as it is lifted away from the water surface but the method still allows for efficient collection of a much thicker coating, which is visibly dark grey. Due to the manual procedure of this method, the dip-coating approach is expected to provide better reproducibility.

Both SWNT coatings were examined by SEM imaging and Raman spectroscopy, and the results are shown in Fig. 3, proving the presence of nanotubes on the fiber surface. From SEM images and variation of the intensity of the Raman spectra from location-to-location, we can deduce that dip-coating provides a thinner and more homogeneous layer of SWNTs on the fiber. In contrast the wrapping technique produces a much thicker coating, but with less control of the uniformity of the wrapping.

An experiment is performed to demonstrate the interaction of light with the SWNT coating via TFBG cladding mode resonances. Nonlinear effects were measured with a pump-

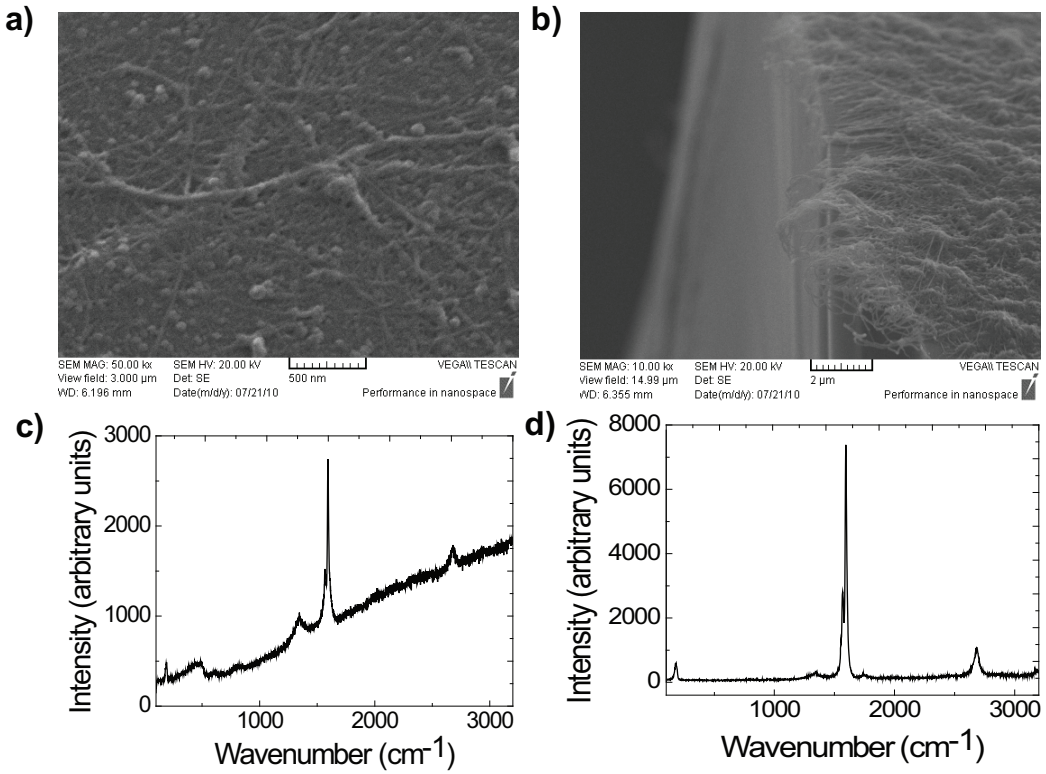

Figure 3: SEM images of deposited nanotubes on the optical fiber cladding for (a) dip-coating and (b) wrapping techniques. In (b) the edge of a cleaved fiber is depicted. Raman spectroscopy for (c) dip-coating and (d) wrapping techniques, where the background slope, due to the relatively small number of SWNTs in the sampling volume that is achieved with the sparse coating method.

probe phase-sensitive set-up described elsewhere [10]. In this technique, a 1ps laser pulse is divided into three pulses, one of them intense (pump) and two identical weak ones (a reference and a probe). All three pulses are combined by setting the pump very close in time to the probe, making this delay variable with a delay line. The amplitude and phase of the probe with respect to the reference pulse is measured with a heterodyne technique and monitored as a function of the delay of the pump. The pulsed light injected into the TFBG had -3.5 dBm and 1535 nm of average power and wavelength respectively, providing 22.5 W of peak power in the fiber. The 1 ps duration determines the measurement resolution. The optical fiber coated by the wrapping method was measured since it provides a thicker coating compared to dip-coating and, therefore, larger nonlinear effects are expected. Fig. 4 shows the nonlinear responses of the SWNT film-wrapped TFBG, a regular TFBG without coating, and standard fiber. These results demonstrate that interaction of the pump with the nonlinear cladding, as mediated by the TFBG, is sufficient to modulate the amplitude of the probe by more than 6% (12% in intensity) on a picosecond time scale. The phase response remains constant, since it is mainly due to Kerr effect from the fiber silica. Therefore, linear and non-linear transmission responses of the tilted grating induce no noticeable effect in the phase of the transmitted pulse. We also have checked that the

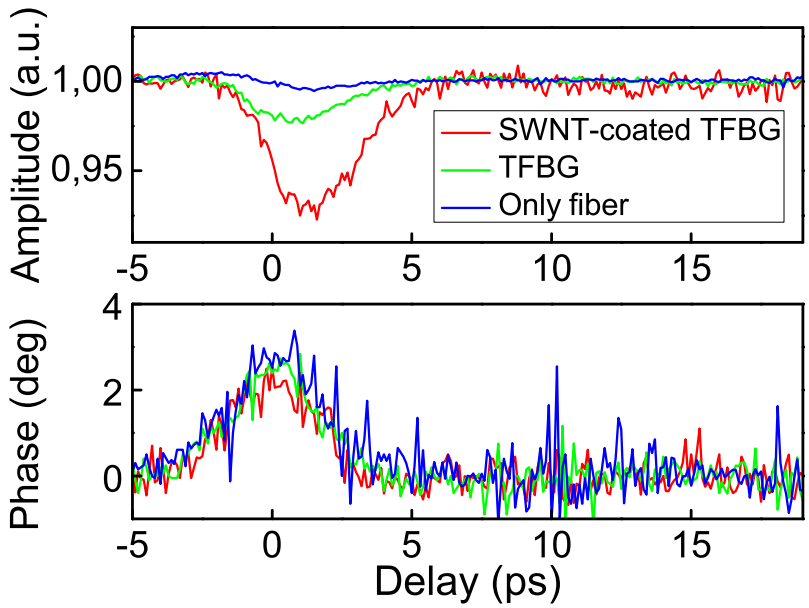

Figure 4: Nonlinear amplitude and phase responses of the SWNT-coated TFBG, of an un-coated regular 4 deg TFBG and of a standard fiber.

magnitude of the amplitude effect depends on the relative spectra of the TFBG and of the probe light, indicating possible optimization strategies.

In conclusion, SWNT-coated single mode optical fibers have been proposed using, for the first time, a standard optical fiber with a TFBG for nonlinear applications. Two simple techniques for nanotube deposition on the cladding surface have been carried out. The use of tilted fiber Bragg grating assisted the interaction of transmitted light with the SWNT-coating. Measurement of cladding mode resonances allowed us to monitor the progressive deposition of nanotubes on the cladding for a dip-coating method. The wrapping method provided a simple and innovative way to deposit thick SWNT layers on optical fibers. Picosecond nonlinear effects were measured by means of pump-probe measurements, showing an effective intensity modulation via TFBG cladding mode coupling.

References

[1] Y. Sakakibara, A. Rozhin, H. Kataura, Y. Achiba, and M. Tokumoto, "Carbon nanotube-poly(vinylalcohol) nanocomposite film devices: applications for femtosecond fiber laser mode lockers and optical amplifier noise suppressors," Jpn. J. Appl. Phys. vol. 44, pp. 1621–1625, 2005.

[2] K. K. Chow, S. Yamashita, and Y. W. Song, "A widely tunable wavelength converter based on nonlinear polarization rotation in a carbon-nanotube-deposited D-shaped fiber," Opt. Express, vol. 17, pp. 7664–7669, 2009.

[3] S. Set, H. Yaguchi, Y. Tanaka, and M. Jablonski, "Ultrafast fiber pulsed lasers incorporating carbon nanotubes," IEEE J. on Select. Top. in Quantum Electron., vol. 10, pp. 137–146, 2004.

[4] K. K. Chow, M. Tsuji, and S. Yamashita, "Single-walled carbon-nanotube-deposited tapered fiber for four-wave mixing based wavelength conversion," Appl. Phys. Lett., vol. 96, pp. 061104, 201).

[5] K. K. Chow and S. Yamashita, "Four-wave mixing in a single-walled carbon-nanotube-deposited D-shaped fiber and its application in tunable wavelength conversion," Opt. Express, vol. 17, pp. 15608–15613, 2009.

[6] S. Y. Choi and F. Rotermund and H. Jung and K. Oh and D. Yeom, "Femtosecond mode-locked fiber laser employing a hollow optical fiber filled with carbon nanotube dispersion as saturable absorber," Opt. Express, vol. 17, pp. 21788–21793, 2009.

[7] C. Chan, C. Chen, A. Jafari, A. Laronche, D. J. Thomson, and J. Albert, "Optical fiber refractometer using narrowband cladding-mode resonance shifts," Appl. Optics, vol. 46, pp. 1142–1149, 2007.

[8] C. Kingston, Z. Jakubek, S. Dénommée, , and B. Simard, "Efficient laser synthesis of single-walled carbon nanotubes through laser heating of the condensing vaporization plume," Carbon, vol. 42, pp. 1657–1664, 2004.

[9] M. Jakubinek, M. Johnson, M. White, J. Guan, and B. Simard, "Novel method to produce single-walled carbon nanotube films and their thermal and electrical properties," J. Nanosci. Nanotechnol., vol. 10, pp. 8151–8157, 2010.

[10] T. Vallaitis, C. Koos, R. Bonk, W. Freude, M. Laemmlin, C. Meuer, D. Bimberg, and J. Leuthold, "Slow and fast dynamics of gain and phase in a quantum dot semiconductor optical amplifier," Opt. Express, vol. 16, pp. 170–178, 2008.

Chapter 4

General discussion

Previous chapters have compiled the main publications derived from the realization of this thesis. Chapter 2 focused on continuous wave dual-wavelength fiber lasers and their applications in microwave signal generation, and Chapter 3 dealt with pulsed mode-locked fiber lasers. This chapter provides a general discussion about the obtained results.

For microwave signal generation applications, the performed work was oriented towards the design of an innovative tunable dual-wavelength DFB fiber laser. The basic principle is the induction of two controllable local phase shifts in a FBG written in an erbium-doped optical fiber. DC-controlled piezoelectric actuators were used to stretch short fiber sections, and they allowed tunability of the wavelength difference between the two single longitudinal emitted modes. In this way, when photodetecting the laser output, a photogenerated signal with a frequency equal to the modes frequency difference is obtained.

For the experimental validation, a 15 cm long FBG was written in an erbium-doped optical fiber. The stopband spectral width was 60 pm. On the one hand, such spectral width sets the maximum frequency difference between modes, i. e., the maximum photogenerated frequency. On the other hand, the minimum frequency is set by the spatial separation of the phase shifts as determined by equation (2.5) on page 26. Stable dual-wavelength lasing is achieved in an optical tuning range of 1-54 pm, which is equivalent to a 0.128-7 GHz photodetected frequency range. One important property resulting from the piezoelectric actuators is the continuous characteristic of the tuning range, in contrast to other discrete proposals [1, 2].

Our dual-wavelength fiber laser frequency range is linked to the grating spectral response. Extension of the frequency range comprises the design of wider stopband gratings. In our case, shortening the grating would increase the stopband bandwidth. Nonetheless, we do not consider this solution as a worthy option to extent the tuning range: a shorter grating in a DFB fiber laser enlarges the passive transmission peak

that appears in the stopband, which derives in an enhancement of emitted linewidth. Common to every laser configuration, the fundamental Schawlow and Townes limit for the linewidth of a laser sets an inverse relation between linewidth and cavity length [3]. In addition, a shorter grating means a shorter length of doped-fiber, reducing the available gain to reach lasing condition.

To further extent the operation frequency range, the second publication of Chapter 2 proposes a cascaded DFB fiber laser. Piezoelectric transducers are exploited even more than the previous structure, establishing two completely different DFB cavities in the same grating. With the cascaded DFB laser, the mode frequencies can separate up to 724 pm. Continuous photogenerated signal frequencies from 0.72 to 92 GHz are obtained, enhancing the tuning range of the previous fiber laser one order of magnitude. While a large piezoelectric actuator (with 5x5x36 mm dimensions) is in charge of stretching one half of the grating and implements a coarse tunability, two small actuators (2x2x2 mm) induce the local phase shifts and provide a fine tuning control. Both fiber lasers presented in Chapter 2 constitute highly compact optical sources, as the cavity comprises 15 cm of erbium-doped optical fiber, and the dimensions of the actuators attached to the fiber are considerably small.

Another aspect to be discussed is the phase noise of the photogenerated microwave signals. In high-frequency signal generation based on two-color photomixing, the phase noise of the electrical signal is closely related to the phase noise of optical modes and their mutual coherence. Two free-running lasers will suffer from independent noise sources, and they will produce a poor photomixed signal in terms of phase noise. Multiple techniques have been adopted to correlate both optical modes, such as the use of injection-locked lasers [4] or filtering of mode-locked lasers [5, 6]. Our dual-wavelength DFB fiber laser generates two longitudinal modes in one cavity, in a similar way to longitudinal modes generated in one cavity for a mode-locked laser. Then, a high coherence degree between both modes is present. From the second approach developed in this thesis, a lower coherence degree is expected, as the laser consists of two DFB cavities. Even though, they share the same grating and fiber, so oscillating modes will experience similar phase and amplitude drifts. A future work extension of this thesis is phase noise characterization of the photogenerated signal for both fiber laser designs, and for two different single-mode DFB fiber lasers to have a common reference to compare with.

Also, some instability due to polarization mode competition has been observed in the fiber laser performance. In the photogenerated microwave signal the polarization mode competition is identified as spurious signals at 135 MHz from the nominal electrical tone (see figure 5 on page 41 and figure 3 (b) on page 49). Some steps to be taken in order to alleviate polarization instability are the use of erbium-doped highly-birefringent fibers with selective pressure points to promote oscillation of one single polarization, or implementing a cavity in an erbium-doped polarizing fiber.

Chapter 3 presented the work carried out regarding pulsed mode-locked fiber lasers. Design, simulation, building and characterization of different active and passive

mode-locked fiber lasers for photonic-assisted analog to digital conversion applications were realized. Main target specifications for PADC applications were a pulse repetition frequency of 1.3 GHz, time jitter below 100 fs and sub-picosecond pulse temporal width.

In this study, active mode-locking was implemented by an optical Mach-Zehnder modulator inserted in a ring fiber cavity. The high bandwidth of the modulator allowed a wide tunability of the pulse repetition frequency up to 50 GHz. Stable mode-locked operation was demonstrated, showing sub-Hz linewidth photodetected signals with signal to noise ratios up to 80 dBs. Experimental results were completed with numerical calculations, and effective pulse formation from white noise due to cavity loss modulation was simulated. On the other hand, Mach-Zehnder modulators have high insertion losses (typically over 6 dB) and need for polarization control at their input, so cavity losses get increased. In addition, active mode-locking is accompanied by electronics to feed the electro-optic modulator, like RF cabling and high frequency synthesizers, raising the cost and complexity of the whole optical source.

In the case of passive mode-locking, a semiconductor saturable absorber was employed. The first passive mode-locked set-up was a ring cavity with a fundamental repetition frequency of 27 MHz. Self-starting mode-locking is easily reached with the SA action, and pulses with 500 fs width and time jitters below 180 fs are obtained under solitonic operation. A couple of techniques to increase the pulse repetition frequency were studied: exploitation of Vernier effect and fiber ring intracavity filtering. Even though these techniques achieve effective repetition frequency multiplication to get the reference 1.3 GHz, both of them failed to provide a good suppression of spurious harmonics. In comparison with active mode-locking, the passive mode-locking set-up constitutes a simpler and lighter optical pulsed source. Reduction of the source complexity is further explored by designing a short linear cavity. In this source, a 7 cm cavity length directly provides a fundamental repetition frequency of 1.4 GHz. The use of an end-facet deposited dichroic mirror and a butt-coupled SESAM makes this cavity extremely compact. Mode-locking operation is evaluated numerically and experimentally. Moreover, a piezoelectric actuator attached to the cavity was able to stretch the cavity, thus performing pulse repetition frequency continuous tunability of 500 kHz. This figure can seem quite modest, but for sub-sampling downconversion PADC configurations, it is practical enough to effectively prevent overlapping of aliased RF components [7].

Intracavity polarizing fibers in passive mode-locked fiber lasers have been studied in Chapter 3. The cladding of the polarizing fiber employed has a highly elliptical design, allowing waveguiding of only one polarization in a wide wavelength range. This fiber not only introduces polarization-dependent losses into the cavity, but also modal birefringence and birefringence dispersion [8]. Depending on the polarization, the propagating optical pulse through the PZ fiber experiments different losses and chromatic dispersion. By means of two polarization controllers asides the PZ fiber section, it was possible to control the operation regime of a passive mode-locked ring fiber

laser. Three regimes were observed; high dispersion and low dispersion solitonic pulsed regimes, and 106 GHz multiwavelength emission regime. Pulse width of 600 fs was achieved for the high dispersion solitonic emission, while apparent multipulse bunching effect was present in the low dispersion solitonic operation. The multiwavelength operation originates from spectral filtering due to the polarizing and birefringence effect of the PZ fiber, and experimental spectra are in accordance with numerical calculations performed from coupled nonlinear Schrödinger equation solution. Even though the laser was unable to emit stable pulsed emission in this multiwavelength regime, we believe this regime is a harmonic mode-locking mechanism. Therefore, this scheme must be further studied to reach stable harmonic mode-locked regimes with repetition frequencies over 100 GHz.

Finally, this thesis includes a study of a carbon nanotube-based fiber device to demonstrate versatile nonlinear interaction of light propagating through optical fiber and nanotubes deposited on the fiber cladding surface. The approach makes use of a tilted fiber Bragg grating, which is able to couple light to the fiber cladding. As a conventional fiber Bragg grating, the coupling phenomenon is resonant, so only some frequencies will be coupled from the co-propagating core mode to counter-propagating cladding modes. In the present work, a TFBG was written in an optical fiber, and carbon nanotubes were subsequently deposited on the fiber cladding. Deposition of carbon nanotubes on optical fibers were carried out using two different methods: dip-coating and film wrapping. The fist deposition technique exploited the spectral response of tilted gratings to monitor the layer growth, since cladding mode resonances are sensitive to outer medium [9]. Alternatively, film wrapping provided a simpler way to deposit CNTs in optical fibers, and produced thicker layers of CNTs, but with lower homogeneity. The resulting CNT-coated optical fibers were checked by scanning electron microscopy and Raman spectroscopy.

Ultrafast nonlinearity of CNTs was measured via a pump probe set-up. The experiment allowed us to measure the temporal nonlinear response of the nonlinear tilted grating. Figure 4 on page 116 shows a 12% intensity modulation, and no phase response. However, the combination of a tilted grating with a nonlinear external medium (the nanotube layer) does not provide the characteristic broad spectral response of single walled carbon nanotubes. Instead, the spectral transmittance is basically the multinotch response imposed by the tilted grating. Excited nonlinear effects in the external medium result in frequency shifts of the cladding mode resonances. Instantaneous cladding mode shifts do not necessarily mean a nonlinear absorbance of the propagating pulse, but an instantaneous change in the multinocth spectral filtering. This effect is not straightforward, and multiple parameters such as polarization of pump and probe pulses as well as spectral TFBG response considerably affect the final nonlinear response. Four-wave mixing has recently been demonstrated for this kind of nanotube-coated TFBG device [10].

Bibliography

[1] R. Sova, C.-S. Kim, and J. Kang, "Tunable dual-wavelength all-PM fiber ring laser," *Photonics Technology Letters, IEEE*, vol. 14, no. 3, pp. 287 –289, Mar. 2002.

[2] H. Ahmad, M. Zulkifli, A. Latif, K. Thambiratnam, and S. Harun, "Dual wavelength fibre laser with tunable channel spacing using an SOA and dual AWGs," *Journal of Modern Optics*, vol. 56, no. 16, pp. 1768–1773, 2009.

[3] A. L. Schawlow and C. H. Townes, "Infrared and Optical Masers," *Physical Review*, vol. 112, pp. 1940–1949, 1958.

[4] L. Thévenaz, D. Alasia, S. Le Floch, and J. Troger, "Generation of high-quality signals for optical sensing using DFB lasers injection locking," in *Second European Workshop on Optical Fibre Sensors*, ser. Proceedings of SPIE - The International Society for Optical Engineering, vol. 5502, 2004, pp. 556–559.

[5] A. Criado, P. Acedo, G. Carpintero, C. de Dios, and K. Yvind, "Observation of phase noise reduction in photonically synthesized sub-THz signals using a passively mode-locked laser diode and highly selective optical filtering." *Optics Express*, vol. 20, no. 2, pp. 1253–60, 2012.

[6] G. Serafino, P. Ghelfi, P. Perez-Millan, G. Villanueva, J. Palaci, J. Cruz, and A. Bogoni, "Phase and amplitude stability of EHF-band radar carriers generated from an active mode-locked laser," *Lightwave Technology, Journal of*, vol. 29, no. 23, pp. 3551 –3559, Dec. 2011.

[7] R. Barrak, A. Ghazel, and F. Ghannouchi, "Design of sampling-based downconversion stage for multistandard RF subsampling receiver," in *Electronics, Circuits and Systems, 2006. ICECS '06. 13th IEEE International Conference on*, Dec. 2006, pp. 577 –580.

[8] D. Marcuse, "Simplified analysis of a polarizing optical fiber," *Quantum Electronics, IEEE Journal of*, vol. 26, no. 3, pp. 550 –557, Mar. 1990.

[9] C. Chan, C. Chen, A. Jafari, A. Laronche, D. J. Thomson, and J. Albert, "Optical fiber refractometer using narrowband cladding-mode resonance shifts," *Applied Optics*, vol. 46, no. 7, pp. 1142–1149, Feb. 2007.

[10] L.-Y. Shao, M. B. Jakubinek, T. Sun, B. Simard, and J. Albert, "Four-wave mixing in carbon nanotube-coated optical fiber gratings," *Applied Physics Letters*, vol. 100, no. 7, p. 071108, 2012.

Chapter 5

Conclusions

A comprehensive study of optical fiber lasers for microwave photonics applications has been presented in this thesis. The consolidated technology of optical fibers offers an extensive portfolio of optical fiber laser systems. In particular, erbium-doped optical fibers have been exploited in this thesis to design all the optical sources emitting in the third optical communication window of 1.5 μm. The commercial availability of telecom fiber devices such as modulators, couplers and isolators makes fiber lasers reliable and compact optical sources.

The content of this thesis focuses on continuous wave dual-wavelength fiber lasers for microwave signal generation and mode-locked fiber lasers for photonic analog to digital conversion. For the first part, dual-wavelength fiber lasers have been approached employing distributed feedback structures. Based on fiber Bragg gratings, DFB lasers represent low cost and highly compact optical sources. An innovative application of piezoelectric transducers is proposed to achieve dynamic tunability of the spectral separation between the two emitting modes. The designed fiber laser provides a continuous tuning range of the photogenerated frequency from 0.128 to 7 GHz. A cascaded DFB cavities design extended the tuning range to 0.72-92 GHz. The obtained results highlight the potential application of piezoelectric actuators in fiber based devices. The cascaded DFB design can be further extended to higher tuning ranges by specialty fibers with higher elasticity, or the direct inscription of two cascaded fiber gratings with different grating periods, easily reaching THz-generation applications.

Mode-locked fiber lasers have been addressed in the second part of the thesis. Different fiber laser structures were designed, simulated, fabricated and characterized to comply with photonic-assisted analog to digital conversion specifications. Active and passive mode-locking operations are explored. The thesis proposes an intracavity polarizing fiber based mode-locked laser. Through polarization state control, this laser is able to switch among three different operation regimes (two solitonic pulsed regimes and one multiwavelength regime). Polarizing fibers offer potential management of

dispersion and polarizing ratio of an optical all-fiber cavity. Further experimentation with different gain budgets will allow us to obtain stable pulsed emission in the harmonic mode-locked regime with repetition rates over 100 GHz. Moreover, polarizing photonic crystal fibers can be proposed to customize desired chromatic dispersion profiles at the same time they polarize light, assisting in a wider range of dispersion controlled operation regimes.

The final part of this thesis deals with the design of a fiber-based device incorporating carbon nanotubes to induce ultrafast nonlinear effects. Carbon nanotubes have found direct application as passive mode-lockers in the recent years. In this work, tilted fiber Bragg gratings have been proposed to assist the interaction of propagating light through the core to the nonlinear nanotube external layer. The inscription of Bragg gratings in standard photosensitive optical fibers avoids the use of special and delicate fibers like D-shaped or tapered fibers in order to integrate carbon nanotubes. Two different processes of carbon nanotube coating were studied, and ultrafast nonlinear effects were experimentally demonstrated through a 1ps resolution pump-probe set-up. The multi-resonant response of a tilted response does not completely exploit the wide flat bandwidth of optical saturable absorption that single walled carbon nanotubes offer, and further structures of optical fibers integrating carbon nanotubes will be analyzed.

List of publications

[1] **G. E. Villanueva**, V. Polo, V. Perales, M. A. Piqueras, and J. Martí, "High purity mm-wave generation employing IM/DD techniques," in *THz Photonics 2007, FP6-ISIS workshop*, Leeds, United Kingdom, 2007.

[2] **G. E. Villanueva**, P. Pérez-Millán, J. Palací, J. L. Cruz, M. V. Andrés, and J. Martí, "Tunable microwave signal generation using dual-wavelength DFB erbium-doped fiber laser," in *IEEE International Topical Meeting on Microwave Photonics, 2009. MWP'09.*, Valencia, Spain, Oct. 2009, p. th.4.33.

[3] **G. E. Villanueva**, P. Pérez-Millán, J. Palací, J. L. Cruz, M. V. Andrés, and J. Martí, "Dual-wavelength DFB erbium-doped fiber laser with tunable wavelength spacing," *Photonics Technology Letters, IEEE*, vol. 22, no. 4, pp. 254–256, Feb. 2010.

[4] **G. E. Villanueva**, J. Palací, J. L. Cruz, M. V. Andrés, J. Martí, and P. Pérez-Millán, "High frequency microwave signal generation using dual-wavelength emission of cascaded DFB fiber lasers with wavelength spacing tunability," *Optics Communications*, vol. 283, no. 24, pp. 5165 – 5168, 2010.

[5] J. Palací, **G. E. Villanueva**, J. V. Galán, J. Martí, and B. Vidal, "Single bandpass photonic microwave filter based on a notch ring resonator," *Photonics Technology Letters, IEEE*, vol. 22, no. 17, pp. 1276 –1278, Sep. 2010.

[6] J. Palací, P. Pérez-Millán, **G. E. Villanueva**, J. L. Cruz, M. V. Andrés, J. Martí, and B. Vidal, "Tunable photonic microwave filter with single bandpass based on a phase-shifted fiber Bragg grating," *Photonics Technology Letters, IEEE*, vol. 22, no. 19, pp. 1467 –1469, Oct. 2010.

[7] G. Serafino, P. Ghelfi, **G. E. Villanueva**, J. Palací, P. Pérez-Millán, J. Cruz, C. Porzi, and A. Bogoni, "Stable optically generated RF signals from a fibre mode-locked laser," in *IEEE Photonics Society, 2010 23rd Annual Meeting of the*, Nov. 2010, pp. 193 –194.

[8] P. Ghelfi, G. Serafino, F. Fresi, **G. E. Villanueva**, P. Pérez-Millán, J. L. Cruz, F. Berizzi, and A. Bogonia, "Photonic generation of RF multiple carriers using a mode-locked laser and a single photodiode," in *Coherent Optical Communication: Components, Subsystems, and Systems*, vol. 7960, no. 1. SPIE, 2011, p. 79600Q.

[9] J. Palací, **G. E. Villanueva**, and J. Herrera, "EAM-SOA millimeter-wave frequency up-converter for radio-over-fiber applications," *Optics Communications*, vol. 284, no. 1, pp. 98 – 102, 2011.

[10] **G. E. Villanueva**, M. Ferri, and P. Pérez-Millán, "Control of the operation regimes of a passively modelocked fiber laser based on an intracavity polarizing fiber," in *CLEO/Europe and EQEC 2011 Conference Digest*. Optical Society of America, 2011, pp. CJ–P29.

[11] **G. E. Villanueva**, M. B. Jakubinek, B. Simard, C. J. Otón, P. Pérez-Millán, and J. Albert, "Tilted fiber Bragg grating assisted nonlinear effects in carbon nanotube-coated optical fibers," in *CLEO/Europe and EQEC 2011 Conference Digest*. Optical Society of America, 2011, pp. CD1–2.

[12] **G. E. Villanueva**, M. Jakubinek, M. Z. Alam, B. Simard, and J. Albert, "Optical properties of a wrapped carbon nanotube layer on optical fiber," in *Photonics North 2011*, Ottawa, Canada, 2011.

[13] **G. E. Villanueva**, M. B. Jakubinek, B. Simard, C. J. Oton, J. Matres, L.-Y. Shao, P. Pérez-Millán, and J. Albert, "Linear and nonlinear optical properties of carbon nanotube-coated single-mode optical fiber gratings," *Optics Letters*, vol. 36, no. 11, pp. 2104–2106, Jun. 2011.

[14] **G. E. Villanueva**, M. Ferri, and P. Pérez-Millán, "Fabrication of actively and passively modelocked fiber lasers for high-speed high-resolution photonic analog to digital conversion," in *7ª Reunión Española de Optoelectrónica OPTOEL*, Santander, Spain, 2011.

[15] **G. E. Villanueva**, M. B. Jakubinek, B. Simard, C. J. Otón, L. Shao, P. Pérez-Millán, and J. Albert, "Nonlinear effects of carbon nanotube coated single mode optical fiber gratings," in *7ª Reunión Española de Optoelectrónica OPTOEL*, Santander, Spain, 2011.

[16] G. Serafino, P. Ghelfi, P. Pérez-Millán, **G. E. Villanueva**., J. Palací, J. L. Cruz, and A. Bogoni, "Phase and amplitude stability of EHF-band radar carriers generated from an active mode-locked laser," *Lightwave Technology, Journal of*, vol. 29, no. 23, pp. 3551 –3559, Dec. 2011.

[17] **G. E. Villanueva**, M. B. Jakubinek, B. Simard, C. J. Otón, L.-Y. Shao, P. Pérez-Millán, and J. Albert, "Nonlinear effects of carbon nanotube coated single mode optical fiber gratings," *Óptica Pura y Aplicada*, vol. 45, no. 2, pp. 177–182, Jun. 2012.

[18] **G. E. Villanueva** and P. Pérez-Millán, "Dynamic control of the operation regimes of a mode-locked fiber laser based on intracavity polarizing fibers: experimental and theoretical validation," *Optics Letters*, vol. 37, no. 11, pp. 1971–1973, Jun. 2012.

[19] **G. E. Villanueva**, M. Ferri, and P. Pérez-Millán, "Active and passive mode-locked fiber lasers for high-speed high-resolution photonic analog to digital conversion," *Quantum Electronics, IEEE Journal of*, vol. 48, no. 11, pp. 1443–1452, Nov. 2012.

[20] **G. E. Villanueva** and P. Pérez-Millán, "Short-cavity erbium-doped mode-locked fiber laser with tunable pulse repetition frequency," in *Photonics in Switching*, Ajaccio, Corsica, France, 2012.

Awards

Award for the 2^{nd} best student paper (sponsored by SPIE) in the 7^{a} *Reunión Española de Optoelectrónica OPTOEL*, Santander, Spain, 2011, for the work "Nonlinear effects of carbon nanotube coated single mode optical fiber gratings". June 2011.

Valencia Idea 2012 award for the innovative project "Ultrafast fiber lasers based on carbon nanotubes" in the Information and Communications Technology category, sponsored by Valencia City Council, Gas Natural Fenosa and InnDEA Valencia. October 2012.

List of Figures